



HAL
open science

Radiocarbon as a Dating Tool and Tracer in Paleoceanography

L. C. Skinner, E. Bard

► **To cite this version:**

L. C. Skinner, E. Bard. Radiocarbon as a Dating Tool and Tracer in Paleoceanography. *Reviews of Geophysics*, 2022, 60, 10.1029/2020RG000720 . insu-03661015

HAL Id: insu-03661015

<https://insu.hal.science/insu-03661015>

Submitted on 6 May 2022

HAL is a multi-disciplinary open access archive for the deposit and dissemination of scientific research documents, whether they are published or not. The documents may come from teaching and research institutions in France or abroad, or from public or private research centers.

L'archive ouverte pluridisciplinaire **HAL**, est destinée au dépôt et à la diffusion de documents scientifiques de niveau recherche, publiés ou non, émanant des établissements d'enseignement et de recherche français ou étrangers, des laboratoires publics ou privés.



Distributed under a Creative Commons Attribution 4.0 International License

Reviews of Geophysics®



REVIEW ARTICLE

10.1029/2020RG000720

Radiocarbon as a Dating Tool and Tracer in Paleoceanography

L. C. Skinner¹  and E. Bard² 

Key Points:

- Radiocarbon is a powerful carbon cycle tracer and radiometric dating tool, that is widely used in paleoceanography
- Marine radiocarbon activities, relative to the contemporary atmosphere, integrate three main effects: gas exchange, transport times, and the mixing of different water masses
- Reconstructions attest to ocean ventilation's role in past CO₂ change, but the long-term closure of the radiocarbon cycle remains unresolved

Supporting Information:

Supporting Information may be found in the online version of this article.

Correspondence to:

L. C. Skinner,
luke00@esc.cam.ac.uk

Citation:

Skinner, L. C., & Bard, E. (2022). Radiocarbon as a dating tool and tracer in paleoceanography. *Reviews of Geophysics*, 60, e2020RG000720. <https://doi.org/10.1029/2020RG000720>

Received 3 DEC 2020
Accepted 29 DEC 2021

Author Contributions:

Writing – review & editing: E. Bard

¹The Godwin Laboratory for Palaeoclimate Research, Department of Earth Sciences, University of Cambridge, Cambridge, UK, ²CEREGE, CNRS, IRD, INRAE, Collège de France, Technopole de l'Arbois, Aix Marseille University, Aix-en-Provence, France

Abstract Radiocarbon is an extremely useful carbon cycle tracer and radiometric dating tool. Here, we review the main principles and challenges involved in the use of radiocarbon in paleoceanography. First, we present a conceptual framework in which there are three possible uses of a radiocarbon measurement: (a) to obtain a calendar age interval, or a fossil entity's age; (b) to obtain an estimate of a carbon reservoir's past radiocarbon activity; or (c) to compare the relative radiocarbon activities of two contemporary carbon reservoirs. We discuss the analysis of marine fossil material, the generation of an atmospheric reference curve, and the interpretation of marine radiocarbon “ventilation metrics” in relation to this reference curve. It is emphasized that marine radiocarbon integrates the influences of: changing radiocarbon production; air-sea gas exchange effects at the sea surface; transport times within the ocean interior; and the mixing of water parcels with different transit times from the sea surface, and different sea-surface sources. These controls are what make radiocarbon such a powerful paleoceanographic tracer, though the difficulty of disentangling them is what makes marine radiocarbon dating and tracer studies so challenging. We discuss the implementation of radiocarbon in numerical models, and explore the theory linking ocean-atmosphere partitioning of radiocarbon and CO₂. Finally, we review existing records of marine radiocarbon variability over the last ~25,000 years, which highlight the influence of ocean-atmosphere carbon exchange on past atmospheric CO₂ and climate, and point to emerging opportunities for resolving the global radiocarbon- and carbon budgets over the last glacial cycle.

Plain Language Summary Radiocarbon is a naturally occurring, albeit rare, isotope of carbon that is widely used in the biogeosciences: as a “dating tool,” to provide the age of carbon bearing materials; and as an environmental “tracer,” to track the movement of carbon in the environment. Radiocarbon is produced in the atmosphere, via the impact of cosmic radiation on nitrogen atoms. Once formed, it participates in the global carbon cycle, while gradually decaying away, providing a “clock” for the movement of carbon in the environment. In the field of paleoceanography (the study of past ocean dynamics and biogeochemistry), the most important areas of activity in the application of radiocarbon include: the ongoing improvement of analytical techniques for measuring ever smaller and more difficult samples; the elucidation of the myriad biological and sedimentary processes that may bias radiocarbon observations; and newly emerging opportunities for combining globally distributed observations with numerical and statistical models to infer increasingly detailed aspects of past ocean circulation and carbon cycle change. A revised synthesis of marine radiocarbon observations accumulated over the last decades attests to the ocean's central role in past global change, and points to a wealth of exciting developments to be pursued in the years to come.

1. Introduction

Radiocarbon (¹⁴C) is one of three naturally occurring isotopes of carbon. Unlike its stable counterparts (¹²C and ¹³C), radiocarbon decays away with a half-life of ~5700 years (i.e., the abundance of radiocarbon in a fixed mass halves every ~5700 years). It is a relatively rare isotope of carbon, representing ~1.2 × 10⁻¹⁰% of the total carbon inventory (compared to ~98.9% for ¹²C, and ~1.1% for ¹³C). Radiocarbon is naturally produced in the atmosphere via the collision of neutrons (themselves produced by cosmic protons) with nitrogen atoms, which capture a neutron and expel a proton to yield a radiocarbon atom. Once a radiocarbon atom is produced in the atmosphere it is cycled through the global carbon cycle (Figure 1), along with the other isotopes of carbon, eventually decaying back to stable nitrogen via beta particle emission (Craig, 1957).

Evidence for the existence of a radioactive isotope of carbon of atomic mass 14 was first discovered by Franz Kurie in 1934 (Kurie, 1934), but most of the fundamental work on its measurement and application as a

© 2022. The Authors.

This is an open access article under the terms of the [Creative Commons Attribution License](https://creativecommons.org/licenses/by/4.0/), which permits use, distribution and reproduction in any medium, provided the original work is properly cited.

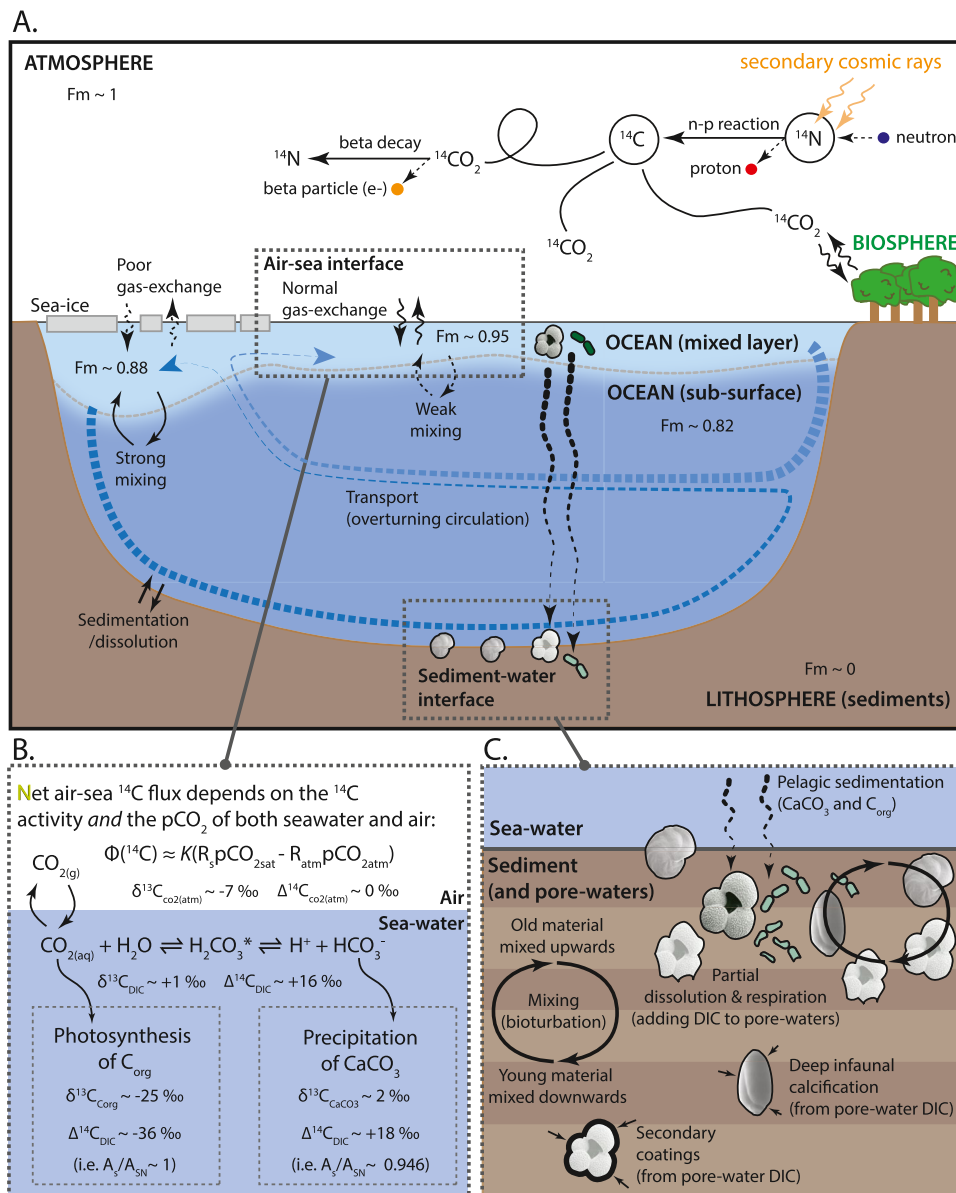


Figure 1. Illustration of some key aspects of the marine radiocarbon cycle (panel A), including processes operating at the air-sea interface (panel B) and the sediment-seawater interface (panel C). Radiocarbon is produced in the atmosphere (e.g., with a “fraction modern” radiocarbon activity, Fm ~ 1), after which it begins to decay away with a constant half-life while being cycled through the carbon cycle. The average timescale for exchange between a carbon bearing reservoir and the atmosphere will determine the extent of its isotopic enrichment relative to the atmosphere (e.g., yielding marine Fm ~ 0.82–0.95, and “radiocarbon-dead” lithosphere Fm ~ 0). The radiocarbon activity of the surface ocean reflects the efficiency of air-sea gas-exchange (e.g., modified by sea-ice cover), as well as the rate of mixing with the more radiocarbon-depleted ocean sub-surface (see panel A). The radiocarbon activity of the ocean (and its spatial distribution) therefore depends on air-sea gas exchange efficiency, combined with ocean interior transport rates and pathways. Net air-sea flux of radiocarbon ($\Phi(^{14}\text{C})$) depends on the CO_2 partial pressures and radiocarbon activities of both seawater and the overlying atmosphere (panel b), as well as the CO_2 solubility and exchange efficiency (represented in panel b by the factor “K”). Gas exchange involves isotopic fractionation of both $^{13}\text{C}/^{12}\text{C}$ and $^{14}\text{C}/^{12}\text{C}$, with the latter twice as large as the former (i.e., $\epsilon_{14} = 2 \times \epsilon_{13}$, $\alpha_{14} = \alpha_{13}^2$). Isotopic fractionation occurs during CO_2 uptake/release, during dissolved inorganic carbon speciation, and during organic carbon fixation or carbonate precipitation. By convention, these fractionation effects are corrected for when reporting radiocarbon activities/dates, by normalizing to equivalent organic carbon activities (measured activity/normalized activity, $A_3/A_{\text{SN}} \sim (1 - 2(25 + \delta^{13}\text{C}_3)/1,000)$). At the sediment-water interface (i.e., at the sea floor; panel [c]), benthic material will ideally reflect bottom-water radiocarbon activity, and co-deposited planktonic material will reflect the activity of overlying surface waters. However, the radiocarbon activity of sedimentary material can be influenced by: for example, mixing of old/young sediments via bioturbation, the supply of old/young carbon to pore-waters via respiration/dissolution of organic carbon/carbonate, and the possible precipitation of secondary carbonate coatings (or primary benthic carbonate) from pore-waters that have been influenced by respiration/dissolution of pelagic material.

radiometric dating tool is attributed to W. F. Libby (Libby, 1946; Libby et al., 1949), who received the 1960 Nobel Prize in chemistry for this work. Libby had initially determined the half-life of radiocarbon to be 5568 years (Libby, 1955), but this was subsequently revised to 5730 by (Godwin, 1962) who averaged three independent estimates presented at the 1962 ^{14}C -symposium held in Cambridge, United Kingdom (Hughes & Mann, 1964; Mann et al., 1961; Olsson et al., 1962; Watt et al., 1961). Although the “Cambridge half-life” (5730 years) has been widely adopted as the accurate value for the radiocarbon half-life, a slightly lower value of 5700 ± 30 years is obtained by averaging the three previous estimates, including a correction (Hughes & Mann, 1964), with a fourth independent estimation by Bella et al. (1968). Recent work indicates that the half-life could be even lower (Roberts & Southon, 2007). However, in order to avoid the need to recalculate all previously reported radiocarbon ages (and in order to avoid the need to do this each time the radiocarbon half-life might be improved in future), it was also decided in 1962 that radiocarbon age determinations would continue to be reported using the original “Libby half-life” of 5568 years, by convention (Godwin, 1962). All measured radiocarbon ages are therefore reported as “conventional radiocarbon ages,” and thus derived from measured radiocarbon activities or isotopic ratios using the Libby half-life (hereafter, for simplicity, we refer to activities and ratios interchangeably as generic measures of relative radiocarbon abundance). Note that the conventional approach of using the Libby half-life is not necessarily (or generally) adopted in other contexts, such as tracer or modeling studies, and that uncertainty in the half-life is not propagated into age calculations because it is systematic.

The current conventions for radiocarbon age reporting are those described by Stuiver and Polach (1977) and updated by Mook and van der Plicht (1999). These reporting conventions (and attendant calculations) seek to address three goals: (a) to normalize the measured radiocarbon abundance in a sample material, by correcting for mass-dependent isotopic fractionation due to physical and biological processes during sample formation, chemical treatment, and analysis (using the measured stable carbon isotope ratio, $^{13}\text{C}/^{12}\text{C}$, of the sample); (b) to reference this fractionation-corrected radiocarbon abundance relative to that of an internationally accepted “primary” radiocarbon standard; and (c) to correct for the time elapsed between 1950 (the year of normalization, or “year 0”) and the year in which the sample was measured (or alternatively the year in which it was collected). However, not all samples need to be treated and reported in exactly the same way, resulting in slightly different reporting conventions for different samples (Stuiver & Polach, 1977). Furthermore, these reporting conventions are not necessarily adopted (or even appropriate) for all radiocarbon applications, including in particular the use of radiocarbon as a carbon cycle tracer, including in numerical models. Care should therefore be taken when comparing radiocarbon activities derived from reported conventional dates (which will always be $\delta^{13}\text{C}$ -normalized, and for which the radiocarbon activity will always be referenced to the $\delta^{13}\text{C}$ -normalized activity of a “primary” standard in 1950 [Stuiver & Polach, 1977]), and those obtained for example, from numerical model simulations (which are likely to adopt the “true” radiocarbon half-life instead of the conventional “Libby half-life,” and are not always “corrected” for mass dependent fractionation relative to ^{12}C). While the main point here is that comparisons should always be made using similar units, a secondary point is that true radiocarbon inventories can only be derived using unnormalized values that are decay corrected to the time period of interest (e.g., $\delta^{14}\text{C}$, as defined by Stuiver and Polach [1977]). Indeed, “correcting” marine radiocarbon to what it would be if the ocean obtained its carbon via photosynthesis, makes the marine carbon reservoir appear to contain less radiocarbon than it actually does (Bard et al., 1988).

Radiocarbon is widely used in the biogeosciences (and archeology, for example) due to the time-dependence of its decay, and/or its participation in the carbon cycle. Radiocarbon is perhaps best known for its use as a radiometric dating tool, and indeed it was developed by W. F. Libby primarily for this purpose (Libby, 1955). However, it is a curious fact that the conditions under which radiocarbon can be used to provide accurate calendar dates are far from universal, and are actually quite restricted. This review focuses on the challenges that arise in the use of radiocarbon in paleoceanography, where radiocarbon is used both as a dating tool and as an ocean circulation and carbon cycle tracer. First, in Section 2, we present a general conceptual framework for understanding the use of radiocarbon in paleoceanography, and discuss the central concepts and challenges associated with: (a) the analysis of marine fossil material; (b) the generation of an atmospheric reference curve; and (c) the interpretation of marine radiocarbon “ventilation metrics” in relation to this reference curve. Then, in Section 3, we address the developments and challenges associated with implementing radiocarbon in numerical models. In Section 4 we explore a basic theory for the link between marine radiocarbon, the marine “disequilibrium” and “respired” dissolved inorganic carbon (DIC) inventories, and atmospheric CO_2 . Finally, in Section 5, we turn to the history

of marine radiocarbon variability over the last ~25,000 years, and its implications for the ocean's role in carbon cycle and climate change.

2. Theory and Concepts for the Use of Radiocarbon as a Dating Tool and Tracer in Paleoceanography

2.1. A General Conceptual Framework for the Use of Radiocarbon in Paleoceanography

If radiocarbon were distributed uniformly alongside the stable carbon isotopes at the Earth's surface (i.e., in the atmosphere, ocean, and biosphere), it would serve as a straightforward chronological tool. However, the journey from its formation in the upper atmosphere to all the waters, soils, minerals and tissues of the world is not instantaneous. In addition, isotopic fractionation associated with phase transitions and chemical reactions can contribute to radiocarbon biases between reservoirs. As a result, different pools of carbon in the environment (e.g., dissolved inorganic carbon at a given location in the surface ocean, vs. carbon dioxide in the troposphere) will have different radiocarbon activities, at the same point in time. This means that different contemporary fossil entities can be formed, and eventually deposited, with different initial radiocarbon activities, depending on the reservoir that they have fixed their carbon from. To complicate matters, due to variable radiocarbon production rates and/or variable fluxes between carbon reservoirs, the radiocarbon activities of the various Earth surface reservoirs will vary over time. The evolving offsets in radiocarbon activity between carbon reservoirs creates the potential to use radiocarbon as an environmental tracer that informs on the physical, chemical, and biological processes that operate within them, and that mediate carbon exchanges between them. At the same time (and in a necessarily *alternative* application), it means that radiocarbon can only be used to *date* fossil material if we know how the radiocarbon activities of the relevant Earth surface reservoirs have evolved over time, thereby allowing us to calibrate “radiocarbon years” to calendar years. This is why accurate radiocarbon dating can be challenging.

The radiocarbon system combines the complexity of the global carbon cycle with the added influences of: *variable cosmogenic isotope production* (and hence the influence of geomagnetic field strength and solar activity variability); *isotopic fractionation* during phase transitions and chemical reactions; and constant gradual *radioactive decay* (see Figure 1). Most radiocarbon measurements further include influences from the biological systems that produce the fossils, tissues or minerals that are analyzed, as well as the sedimentary systems that these fossils “filter” through, into the geological record. The isotopic rarity of radiocarbon lends further analytical challenges, particularly for the analysis of small aliquots of relatively old material. These complexities make it particularly useful to adopt a consistent theoretical framework and rigorous nomenclature to avoid confusion and/or misinterpretation of the radiocarbon system (Mook & van der Plicht, 1999; Soulet et al., 2016; Stuiver & Polach, 1977). Because attendant complexities render such a framework and nomenclature somewhat cumbersome, we restrict ourselves to summarizing here just the most central axioms for interpreting measured radiocarbon activities in this context:

1. The basic known quantity for any radiocarbon-dated sample is the activity ratio, or “**fraction modern carbon**,” of the sample (Reimer et al., 2004), defined as: $Fm_{\text{entity name}}^{\text{reporting time}}$. This is the ratio of the measured (and mass-dependent isotopic fractionation-normalized) radiocarbon activity in the sample, relative to the radiocarbon activity that is defined as representing the year 0 before present (BP), that is, the year 1950, via primary oxalic acid standards (Stuiver & Polach, 1977). Note that 1950 is therefore defined as “the present” in this system.
2. The measured fraction modern of a sample (i.e., Fm_{sample}^0) simply represents a point on a decay curve that extends from the past, through the present, and into the future, along a trajectory that is defined by the radiocarbon decay constant, λ_C (i.e., where the “true” or “Cambridge” half-life, $\tau_C = \ln(2)/\lambda_C$). The decay constant thus allows us to “adjust” a measured fraction modern, Fm_{sample}^0 , to the value it would have been at any given “time before present” (T) in the past: that is, Fm_{sample}^T (see Figure 2).
3. If we assume that the Fm_{sample}^T of the measured sample faithfully recorded the radiocarbon activity of its “parent” carbon reservoir at the time (T) that it formed (i.e., it has not been biased by biological, sedimentary, diagenetic, analytical or other influences), then we can use the measured Fm_{sample}^0 value, along with the radiocarbon decay constant, to do one of three things (see Figure 3):
 - a. we can *determine the radiocarbon activity of the parent reservoir* at the time the fossil entity formed (e.g., the atmospheric radiocarbon activity in the past, Fm_{atm}^T), if we also know the true “calendar” age of the sample (i.e., T, how far back in time to trace the decay curve);

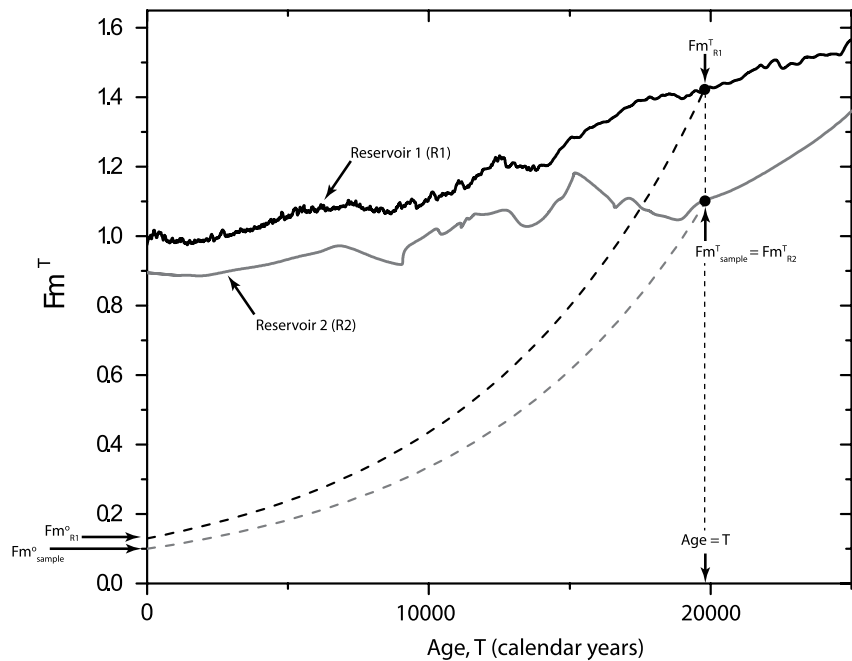


Figure 2. Illustration of the relationships between the “fraction modern” radiocarbon activity (Fm^T): measured today (where at 1950, age = 0, Fm^0_{sample}), fixed in the past by the sampled fossil entity (at age = T , Fm^T_{sample}); and evolving over time in various natural reservoirs. The solid black line indicates the evolving hypothetical fraction modern for reservoir 1 (e.g., the atmosphere), while the solid gray line indicates the evolving hypothetical fraction modern for reservoir 2 (e.g., a region of the surface ocean). The dashed lines indicate decay trajectories for aliquots of each reservoir, for example, as sampled at a given point in time (age = T) by fossil entities, such as tree cellulose or marine carbonate shells. Note that the ratio of $Fm^0_{\text{sample}}/Fm^0_{R1} = Fm^T_{\text{sample}}/Fm^T_{R1} = \alpha^T_{\text{sample}-R1}$ remains constant over time.

- b. we can *determine the age of the fossil entity* (i.e., T , how long its radiocarbon has been decaying away), if we also know its initial radiocarbon activity, or equivalently the activity of its parent reservoir at the time the entity formed; or
- c. we can *determine the relative isotopic enrichment of the “parent” reservoir versus another*, if we know the calendar age of the fossil entity and the radiocarbon activity of the second carbon reservoir at the time the fossil formed; for example, we can infer the ratio of the radiocarbon activity of reservoir R_2 versus the contemporary atmosphere, at time = T , defined here as $\alpha^T_{R2-\text{atm}}$ (this was defined as the slightly more cumbersome $F^{14}R^T_{R2-\text{atm}}$ in Soulet et al. [2016]). Notably, this can also be done using radiocarbon dates from two entities/reservoirs that are known to be co-eval, without knowledge of their calendar age, since both entities will experience the same rate of radiocarbon decay over time (see Case 3 in Figure 3). In paleoceanographic applications this would typically be used to derive marine “reservoir age” offsets, or some other measure of “radiocarbon ventilation” for example (this is explored further below).

Note that the ocean is typically depleted in radiocarbon relative to the atmosphere; however, we refer here to metrics for the isotopic enrichment of radiocarbon relative to ^{12}C (i.e., Fm^T_{sample}), or the relative isotopic enrichment of radiocarbon in one reservoir versus another (i.e., $\alpha^T_{R2-\text{atm}}$), such that greater enrichment is indicated by more positive values in these terms (or relative enrichment >1), and greater depletion is indicated by more negative terms (or a relative enrichment <1).

Implicit in the three (exclusive) applications of a single radiocarbon measurement listed above, are three basic requirements, in addition to knowledge of the radiocarbon half-life. The first is the ability to obtain accurate radiocarbon activity measurements, performed on a variety of materials obtained from marine sediments. The second, ideally, is accurate knowledge of how the radiocarbon activities of the main Earth surface carbon reservoirs (and their constituent parts, if they are not well mixed, e.g., the ocean) have evolved over time. Clearly, such knowledge would “beg the question” of most paleoceanographic research that seeks to use radiocarbon as a tracer. However, as a starting point, we might hope to have accurate knowledge of how the atmospheric radiocarbon activity has

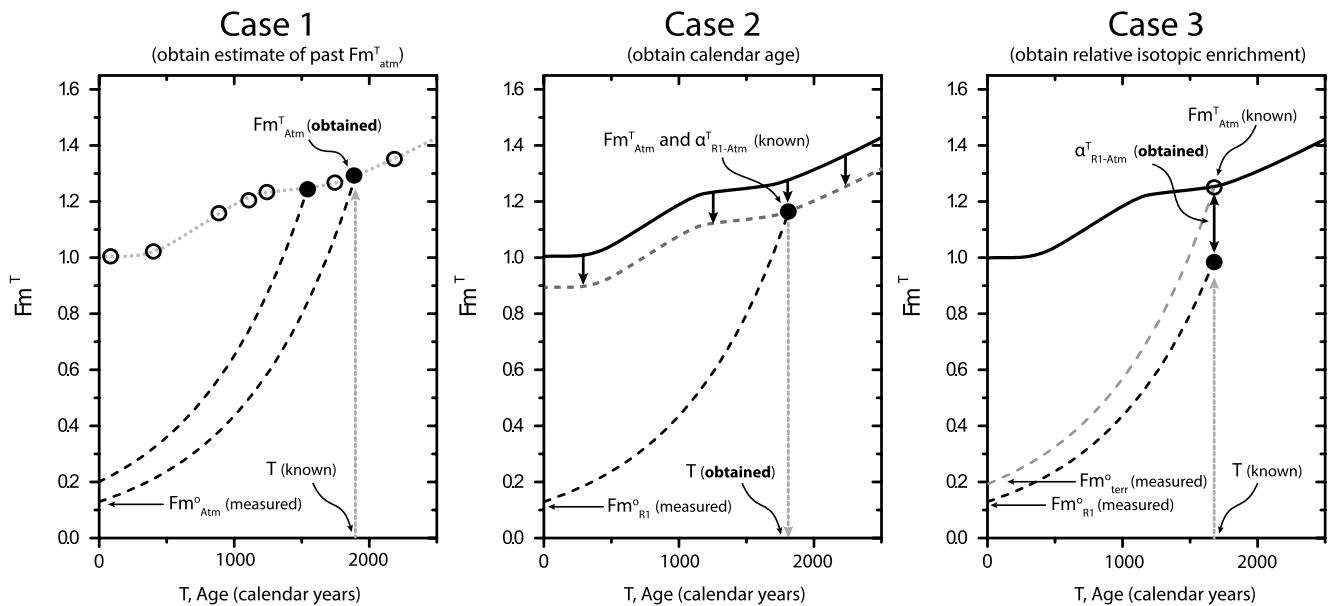


Figure 3. Illustration of the three different applications of a single radiocarbon measurement, provided a known decay constant for radiocarbon. In each panel fraction modern (Fm^T) is plotted against calendar age (T). Case 1: a measured radiocarbon activity and a known calendar age for the fossil entity is used to obtain the initial radiocarbon activity of the fossil's parent reservoir, such that many such measurements can be used to derive a history of the parent reservoir's radiocarbon activity (e.g., as for an atmospheric calibration curve). Case 2: A measured radiocarbon activity is combined with a known radiocarbon activity history for the parent reservoir (here given by a known atmospheric history and α^T_{R1-Atm}) to obtain a calendar age, that is, to date a fossil entity. Case 3: a measured radiocarbon activity is combined either with a known calendar age and a known radiocarbon activity history for a given reservoir (e.g., the atmosphere, Atm), or with a measurement performed on a contemporaneous sample (e.g., a co-deposited terrestrial fossil entity that obtained its carbon from the atmosphere), to obtain the relative isotopic enrichment of ^{14}C in the fossil entity (or equivalently its parent reservoir) as compared to the second reservoir or entity, at the time the fossil formed. Note that in Case 3, $\alpha^T_{R1-Atm} = \alpha^0_{R1-atm} = \alpha^0_{R1-terr}$ is constant, implying that if two fossil entities are known to be contemporaneous, their past relative isotopic enrichment can be accurately known without knowledge of their calendar age.

evolved over time (and to what extent this reflects changes in the radiocarbon production rate), thus allowing us to compare our past marine radiocarbon activity estimates to a common, time-varying, atmospheric reference (notwithstanding subtle heterogeneities that also exist in the atmosphere [Capano et al., 2019; Hogg et al., 2020]). The third basic requirement is an independent calendar age dating method, applicable to marine samples, as well as a theoretical framework for understanding marine radiocarbon activities and interpreting their evolution over time. While the first of these three requirements is needed in all cases, the second and third are needed in only two of the three cases listed above (Figure 3). We take up each of these requirements below.

2.2. Radiocarbon Measurements: Inherent Challenges and Technical Advances

The radiocarbon abundance in a sample can be measured by counting its “radio-activity” (e.g., disintegrations per minute per gram carbon, dpm/gC) or by measuring its $^{14}C/^{12}C$ isotopic ratio by accelerator mass spectrometry (AMS). Both measurements are normalized to those of a reference sample with the same techniques and under the same conditions. This ensures an accurate determination of the radiocarbon abundance that can be expressed either as an absolute activity or as an isotopic ratio (Mook & van der Plicht, 1999), or just as a deviation with respect to the reference sample. Prior to the development of ion counting methods and AMS, radiocarbon measurement was exclusively possible by beta disintegration counting techniques. Such analysis methods require large samples in order to have enough carbon atoms present to have the chance of counting a sufficient number of disintegrations to permit a statistically reasonable estimate of the true radiocarbon activity of the sample. AMS methods have revolutionized the analysis of radiocarbon by permitting the accurate analysis of very small amounts of carbon. A 2009 review of radiocarbon analysis methods and their historical development can be found in Povinec et al. (2009).

The key principles of radiocarbon measurement by accelerator mass spectrometry are: (a) the ion source usually consists of negatively charged C ions, created in a secondary mode via sputtering a solid carbon target by

Cs + ions; (b) the presence of isobars (^{13}CH and $^{12}\text{CH}_2$, i.e., masses that “masquerade” as ^{14}C) is solved by stripping negative ions at high energy (hence the accelerator); (c) AMS is based on multiple magnetic and electrostatic sectors, which select ions according to their $M\cdot E/q^2$ and E/q ratios, respectively (M is mass, E is energy, q is charge state); and (d) detection of radiocarbon is finally achieved using gas ionization chambers, which select ions according to their $M\cdot Z^2/E$ ratio (Z being the atomic number). AMS has been routinely used for ^{14}C measurements since the mid 1980s. One of the most significant recent analytical developments is the routine, accurate and relatively precise, gas ion source AMS measurements on small carbonate or organic carbon samples, down to ~ 50 μgC versus ~ 1 mgC for traditional AMS methods (Bard et al., 2015; Fagault et al., 2019; Gottschalk et al., 2018; Wacker et al., 2013). Even smaller quantities can be measured, albeit with a sacrifice in analytical precision. This analytical development has accelerated a host of specialized lines of enquiry, including in particular the routine analysis of compound-specific radiocarbon activities (Mollenhauer et al., 2019), or investigations of the distribution of radiocarbon between or even within individual foraminifera or coral skeletons etc. (e.g., Fagault et al., 2019; Lougheed et al., 2018; Wacker et al., 2013; Welte et al., 2016).

For paleoceanographic applications, radiocarbon measurements are performed on “fossil” material, containing either organic carbon or biogenic/inorganic carbonate, that has been incorporated into the marine sedimentary record. As such, it is important to take account of the depositional and diagenetic history, or “taphonomy,” of the material that is dated (e.g., Mekik, 2014). For biogenic material, it is also often important to consider the life habits, including the stenotopy and (micro-) habitat preferences, of the organisms that produced the fossil material being dated. In paleoceanographic contexts, fossil material for dating will typically include foraminifera (planktonic, and both infaunal- and epifaunal benthic), corals, gastropods, bivalves or coccoliths, as well as organic matter (undifferentiated or as isolated molecular types). In all these cases, life habits, taphonomy, and diagenesis are important issues to consider, in particular as they affect three key factors: (a) synformational/syndeformational contamination or habitat bias (e.g., from specific carbon sources during shell/skeleton/biomarker formation); (b) time-averaging, for example, due to bioturbation or lateral transport (affecting the age distribution amongst individual shells/fragments/molecules included in a single sample; Bard et al., 1987; Mollenhauer et al., 2005; Ohkouchi et al., 2002); and (c) post-depositional contamination/over-printing (e.g., from cementation or other post-depositional carbonate precipitation; Wycech et al., 2016), or selective destruction of labile phases via oxidation or dissolution (Barker et al., 2007; Broecker & Clark, 2011; see Figure 1c).

The first of the above factors would include habitat bias in shallow (surface) versus deep (thermocline) dwelling planktonic foraminifera, affecting the degree of offset from atmospheric radiocarbon activity (i.e., reservoir age offsets; see below). Habitat biases on epifaunal versus infaunal benthic foraminifera may also occur (e.g., Ezat et al., 2017, 2019; Keigwin & Lehman, 2015; Magana et al., 2010), although the relatively high concentration of dissolved inorganic carbon (DIC) in deep water means that significant biases from the ambient bottom water radiocarbon activity are most likely to occur in the context of major carbon fluxes from for example, hydrocarbon seeps or clathrate dissociation (Magana et al., 2010). Under “normal” infaunal conditions, with relatively high sedimentation rates, where the carbon inventory of pore-waters is dominated by the DIC of bottom water and secondarily influenced by organic carbon fluxes from the surface ocean, the direct addition of respired organic carbon, producing a pore-water $\delta^{13}\text{C}$ depletion of -1 to -2 permil, might be expected to also coincide with a radiocarbon activity bias in pore-waters of <100 ^{14}C years equivalent (assuming a radiocarbon activity offset between deep-water and respired organic carbon equivalent to the typical average radiocarbon offset between deep- and surface waters). However, the observation of mono-specific radiocarbon dates on co-deposited benthic foraminifera that differ by several thousand years (Ezat et al., 2017; Magana et al., 2010), despite coherent stable isotopic compositions in some cases, indicates that much has yet to be learned regarding the cycling of radiocarbon in the benthic realm. Here, the shallow infaunal (high-Mg, miliolid) benthic foraminifer species *Pyrgo sp.*, which tends to exhibit higher radiocarbon ages than other co-deposited benthic species, stands out as one example of a benthic foraminifer whose closer investigation holds potential to gain insights into the generation of radiocarbon biases between co-deposited benthic foraminifera (Magana et al., 2010).

Where carbonate dissolution also contributes DIC to pore-waters, the magnitude and direction of the resulting pore-water radiocarbon activity bias affecting infaunal benthics is hard to know *a priori*, as it will depend on a range of factors, including: the balance of respired organic carbon versus dissolved carbonate contribution to DIC, the deposition-age distribution of carbonate particles in the benthic foraminifer's habitat range and their solubility, and the degree of radiocarbon enrichment of those particles relative to contemporary bottom waters. In a context

of very low sedimentation rates (e.g., a few cm per kyr), it has been shown that carbonate dissolution can cause pore-waters in the upper several centimeters of the sediment column to become significantly radiocarbon-depleted relative to bottom waters, equivalent to thousands of years older (Martin et al., 2000). This serves to underline the potential difficulties that arise at low sedimentation rate sites. Setting aside poorly understood species-specific effects (Magana et al., 2010), it is likely that where moderate to high sedimentation rates prevail, bioturbation of foraminifera (acting in conjunction with changes in their abundance) will exert the most significant impact on measured radiocarbon ages (Bard et al., 1987; Broecker et al., 1984; Missiaen et al., 2020). Furthermore, bioturbation will affect planktonic as well as benthic substrates, and will interact with particle abundance variations and particle preservation biases (Barker et al., 2007; Broecker, Andree, Bonani, Wolfli, Klas, et al., 1988) to create offsets between radiocarbon ages and sediment deposition age (and between radiocarbon ages for entities with different abundance histories and/or preservation potential; Bard et al., 1987; Broecker, Andree, Bonani, Wolfli, Klas, et al., 1988). Although it is possible to minimize radiocarbon age biases relative to deposition ages by performing radiocarbon dates exclusively at abundance maxima for the dated substrate (Bard et al., 1987; Cook & Keigwin, 2015), this approach will not eliminate radiocarbon age biases between co-deposited particles (e.g., benthic and planktonic foraminifera) whose abundance maxima do not happen to coincide. Thus, for example, obtaining planktonic radiocarbon dates at local abundance maxima might help to obtain an accurate radiocarbon age-depth model (e.g., for sediment chronology), but it will not help to obtain accurate benthic versus planktonic radiocarbon age offsets (see below) unless benthic and planktonic abundance maxima coincide.

In general, it is fair to say that the effects of syndepositional contamination, habitat biases, bioturbation, and post-depositional overprinting/preservation have been relatively under-studied, largely due to the relatively large sample sizes needed for radiocarbon analyses, even with accelerator mass spectrometry methods. However, this is set to change with the advent of accurate gas-source AMS methods capable of routinely measuring very small aliquots of carbon (e.g., single foraminifera; Fagault et al., 2019; Wacker et al., 2013), potentially in sequential or continuous fashion (e.g., on carbonate leachates, or by laser-ablation; Ausín et al., 2019; Missiaen et al., 2020; Welte et al., 2016). Thus, age distributions for fossil entities (Dolman et al., 2021; Fagault et al., 2019), or age biases in sample leachates (Ausín et al., 2019; Missiaen et al., 2020), might be used to inform on the effects of bioturbation, population sampling, preservation or diagenesis. Auxiliary assessments of diagenetic overprinting or recrystallization may also be obtained from scanning electron microscope (SEM) imaging, for example to provide evidence of secondary phases/coatings or altered surface structures (Stott et al., 2009; Wycech et al., 2016). In this context, quantifying the effects of diagenesis or alteration can be a major challenge, even when age differences between visually distinct fossils or species (Ausín et al., 2019; Barker et al., 2007; Broecker, Andree, Bonani, Wolfli, Klas, et al., 1988; Wycech et al., 2016), or between leachates and bulk samples (Ausín et al., 2019; Missiaen et al., 2020), can be identified. Furthermore, any such impacts are very likely to be specific to a given site, sediment core, or even a given set of samples, depending on the conditions of sedimentary deposition, sediment core recovery, and sample treatment. While it might be expected that benthic fossils are less likely to undergo sea floor diagenesis or alteration, the existence of as yet unexplained radiocarbon age offsets between co-deposited benthic species (Ezat et al., 2017; Magana et al., 2010) should give us pause. As for most paleoceanographic applications, the greatest challenge (and the greatest contribution to uncertainty) in this context is typically not analytical; rather, it relates to what our careful, and probably quite accurate, measurements actually *represent*.

Accordingly, an important avenue for future work will almost certainly involve plying newly available analysis methods to the “Pandora’s Box of taphonomic nightmares” that can affect marine radiocarbon dates, while at the same time developing a mindful pragmatic approach to producing informative paleoceanographic reconstructions. Clearly, the most pressing objective will be to rule out the possibility that a sedimentary/depositional bias is misinterpreted as a primary environmental/hydrographic signal. Perhaps the most feasible and useful first step in this direction would be the systematic collection and reporting of down-core changes in the abundance of proxy carriers and radiocarbon-dated entities (e.g., foraminifer counts, in absolute numbers), which would permit an initial assessment of time-averaging and/or preservation biases. While it may not always be feasible or practical to perform SEM imaging of all dated fossil entities, or to perform extensive radiocarbon dating of multiple co-deposited species, individual foraminifera, or leachates, some routine practices can help to minimize certain biases. Thus even a limited amount of routine screening of radiocarbon samples, for example, through SEM imaging of foraminifera, and dating of multiple species in parallel, will increase the likelihood of identifying major issues, even if it will not be able to rule out all forms of potential bias. This may be aided by routinely recording and reporting benthic faunal composition and foraminifer aspect, and by opting wherever possible for

high sedimentation rate study sites, which will limit the effects of bioturbation and its interaction with fossil abundance variations (e.g., working with laminated sediments will avoid bioturbation effects entirely). High sedimentation rates might also help to limit the effects of sea floor diagenesis where this is caused by exposure to deep-waters (Wycech et al., 2016), rather than pore-waters. The use of large specimen numbers in sample aliquots (even where analytical capabilities do not require this), will limit scatter in radiocarbon dates that arises from differences between the age of a sub-set of entities drawn from a mixed (i.e., bioturbated) population, versus the mean age of the population (Dolman et al., 2021). That said, obtaining numerous radiocarbon ages on entities or sub-samples drawn from a single interval may allow the age-distribution within the interval to be determined, which can be extremely informative (Dolman et al., 2021). While this is unlikely to be practical in most down-core studies, it may be advisable in very low sedimentation rate settings, where the mean age of fossil entities within a stratigraphic interval may represent such a broad distribution as to contain very little information on its own. Furthermore, as discussed above, even well constrained “mean ages” can be significantly biased by habitat effects, bioturbation, diagenesis etc., such that a high degree of reproducibility carries no guarantee of the significance of the age obtained. In all cases, care should be taken to exclude agglutinated benthic foraminifera, and species such as *Pyrgo*, or even deep infaunal species if possible, when attempting to reconstruct past deep-water radiocarbon signatures. Ultimately, a pragmatic approach must be adopted (e.g., mono-specific, single-foram, dating of at least 30 benthic and planktonic individuals, drawn exclusively from abundance maxima, is unlikely to be practical in most instances); however, such pragmatism must be tempered by an awareness of the distinction between a radiocarbon measurement and the marine “reservoir” that it hypothetically represents.

2.3. Atmospheric Radiocarbon and Radiocarbon “Calibration”

As noted above, knowing how the radiocarbon activities of the main Earth surface reservoirs have evolved over time (and in relation to each other) is the key to the use of radiocarbon both as an environmental tracer and as a dating tool. To date, most efforts have focused on reconstructing the evolution of atmospheric radiocarbon activity over time, as the atmosphere is well mixed (though not perfectly well mixed [e.g., Capano et al., 2019; Hogg et al., 2013; Roth & Joos, 2013]), and is the most significant source of radiocarbon to all the other Earth surface carbon reservoirs (in situ production in rocks by cosmic rays, or via radioactive decay in rocks, is an additional, albeit negligible, source). Armed with an atmospheric radiocarbon activity record, we could in principle derive the radiocarbon activities of other Earth surface reservoirs, and their constituent parts, given complete knowledge of all the physical and chemical fluxes that are involved in the global carbon cycle. In theory, this would allow any fossil entity to be accurately “dated” using radiocarbon. Alternatively (and a more likely scenario), if we had knowledge of the evolution of radiocarbon disequilibria over time (i.e., between various carbon reservoirs vs. the atmosphere), we might instead draw inferences regarding the cycling of carbon between these reservoirs and the atmosphere. The latter could clearly be useful for understanding the past evolution of atmospheric CO₂, for example.

Secular changes in atmospheric radiocarbon activity were initially confirmed by de Vries (1958) using radiocarbon dates on tree rings. Further dendrochronological work on particularly long-lived *Pinus longaeva* and *Sequoia gigantea* trees (i.e., comparing the number of calendar years indicated by annual tree ring counts with the number of radiocarbon-years indicated by radiocarbon dates on the same tree rings) provided ultimate confirmation of this (e.g., Willis et al., 1960). Today, the continuous dendrochronological radiocarbon record extends to ~14,000 years BP (Reimer et al., 2013, 2020), and arguably remains the most robust radiocarbon calibration basis over this time interval (Kromer, 2009; Reimer et al., 2004, 2009, 2013; Stuiver et al., 1998). Other approaches to directly reconstructing past atmospheric radiocarbon variability have used radiocarbon analyses on independently dated terrestrial material deposited in lake sediments (e.g., by annual “varve” layer counting; Bronk Ramsey et al., 2012; Goslar et al., 1995; Kitagawa & van der Plicht, 2000). Yet others have employed more indirect means (i.e., using radiocarbon dating of reservoirs that are offset from the atmosphere), including the dating of marine foraminifera (Bard et al., 2004, 2013; Hughen et al., 1998, 2006; Hughen, Eglington, et al., 2004), marine corals (Bard et al., 1990, 1998; Fairbanks et al., 2005) or speleothem (cave) deposits (Cheng et al., 2018; Southon et al., 2012).

In all attempts to reconstruct past atmospheric radiocarbon activity, one principal challenge is obviously the determination of independent calendar ages, typically by layer counting (e.g., using tree rings or annual laminations/varves), uranium-series dating (e.g., in corals or speleothems), or chronostratigraphic alignments (e.g., for marine

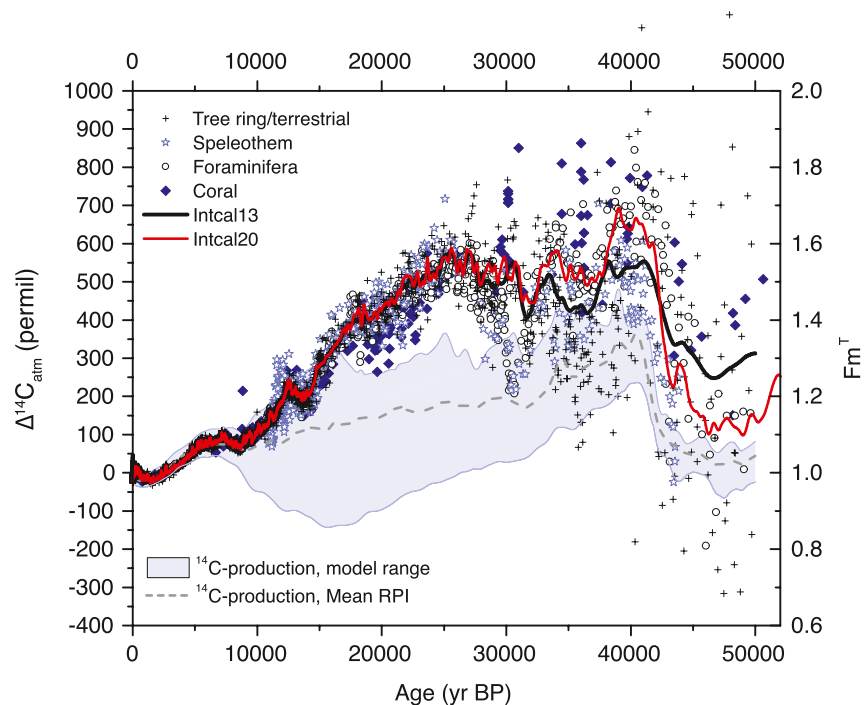


Figure 4. Reconstructions of past atmospheric radiocarbon activity (expressed both as $\Delta^{14}\text{C}$ and Fm^T) used to derive the Intcal13 calibration curve (solid black line; Reimer et al., 2013), based on measurements from a range of archives (symbols), including planktonic marine foraminifera, speleothem carbonate, coral carbonate, tree rings, and terrestrial macrofossils. The updated Intcal20 curve is also shown for comparison (solid red line; Reimer et al., 2020). The shaded area shows the full range of modeled atmospheric radiocarbon activity variability that can be accounted for by radiocarbon production rate estimates alone (i.e., with no additional carbon cycle changes; Dinauer et al., 2020). The dashed gray line shows modeled atmospheric radiocarbon activity based on production rate changes given by averaged estimates of relative paleomagnetic intensity (RPI) (Dinauer et al., 2020).

foraminifera). However, a second, and often more significant challenge, is the reliable inference of *atmospheric* radiocarbon activity on the basis of radiocarbon measurements performed on for example, lacustrine, marine or speleothem material. Essentially, the challenge is to determine (or to guess, as accurately as possible) the degree of equilibration between the radiocarbon-dated carbon reservoir and its contemporary atmosphere. For marine samples, which are typically depleted in radiocarbon relative to the atmosphere due to the slow air-sea equilibration timescale for $^{14}\text{CO}_2$ (Bard, 1988; i.e., with $\alpha_{\text{Ocean-Atm}}^T < 1$), this amounts to knowing the applicable ocean-atmosphere “reservoir ^{14}C -age offset” (Soulet et al., 2016); more commonly known simply as the “*reservoir age*.” For speleothem samples, which will derive a significant portion of their carbon from the soil and/or rocks above a cave, this is equivalent to knowing what is often called the “*dead carbon proportion*” (also called the dead carbon fraction) of the sample (Genty & Massault, 1997).

It is important to underline that, when inferring past atmospheric radiocarbon activity from radiocarbon-dated samples that derived their carbon from a non-atmospheric source (e.g., marine corals, or foraminifera, or speleothems), the only way to do so is by claiming a priori knowledge of the relative isotopic enrichment of radiocarbon in the source reservoir versus the atmosphere (i.e., $\alpha_{R-\text{atm}}^T$) at the time (T) the sample formed. Typically, the approach taken is to assume that the relative isotopic enrichment of the dated reservoir, relative to the atmosphere (i.e., the “reservoir age” of the marine sample, or “proportion dead carbon” of the speleothem) has not changed over time and can therefore be approximated by a modern or pre-industrial estimate. Clearly, such an approach is less than ideal, especially over time intervals that involved significant climatic-, carbon cycle and/or atmospheric CO_2 changes (e.g., Bard, 1988; Skinner, Muschitiello, & Scrivner, 2019).

Figure 4 illustrates a selection of current estimates of past atmospheric radiocarbon activity, based on a range of techniques, compared with an assessment of the history of past atmospheric radiocarbon activity, based on the *IntCal13* and *IntCal20* calibration products (Reimer et al., 2013, 2020). The latter calibration products (the 2013

and 2020 iterations in a series of updates [Reimer et al., 2004, 2009; Stuiver et al., 1998]) represent estimates of the history of past atmospheric radiocarbon activity that have been derived using a Bayesian statistical approach (Niu et al., 2013), applied to selected radiocarbon datasets (Reimer et al., 2013, 2020). Notably, because of the finite mixing time of the atmosphere, combined with differences in air-sea radiocarbon exchange in the northern and southern hemispheres (i.e., strong air-sea $^{14}\text{CO}_2$ fluxes over the large area of the Southern Ocean; Brazunias et al., 1995; Rodgers et al., 2011), the southern hemisphere atmosphere is approximately +50 ^{14}C years offset relative to the northern hemisphere (Capano et al., 2017, 2019; Hogg et al., 2020; Levin et al., 1987). For some applications, this may require the use of an “austral” calibration curve, such as SHCal20 (Hogg et al., 2020). An extension of this is that temporal variations in this interhemispheric atmospheric radiocarbon gradient have the potential to inform on variations in convection and air-sea gas exchange in the high northern- and/or southern latitudes (Capano et al., 2019; Hogg et al., 2016).

The *Intcal* radiocarbon datasets incorporate tree-ring, lacustrine, marine and speleothem radiocarbon data, on independent calendar ages, which have been “corrected” for estimated relative isotopic enrichments to give atmospheric radiocarbon activities, and therefore an atmospheric radiocarbon- versus calendar age “calibration curve.” At the time of writing, the *Intcal13* calibration curve has just been superseded by the *Intcal20* iteration (Reimer et al., 2020). Most recent work in this field will have made use of the *Intcal13* atmospheric curve; where possible in the figures that follow we have re-referenced marine data to the *Intcal20* atmospheric curve. Notably, *Intcal20* differs very little from *Intcal13* back to ~ 27 ka BP (see Figure 4); however, it does represent a less “smoothed” record, and therefore contains a greater amount of very high-frequency (annual to decadal) variability. For the most part, marine records, in particular from the deep ocean interior, are not expected to resolve the highest register of this variability (e.g., Miyake et al., 2013), due to the longer time-scale of marine carbon turnover and the resulting attenuation of atmospheric-driven signal amplitude in the ocean reservoir.

As described above, the calibration of non-atmospheric radiocarbon dates using an atmospheric calibration curve requires knowledge of the relative isotopic enrichment of the dated reservoir versus the atmosphere at the time the sample formed (i.e., a so-called “reservoir age” correction must be made for marine samples). To circumvent this problem, one might consider constructing different *reservoir-specific calibration curves*. This has been attempted for the surface mixed layer of the ocean, for example with the *Marine13* counterpart to *Intcal13* (Reimer et al., 2013), and its predecessors, which were derived in part by forcing an ocean box-model with variable atmospheric radiocarbon boundary conditions (but with constant ocean dynamics and carbon cycling) in order to simulate an “average surface ocean” radiocarbon activity (Hughen et al., 2006). However, this approach can be particularly problematic for a carbon reservoir like the ocean, which (unlike the surface reservoir of a box-model) is not well mixed and therefore has relative isotopic enrichments or “reservoir ages” that are highly variable, both regionally and temporally (e.g., Bard, 1988, 1998; Gottschalk et al., 2020; Peck et al., 2006; Sikes & Guilderson, 2016; Skinner, Muschitiello, & Scrivner, 2019). In light of these issues, the most recent marine calibration product, *Marine20* (Heaton et al., 2020), has been constructed by forcing the BICYCLE carbon-cycle box model (Köhler et al., 2006) in a slightly more sophisticated manner, so as to take account of observed changes in atmospheric $\Delta^{14}\text{C}$ and CO_2 (the latter influences the partitioning of radiocarbon between ocean and atmosphere; Galbraith et al., 2015), as well as parameterized values for ocean overturning and air-sea gas exchange (i.e., piston velocities), including estimates of their uncertainties. Estimates of time varying “climate impacts” (e.g., from temperature, salinity, Southern Ocean convection etc.) were also incorporated, without accounting for their uncertainties (Heaton et al., 2020). In addition to providing useful estimates of the uncertainty in the calculated average surface ocean marine radiocarbon activity (derived from a large number of “Monte-Carlo” simulations using the box-model runs), this approach also makes an initial attempt to incorporate the influence on surface ocean $\Delta^{14}\text{C}$ from changing ocean circulation (and ocean biogeochemistry). This is achieved through a parameterized switch in the strength of North Atlantic convection at ~ 15 ka BP from a hypothetical “glacial mode” to a baseline “modern” mode, as well as further parameterized changes in Southern Ocean convection, global marine carbonate sedimentation, and terrestrial biosphere evolution (Köhler et al., 2006). A strong argument in favor of this approach is that, by not ignoring changes in ocean circulation and biogeochemistry (which must have occurred, even if they remain difficult to quantify), it provides a more accurate estimate of average marine $\Delta^{14}\text{C}$ variability, while also providing a measure of the estimate's precision (i.e., uncertainty). However, it must be said that the improved accuracy of the resulting *Marine20* calibration curve relies entirely on the accuracy of the parameterizations that it employs: parameterizations of ocean convection and mixing in particular. Ultimately the central issue here (setting aside potential errors in the atmospheric record, which serves as a model input) is

a tension between the need to take account of past changes in for example, ocean circulation or sea ice variability when simulating past marine $\Delta^{14}\text{C}$, and the inherent uncertainty in our estimates of these changes. The history of past ocean circulation change (including Southern Ocean convection, North Pacific overturning, North Atlantic deep water formation etc.) is an “unknown,” and it is therefore hard to decide with appropriate confidence how to implement it as a forcing function when attempting to generate an “average mixed layer” calibration curve such as *Marine20* (Heaton et al., 2020).

The use of a reservoir-specific calibration curve may be adapted to take into account spatial heterogeneity in “reservoir age offsets,” if such heterogeneities are assumed to be invariant, or to vary in a predictable manner. As originally described by Stuiver et al. (1986), *under the special circumstance of the ocean circulation and carbon cycle remaining constant, and of ocean radiocarbon activity changes being driven exclusively from the atmosphere* (e.g., due to variable radiocarbon production rates), this may be achieved by applying regional corrections to a global average (reservoir-specific) marine calibration curve, such as *Marine20*. Thus, while the atmosphere would drive the ocean’s mean radiocarbon activity up or down, regional deviations from the mean would remain relatively invariant (again, as long as factors such as ocean circulation, sea ice distributions etc. remained unchanged; Stuiver et al., 1986). These regional deviations from the mean shallow marine radiocarbon activity can be described in terms of deviations from the mean shallow marine “reservoir age” (i.e., its relative isotopic enrichment vs. the atmosphere), or what have been called “ ΔR ” values (Reimer & Reimer, 2001). These principles, and importantly the attendant restrictions also, underpin the application of ΔR values in conjunction with “average marine calibration curves” such as *Marine13* or *Marine20* (Heaton et al., 2020; Reimer et al., 2013; Stuiver et al., 1986). It is therefore important to stress that this approach should not in principle be applied in contexts where the carbon cycle and/or ocean circulation have changed significantly (this is the main reason its application was only initially extended to the last 9,000 years [Stuiver et al., 1986]). As described above, while the *Marine20* calibration curve (Heaton et al., 2020) goes some way toward incorporating the impacts of past Earth System changes, it relies on highly parameterized changes in the ocean circulation in particular, and does not take into account centennial/millennial scale changes in for example, ocean circulation and sea-ice that are known to have occurred throughout the last glacial period and across the last deglaciation, and that remain difficult to quantify (e.g., Henry et al., 2016; McManus et al., 2004; Ng et al., 2018; Sadatzki et al., 2020; Spolaor et al., 2016). The inaccuracy of applying ΔR values to a “mean surface ocean” radiocarbon calibration across/beyond the last deglaciation for example (when significant, yet only loosely constrained, ocean circulation and carbon cycle changes certainly did occur) must therefore be weighed very carefully against inaccuracies or uncertainties involved in alternative approaches, such as the direct estimation of past shallow sub-surface ocean-atmosphere radiocarbon disequilibria/reservoir ages (e.g., Austin et al., 2011; Bard, 1988; Bard et al., 1994; Cao et al., 2007; Peck et al., 2006; Sarnthein et al., 2020; Siani et al., 2001; Sikes & Guilderson, 2016; Sikes et al., 2000; Skinner et al., 2010, 2015; Waelbroeck et al., 2001). Resolving this major and persistent issue for radiocarbon dating of marine sequences represents an important challenge for the future. One approach to addressing this challenge would involve the development of viable *regional* marine radiocarbon calibration curves (Skinner, Muschitiello, & Scrivner, 2019) that are not based on modern estimates of regional deviations from the global mean (i.e., ΔR values), and are based instead on direct estimates of past reservoir age variability, possibly supported by numerical modeling analyses of regional coherence and process-dependence of reservoir age offsets.

While knowledge of past atmospheric radiocarbon activity can provide a basis for radiocarbon dating of marine samples, it can also be used to infer changes in the global radiocarbon cycle. Atmospheric radiocarbon activity will vary as a function of: (a) changes in the rate of radiocarbon production and/or (b) changes in the global carbon cycle. Radiocarbon production rates will in turn depend on the cosmic radiation flux to Earth, which is modulated both by solar activity and by shielding provided by the Earth’s magnetic field (Damon & Linick, 1986; Elsasser et al., 1956; Korff & Mendell, 1980; Kovaltsov et al., 2012; Lal & Peters, 1967; Masarik & Beer, 1999; Stuiver, 1961). If these can be constrained with observations, it should be possible to infer changes in radiocarbon cycling from discrepancies between observed atmospheric radiocarbon activities and modeled atmospheric radiocarbon activities that have been derived from radiocarbon production rate estimates and box-model simulations that specifically assume a constant carbon cycle (Bard, 1998; Bard et al., 1990; Cheng et al., 2018; Hughen, Lehman, et al., 2004; Laj et al., 2002; Mazaud et al., 1991; Muscheler et al., 2000, 2004). The idea is that discrepancies between the “constant carbon-cycle model” and direct observations will reflect the occurrence of carbon cycle changes. Radiocarbon production rate estimates for this approach might be based on ^{10}Be or ^{36}Cl cosmogenic nuclide records (e.g., Beer et al., 1988; Muscheler et al., 2005; Raisbeck et al., 1992), or they might

instead be inferred from geomagnetic field strength reconstructions, derived from measurements of the remanent magnetization of volcanic rocks or marine sediments (Channell et al., 2009, 2018; Guyodo & Valet, 1999; Laj et al., 2004; McElhinny & Senanayake, 1982; Stoner et al., 2002; see Figure 4).

While discrepancies between observed and modeled atmospheric radiocarbon will indicate where the assumption of constant radiocarbon cycling (i.e., constant carbon cycle) is inconsistent with observed changes in atmospheric radiocarbon activity and reconstructed changes in the radiocarbon production rate, the method is subject to uncertainties in *both* the atmospheric radiocarbon observations and the production rate reconstructions. Furthermore, even for very accurate atmospheric radiocarbon activity and production rate reconstructions, this approach does not provide direct information on exactly *what* carbon cycle changes have occurred. Nevertheless, it will indicate *when* such changes may have occurred and how they will have affected the atmospheric radiocarbon activity (thus providing a possible “fingerprint” for the processes involved). As such, this approach provides a means of formulating hypotheses regarding past changes in (radio-) carbon cycling that can be tested using other observations (Bard, 1998; Muscheler et al., 2004). Because of the importance of the global ocean for carbon cycling, especially on the timescales that are relevant to radiocarbon production variability and radiocarbon decay (i.e., centuries to several millennia), reconstructions of the marine radiocarbon inventory, and of mean ocean-atmosphere carbon exchange rates in particular, are especially relevant in this regard. This topic is addressed in the next section.

2.4. Radiocarbon in the Ocean

2.4.1. Controls on Marine Radiocarbon Activity

The marine and atmospheric carbon pools are tightly coupled by virtue of the solubility of CO_2 in seawater. Changes in the magnitude or activity of one of these carbon pools (for example due to exchanges with other carbon reservoirs, such as the terrestrial biosphere or the lithosphere) will therefore inevitably be met by an adjustment in the other. Because an equilibrium in the exchange of carbon between the atmosphere and ocean is achieved via a balance of very large fluxes into and out of the ocean (e.g., summed across the ocean surface and throughout the annual cycle), small changes in these fluxes can also lead to significant adjustments in the carbon and/or radiocarbon inventories of either reservoir. However, because the ocean contains ~ 60 times more carbon than the atmosphere, and ~ 50 times more radiocarbon than the atmosphere, it is the atmospheric radiocarbon activity that will be most sensitive to any imbalances in the fluxes of (radio-) carbon between the ocean and atmosphere.

Radiocarbon enters the ocean from the atmosphere via air-sea CO_2 exchange at the sea surface, which in turn is influenced by temperature and salinity effects on CO_2 solubility, chemical controls on surface ocean $p\text{CO}_2$ (and therefore the ocean-atmosphere $p\text{CO}_2$ offset), and (kinetic) air-sea gas exchange rates (i.e., the piston velocity; influenced by factors such as temperature, wind speed and ice cover). Once radiocarbon has entered the surface ocean, it is re-distributed within the “mixed layer” relatively quickly (the top ~ 100 m or so of the water column is mixed on a timescale of order \sim years), and can then be transported into the ocean interior via advective and diffusive processes, with radiocarbon decaying away over time as this occurs.

Here, it is worth noting that dissolved inorganic carbon (DIC) has four chemical species in seawater: $\text{CO}_{2\text{aqueous}}$ and H_2CO_3 , which together constitute dissolved CO_2 , and contribute to the partial pressure of CO_2 above the seawater, $p\text{CO}_2$ (equivalent to $[\text{CO}_2]/K_0$, where K_0 is the apparent solubility coefficient); bicarbonate ion, HCO_3^- ; and carbonate ion, CO_3^{2-} . The sum of all species is typically referred to as “total CO_2 ” (TCO_2), or DIC. In seawater, dissolved CO_2 is $\sim 0.5\%$, HCO_3^- $\sim 89\%$, and CO_3^{2-} $\sim 11\%$ of DIC, respectively. CO_2 dissolved in the mixed layer is exchanged rapidly with the atmosphere, but it also exchanges via dynamic equilibria with the large pool of ionic carbonate species. As a consequence, the equilibrium time constant for ocean-atmosphere adjustment is shorter for dissolved CO_2 (\sim monthly), longer for DIC (\sim annual), and even longer for carbon isotope ratios (\sim decadal; Broecker & Peng, 1974; Galbraith et al., 2015; D. C. Jones et al., 2014). For these reasons, the ^{14}C -distribution in the mixed layer is buffered against rapid changes, on seasonal to interannual timescales. These chemical and isotopic processes, together with intense mixing in the mixed layer, collectively smooth out complexities linked to the local and high frequency variability of the mixed layer depth (de Boyer Montégut et al., 2004), and of the depth of phytoplankton growth, which tends to be shallow and highly seasonal at high latitudes, but often deeper (>50 m) in most of the ocean (Cornec et al., 2021; Sauzède et al., 2015). Notwithstanding relatively minor local anomalies in the air-sea $p\text{CO}_2$ gradient ($\Delta p\text{CO}_2$) associated with biological drawdown, the primary

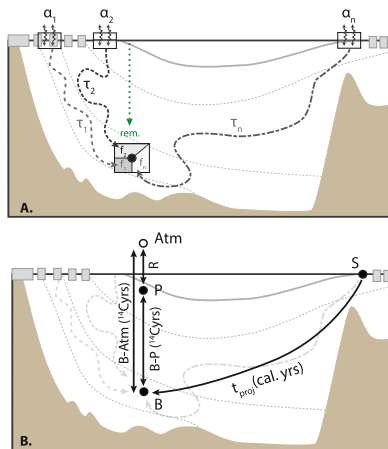


Figure 5. (a) Illustration of the contributions to the radiocarbon activity of a parcel of seawater, including: air-sea gas exchange effects, resulting in air-sea disequilibrium, at a large number of contributing surface ocean source regions (e.g., a_1, a_2, \dots, a_n); transit time effects, resulting in radiocarbon decay during transport from each contributing surface ocean source region to a given location in the ocean interior (e.g., $\tau_1, \tau_2, \dots, \tau_n$); and mixing effects, due to the fractional contribution (e.g., f_1, f_2, \dots, f_n) of each surface source region and its associated air-sea gas exchange and transit time impacts. A minor addition of “young” carbon to the dissolved inorganic carbon pool from remineralized organic carbon and biogenic carbonate is indicated by the dotted green arrow. Note that imperfect gas-exchange efficiency in deep-water source regions (leading to a significant “preformed age”) can lead to a distinction between a water parcel’s last point of contact at the surface and the location at which it last equilibrated with the atmosphere. (b) Illustration of three “metrics” used for marine radiocarbon activity in paleoceanography: (1) the benthic-planktonic radiocarbon age offset (B-P, measured in radiocarbon years); (2) the benthic-atmospheric radiocarbon age offset (B-Atm, measured in radiocarbon years); the planktonic-atmospheric radiocarbon age offset (R, or the “reservoir age offset,” measured in radiocarbon years), which represents the difference between B-Atm and B-P; and (3) the “projection age” (t_{proj} , measured in calendar years), which represents a hypothetical transit time from a single putative surface water source region (S) to the location in the ocean interior. In principle, all of these metrics can be expressed as “age intervals” or as relative isotopic enrichments in fractional, percentage or “permil” notation.

control on $\Delta p\text{CO}_2$ is not local photosynthesis, but the cumulative impacts of physical parameters such as wind stress and temperature, and of large-scale ocean dynamics. For example, large parts of the oceans that are biologically productive, such as latitudes $<20^\circ$, high latitudes of the Southern Ocean and North Pacific, or the upwelling zones of the Northern Indian Ocean, are even characterized by supersaturation on average, with net carbon flux out of the ocean (Landschützer et al., 2020; Takahashi et al., 2009; Wanninkhof et al., 2013).

An additional contribution to the radiocarbon pool of the ocean interior derives from the vertical flux of particulate organic matter and carbonate, raining down into the ocean interior. This carbon, which represents $\sim 6\%$ of the total DIC pool (Williams & Follows, 2011), is typically exported from the mixed layer within days (Lande & Wood, 1987), and converted to DIC through respiration/dissolution within days to decades (Walker et al., 2016). Export productivity therefore provides a “trickle” of young carbon to the ocean interior. Other sources of carbon to the ocean interior include the flux of remineralized dissolved organic carbon (DOC, which tends to be on the order to thousands of years old relative to the contemporary atmosphere [Walker et al., 2016; Williams & Druffel, 1987]); and volcanic/hydrothermal CO_2 (Jenkins et al., 2018). However, in both cases the magnitude of these “old carbon” sources is very small as compared to the total DIC pool (Jenkins et al., 2018; Key et al., 2004), and tends to counteract the small contribution from newly respired particulate organic matter.

As illustrated in Figure 5, the radiocarbon activity of a parcel of water in the ocean interior will therefore overwhelmingly reflect a combination of three components:

1. An “air-sea exchange rate component,” due to ocean-atmosphere gas exchange and the associated isotopic fractionation that determines the “preformed” radiocarbon activity of water in the mixed layer before it is transported into the ocean interior;
2. A “transport time component,” due to radiocarbon decay along the transport trajectory that brought water from the mixed layer to its current position in the ocean interior; and
3. A “mixing component,” due to the fractional contribution to the carbon mass in any given parcel of water in the ocean interior, from a range of different mixed layer origins, each associated with different transport trajectories and transit times. (For radiocarbon, it should be further noted that mixing two volumes of water with different radiocarbon activities, and possibly carbon concentrations, averages the isotopic mass-concentrations of the water parcels, rather than the isotopic ratios or radiocarbon “ages” of the water parcels.)

The first two of these influences account for the fact that a water “parcel” (a small but finite volume of water) may have last equilibrated with the atmosphere at a different location from its last point of contact with the atmosphere (Koeve et al., 2015; Matsumoto, 2007; see Figure 5a). Given estimates of the radiocarbon activity of a parcel of water in the ocean interior (or better still, a large spatial array of such measurements), the ultimate goal might be to decompose these measurements into the three components indicated above. However, this presents a significant challenge, to say the least—a challenge that has yet to met using paleoceanographic observations, for example, through a combination of data and (inverse) numerical modeling techniques. Even without precisely decomposing marine radiocarbon activities into their constituent “preformed,” “transport” and “mixing” components (which is rarely possible), informative measures of isotopic disequilibria and/or decay times can still be derived. Typically, this is done by comparing the measured or inferred radiocarbon activity at a location in the

ocean interior with the radiocarbon activity of the contemporary atmosphere or of other locations in the contemporary (or even pre-existing) ocean. The most common comparisons that are made in this way are illustrated in Figure 5. These consist of different ways of expressing the relative isotopic enrichment of ^{14}C as compared to ^{12}C in: (a) the surface ocean/planktonic habitat versus the contemporary atmosphere (i.e., near-surface “reservoir age” offsets); (b) the deep ocean/benthic habitat versus the contemporary atmosphere (i.e., B-Atm age offsets); (c) the deep ocean/benthic habitat versus a contemporary shallow ocean/planktonic habitat at the same location (i.e., B-P offsets); or (d) the deep ocean/benthic habitat versus its presumed mixed layer source region at some time in the past (i.e., “projection ages”).

It is important to note that it is mostly a matter of choice whether to express these different comparisons in terms of an *isotopic enrichment or ratio*, a *decay time interval* (in radiocarbon- or calendar years), or a *relative offset* (e.g., in permil notation). Here we follow the framework devised by Guillaume Soulet (summarized in brief by Soulet et al., 2016), whereby the first of these modes of expression can be defined as the ratio of the radiocarbon activity of one reservoir versus another, or the “*relative isotopic enrichment*,” defined here as:

$$\alpha_{R2-R1}^T = \frac{\text{Fm}_{R2}^T}{\text{Fm}_{R1}^T} = \frac{\text{Fm}_{R2}^0 \cdot \exp\left(\frac{T}{8267}\right)}{\text{Fm}_{R1}^0 \cdot \exp\left(\frac{T}{8267}\right)} = \frac{\text{Fm}_{R2}^0}{\text{Fm}_{R1}^0} \quad (1)$$

Above, Fm_{R1}^0 refers to the fraction modern radiocarbon that Reservoir 1 had at time T , but reported (adjusted) for the “present.” Note that 8267 in the above equation represents the “true” mean lifetime of radiocarbon, based on the “true” Cambridge half-life of 5730 (such that $5730/\ln(2) = 8267$). The relative isotopic enrichment factor α_{R2-R1}^T can also be expressed as an inter-reservoir *radiocarbon age offset* (i.e., in ^{14}C years):

$$R_{R2-R1} = -8033 \times \ln(\alpha_{R2-R1}^T) \quad (2)$$

which is equivalent to the difference between the corresponding radiocarbon ages of each reservoir (e.g., Bard, 1988):

$$R_{R2-R1} = t^{14}\text{C}_{R2} - t^{14}\text{C}_{R1} \quad (3)$$

In the above equation, $t^{14}\text{C}$ represents the radiocarbon age of a given reservoir, which is simply given by the conventional radiocarbon age of the sample that we are taking as representative of that reservoir:

$$t^{14}\text{C}_{\text{sample}} = t^{14}\text{C}_{R1} = -8033 \times \ln(\text{Fm}_{\text{sample}}^0) \quad (4)$$

Note that here the Libby half-life (5568 years), and therefore the Libby mean radiocarbon lifetime ($5568/\ln(2) = 8033$) are used by convention. When converted to an age offset, the relative isotopic enrichment, α_{R2-R1}^T , of one reservoir versus another contemporaneous reservoir therefore encompasses paleoceanographic radiocarbon metrics such as benthic-planktonic foraminifer radiocarbon age offsets (B-P; Broecker, Andree, Bonani, Wolfli, Oeschger, et al., 1988), deep-water versus atmosphere radiocarbon age offsets (B-Atm, or “radiocarbon ventilation ages”; e.g., Skinner et al., 2010), and shallow sub-surface ocean versus atmosphere “reservoir ages” (e.g., Bard, 1988).

Finally, the relative isotopic enrichment of one reservoir versus another (at a given point in time, T) can also be expressed as a *relative offset* between two fraction modern carbon values:

$$\delta^{14}R_{R2-R1}^T = \frac{\text{Fm}_{R2}^T - \text{Fm}_{R1}^T}{\text{Fm}_{R1}^T} = \alpha_{R2-R1}^T - 1 \quad (5)$$

This in turn can be expressed in *permil* notation by multiplying by a factor of 1,000:

$$\delta^{14}R_{R2-R1}^T (\text{‰}) = (\alpha_{R2-R1}^T - 1) \times 1000 \quad (6)$$

The above is essentially equivalent to the $\Delta^{14}\text{C}_{0,\text{adj}}(\text{‰})$ metric defined by Cook and Keigwin (2015). It is also worth noting that the commonly encountered $\Delta^{14}\text{C}(\text{‰})$ (e.g., as defined by Stuiver and Polach (1977), taking into account applicable $\delta^{13}\text{C}$ -normalization), can be seen as a special case of $\delta^{14}R_{R2-R1}^T(\text{‰})$, where R_2 is the reservoir

of interest (e.g., the atmosphere, for $\Delta^{14}\text{C}_{\text{atm}}(\text{‰})$) and R_1 is the fraction modern carbon of the modern reference, which is 1 by definition. Therefore:

$$\Delta^{14}\text{C}_{R2}(\text{‰}) = (\text{Fm}_{R2}^T - 1) \times 1000 \quad (7)$$

Note again that Fm_{R2}^T represents the measured fraction modern (Fm_{R2}^0) that has been corrected to its value at time T in the past.

Many paleoceanographic studies have sought to compare the radiocarbon activity of contemporaneous reservoirs by differencing their $\Delta^{14}\text{C}(\text{‰})$ values, for example:

$$\Delta\Delta^{14}\text{C}_{R2-\text{atm}}(\text{‰}) = \Delta^{14}\text{C}_{R2}(\text{‰}) - \Delta^{14}\text{C}_{\text{atm}}(\text{‰}) \quad (8)$$

However, as noted elsewhere (Burke et al., 2015; Cook & Keigwin, 2015; Soulet et al., 2016), this metric scales with the absolute values that are being differenced, and therefore the time-varying $\Delta^{14}\text{C}_{\text{atm}}(\text{‰})$, which means that a given value for $\Delta\Delta^{14}\text{C}_{R2-\text{atm}}(\text{‰})$ will represent *different* degrees of isotopic disequilibrium between two reservoirs depending on their absolute radiocarbon activities. The value of $\Delta\Delta^{14}\text{C}_{R2-\text{atm}}(\text{‰})$ can therefore change without any real change in relative isotopic enrichment between “reservoir 2” and the atmosphere. For this reason, the use of $\Delta\Delta^{14}\text{C}_{R2-\text{atm}}(\text{‰})$ offsets, without adjusting for changes in absolute radiocarbon activity (Cook & Keigwin, 2015), should probably be discouraged. It is preferable to use the “relative isotopic enrichment” ratio, or radiocarbon age offsets, especially in the context of varying absolute radiocarbon activity (Cook & Keigwin, 2015; Soulet et al., 2016).

To summarize: all of the formalism above is intended to underline the fact that there is a degree of equivalence between the various ways of representing radiocarbon enrichment in one reservoir versus another. Therefore, a $\Delta^{14}\text{C}_{0,\text{adj}}$ value does not “mean” something different from a “B-Atm” age-offset (and neither can it be said to be more accurate in any way). Rather, the central problem is always to understand, or to interpret, how either metric reflects the combined influences of air-sea exchange, transport, and/or mixing in the marine environment (Cook & Keigwin, 2015).

2.4.2. Radiocarbon “Ventilation” Metrics

In seeking to interpret a given measure of marine radiocarbon disequilibrium in terms of the three main components of marine radiocarbon disequilibrium noted above (i.e., the “air-sea exchange,” “transport time” and/or “mixing” components), it is important to emphasize the distinction between metrics of isotopic disequilibrium and the diverse physical processes that affect them. Thus, for example, mass transport rates in the ocean will affect the deep ocean’s radiocarbon age offset from the contemporary atmosphere (e.g., B-Atm in Figure 5), but the latter does not directly and exclusively provide a measure of ocean transport times or rates (Marchal & Zhao, 2021). Despite this major limitation, all of the isotopic disequilibrium metrics noted above (and illustrated in Figure 5) relate in some way to physical processes that transfer radiocarbon from the atmosphere (where radiocarbon is produced) to the surface ocean, and in turn that transport radiocarbon (in solution) from the surface ocean into the ocean interior and back again. As such, these metrics are often referred to as measures of ocean “ventilation.”

A discussion of the term “ventilation” is warranted. “Ventilation” is defined here as *the collective effect of the physical and chemical processes that convey atmospheric properties into the ocean interior*. The term “radiocarbon ventilation” therefore refers more specifically to the net effect of the processes that act to convey (“young”) atmospheric radiocarbon to the ocean interior. Other definitions of ventilation exist, and the paleoceanographic literature contains a plethora of different (often conflicting, and sometimes imprecise or only implicit) definitions of the term “ventilation” (e.g., applied to stable carbon isotopes, Nd isotopes etc.). Furthermore, the terms “ventilation” and “ventilation age” are generally used to refer to *water transit times* in studies of physical oceanography (England, 1995). This can lead to confusion regarding the intended goal of paleoceanographic radiocarbon studies as reconstructions of *water* renewal rates, versus *carbon* renewal rates (Marchal & Zhao, 2021). In this context, defining ventilation (which has a Latin linguistic root pertaining to the movement of air) in terms of the conveyance of *atmospheric* properties into the ocean interior will depart from common practice in physical oceanography, but is nevertheless an obvious choice for radiocarbon, which is produced in the atmosphere. However, to avoid confusion, when discussing the collective effects of air-sea gas exchange and transport/mixing on marine radiocarbon, it is recommended to refer exclusively to “relative isotopic enrichment” or “radiocarbon age

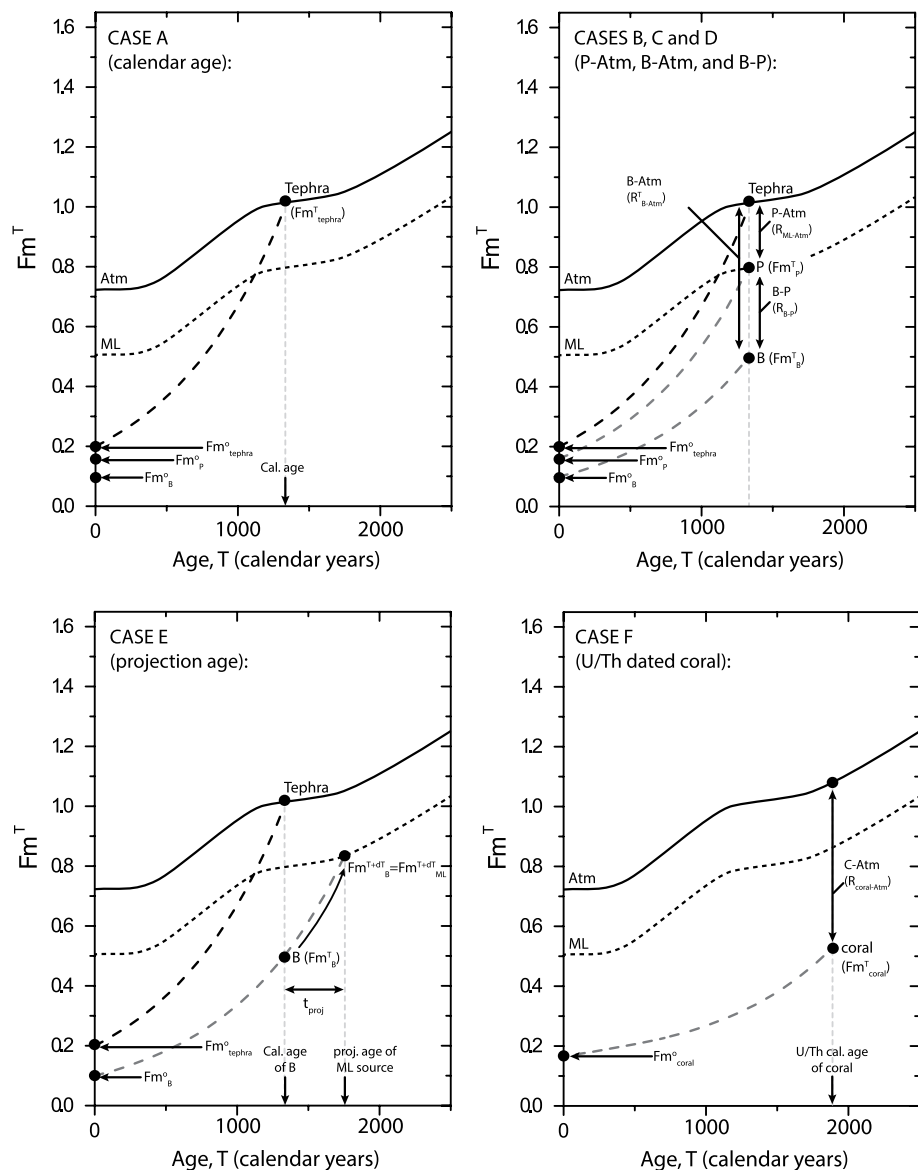


Figure 6. Four scenarios illustrating the reconstruction of a variety of radiocarbon metrics, as discussed in the text. In each plot, fraction modern radiocarbon activity (Fm^T) is plotted against calendar age, the solid black line represents the evolving atmospheric (Fm^T_{Atm}) radiocarbon activity, the dashed black line represents the evolving shallow marine mixed layer (Fm^T_{ML}) radiocarbon activity, and the long-dashed gray and black curves represent decay trajectories for various fossil entities. Note that R^T_{R1-R2} values represent radiocarbon age offsets, which are derived from Fm values by: $R^T_{R1-R2} (^{14}C_{yrs}) = -8033 \times \ln(\alpha^T_{R1-R2})$, where $\alpha^T_{R1-R2} = Fm^T_{R1} / Fm^T_{R2}$ (see text).

offsets,” or at least to specify “radiocarbon ventilation (ages).” Accordingly, “ideal age” (or transit time) might be reserved for the timescale associated with water renewal rates and mass transport (Hall & Haine, 2002). Thus, by clearly incorporating air-sea gas exchange effects into the definition of “radiocarbon ventilation,” one might obviate any confusion as to whether or not radiocarbon ventilation ages, such as B-Atm offsets (Figure 5), reflect transit times: they simply do not, even if there might be ways of using radiocarbon to constrain such transit times or ideal ages (DeVries & Primeau, 2010).

In order to demonstrate how different radiocarbon ventilation metrics can be derived in practice, Figure 6 illustrates an example scenario of paired radiocarbon dates on benthic (bottom dwelling) and planktonic (mixed layer dwelling) foraminifera, that have been co-deposited with a volcanic tephra that provides a time-marker for an eruption that has been previously radiocarbon dated on land using plant macrofossils (i.e., we have an estimate

of the atmospheric radiocarbon activity at the time of the volcanic eruption). We might further assume in this example that the history of atmospheric radiocarbon activity is also known (e.g., from radiocarbon dates on independently calendar-dated tree rings and/or speleothems, as described in Section 2.3). The information contained in this example scenario can be described in the following manner:

1. *Calibration of the tephra age to obtain a calendar age for the co-deposited foraminifera* (Case A in Figure 6): this consists of determining the calendar age for which the decay trajectory for the (terrestrial) tephra's measured fraction modern (Fm_{tephra}^0) intersects the history of atmospheric radiocarbon activity.

$$Fm_{\text{atm}}^T = Fm_{\text{tephra}}^0 \exp^{\lambda_C T} \quad (9)$$

where:

$$T = \frac{1}{\lambda_C} \ln \left(\frac{Fm_{\text{atm}}^T}{Fm_{\text{tephra}}^0} \right) \quad (10)$$

Note that here the “true” Cambridge half-life ($\lambda_C = \ln(2)/\lambda_C = 5730$ years), or equivalently the “true” mean life ($1/\lambda_C = 5730/\ln(2) = 8267$), should be used so as to obtain the calendar age of the volcanic tephra.

2. *The planktonic radiocarbon activity in relation to the atmosphere* (Case B in Figure 6): The fraction modern of the planktonic foraminifer at the time it was living will reflect the radiocarbon activity of the shallow sub-surface ocean where the planktonic foraminifer lived (i.e., the fraction modern of the mixed layer, Fm_{ML}^T). We can obtain this by correcting the measured fraction modern of the planktonic foraminifer sample (Fm_p^0) for the decay time experienced by the sample (i.e., for the calendar age of the co-deposited tephra, T), using the following equation:

$$Fm_{\text{ML}}^T = Fm_p^T = Fm_p^0 \exp^{\lambda_C T} \quad (11)$$

Note that the measured fraction modern of the foraminifer sample (Fm_p^0) is related to its conventional radiocarbon age ($t^{14}C_p$), using the conventional (Libby) mean radiocarbon lifetime of 8033 years, such that:

$$t^{14}C_p = -8033 \times \ln(Fm_p^0) \quad (12)$$

With this information, we can compare the fraction modern of the mixed layer/shallow sub-surface ocean with that of the contemporary atmosphere, via the “relative isotopic enrichment” ratio (Soulet et al., 2016), defined here as:

$$\alpha_{\text{ML-atm}}^T = \frac{Fm_{\text{ML}}^T}{Fm_{\text{atm}}^T} \quad (13)$$

This metric can be expressed as an isotopic ratio as above, or else as a relative deviation (e.g., in permil notation, $\delta^{14}R_{\text{ML-atm}}^T$ (‰)) or a radiocarbon age offset ($R_{\text{ML-atm}}^T$):

$$\delta^{14}R_{\text{ML-atm}}^T$$
 (‰) = $(\alpha_{\text{ML-atm}}^T - 1) \times 1000$ (14)

and

$$R_{\text{ML-atm}}(^{14}\text{C}_{\text{yrs}}) = -8033 \times \ln(\alpha_{\text{ML-atm}}^T) \quad (15)$$

The latter is simply equivalent to the difference between the conventional radiocarbon age of the planktonic foraminifer and that of the atmosphere at the time the foraminifer lived (T), and is typically referred to as a “reservoir age”:

$$R_{\text{ML-atm}}(^{14}\text{C}_{\text{yrs}}) = t^{14}C_p - t^{14}C_{\text{atm}} \quad (16)$$

The above definition of a “reservoir age” is equivalent to that introduced by Bard (1988), as the age offset between planktonic foraminifera and terrestrial organic matter that are stratigraphically linked by an isochronous

volcanic ash layer. It is worth noting that this simple difference of two radiocarbon ages of contemporaneous samples (as for the ratio of their radiocarbon activities, $\alpha_{\text{ML-atm}}^T$) is independent of the atmospheric and marine radiocarbon calibration curves; it depends only on the two samples having been formed contemporaneously.

3. *The benthic radiocarbon activity in relation to the atmosphere* (Case C in Figure 6): The fraction modern of the benthic foraminifer at the time it was living (Fm_b^T) will (ideally) reflect that of bottom water (Fm_{BW}^T) at the location in the deep ocean where the foraminifer lived, and can be obtained in the same way as described above for the planktonic foraminifer by correcting for its calendar age (T), given here by calibrating the atmospheric radiocarbon age of the co-deposited tephra. This in turn can be compared with the activity of the contemporary atmosphere to derive an estimate of the relative isotopic enrichment of the deep ocean versus the atmosphere, which can be expressed as an isotopic ratio ($\alpha_{\text{BW-atm}}^T$), a relative deviation for example, in permil notation ($\delta^{14}R_{\text{BW-atm}}^T$ (‰)) or a radiocarbon age offset ($R_{\text{BW-atm}}(^{14}\text{C}_{\text{yrs}})$, often referred to as B-Atm), as described above for the planktonic foraminifer radiocarbon activity.
4. *The benthic foraminifer's radiocarbon activity in relation to its planktonic counterpart* (Case D in Figure 6): In addition to comparing the radiocarbon activities of the benthic and planktonic foraminifer habitats (i.e., the deep ocean and the shallow sub-surface ocean) to that of the contemporary atmosphere, we might also compare these directly to each other, providing an estimate of the radiocarbon activity gradient that existed between the shallow sub-surface and the deep ocean at the time (and at the location) that the foraminifera lived. This comparison is simplified by the fact that we do not need to know the calendar age of the foraminifer samples; we only need to know that the benthic and planktonic foraminifera have the same calendar age. Once again, the comparison can be expressed as an isotopic ratio, a relative deviation (e.g., in permil notation) or as a radiocarbon age offset. The latter would simply be the difference between the conventional radiocarbon ages of the benthic and planktonic foraminifera ($t^{14}C_p - t^{14}C_b$, often referred to as B-P).
5. *The benthic radiocarbon activity in relation to its presumed mixed layer source regions* (Case E in Figure 6): A further comparison can be made between the radiocarbon activity of the bottom water (derived from the benthic foraminifer's fraction modern/conventional radiocarbon age) and the activity of its presumed mixed layer source region(s). Thus, if we assume that the deep water the benthic foraminifer lived in originally came from a *single* region of the ocean's surface mixed layer (ML) and that we know the relative isotopic enrichment of this mixed layer source region versus the atmosphere (e.g., $R_{\text{ML-atm}}^T \sim 500$ ^{14}C -years, or $\alpha_{\text{ML-atm}}^T = 0.94$ etc.), then we can estimate the number of calendar years that have elapsed since the water left that mixed layer source region. This time interval would represent a hypothetical estimate for the “transit time” of water moving from the mixed layer to the location of the benthic foraminifer on the sea floor, and would be given as the difference between the calendar age of the benthic foraminifer and the calendar age of a reservoir that would have the same measured fraction modern as the benthic foraminifer (if measured today), but that had an *initial* fraction modern that was the equivalent of 500 ^{14}C -years offset from the atmosphere. This is typically referred to as a “projection age” in the literature (Adkins & Boyle, 1997), and as will be apparent from the assumptions involved in its application (i.e., of a single deep water source region, and of known initial relative isotopic enrichment of the source waters), which are not likely to be realistic in most cases, this metric should be applied with caution (DeVries & Primeau, 2010). Note that the approach of adjusting a projection age interval (i.e., in calendar years), by a presumed source water “reservoir age” (i.e., in radiocarbon years) is incorrect (Lund, Adkins, & Ferrari, 2011; Lund, Mix, & Southon, 2011); rather the projection age should be determined by projecting to a presumed source water Fm^{T+dT} (Skinner & Shackleton, 2004), as illustrated in Figure 6 (Case E).

In the hypothetical example above, a tephra “time marker” horizon was used as a way of linking marine radiocarbon activities obtained from paired benthic and planktonic foraminifera, to a contemporary atmospheric radiocarbon activity obtained from terrestrial sites (e.g., Bard et al., 1994; Siani et al., 2001, 2013; Sikes et al., 2000; Sikes, Cook, & Guilderson, 2016; Skinner et al., 2015). Any other chronostratigraphic approach could also be used (e.g., alignment of the marine sequence to an independently dated ice-core archive; Marchitto et al., 2007; Peck et al., 2006; Skinner et al., 2010, 2014; Thornalley et al., 2011). As an alternative one might also consider a scenario where for example, a coral sample has been both radiocarbon- and uranium-series dated (e.g., Adkins et al., 1998; Bard et al., 1998; Burke & Robinson, 2012; Chen et al., 2015; Goldstein et al., 2001; Hines et al., 2015; Mangini et al., 1998; Robinson et al., 2005). The U-series age would thus provide a calendar age for

the coral radiocarbon date, and thus permit a comparison of the coral's initial fraction modern radiocarbon at the time it formed with that of the contemporary atmosphere (Case F in Figure 6).

The unique paleoceanographic significance of each these metrics should be clear from their respective definitions and derivations; however, it is important to emphasize that *all of them simply reflect measures of isotopic disequilibrium between two different carbon reservoirs* (estimated via measurements on samples that formed in those different reservoirs). Their relative merits relate primarily to their ease of derivation in different contexts, as well as the different potential biases and uncertainties that each is subject to. Thus, for example, the calendar age of a sample estimated through stratigraphic correlation or with a U-series age, must first be used to obtain an atmospheric ^{14}C age before calculating the difference with the contemporaneous marine ^{14}C age. This implies that the ^{14}C reservoir age, estimated this way, depends on the atmospheric ^{14}C calibration curve (unlike for co-deposited and coeval tephra or terrestrial material, as described above). There are two implications of this: first, the uncertainty in the “de-calibration” step also needs to be taken into account in the overall error propagation (Soulet, 2015); and second, direct comparisons can only be made between reservoir age offsets that have been calculated in this way using the same atmospheric reference curve (e.g., successive Intcal updates).

In summary, marine radiocarbon serves as a carbon cycle tracer that is influenced by radiocarbon production rates, air-sea gas exchange, mass transports, and the time varying interaction of these processes. It does not provide a straightforward “transport time clock.” However, marine radiocarbon can in principle be used to study past ocean dynamical processes, via a three-step process: (a) by using marine radiocarbon measurements to derive a clearly defined metric of isotope disequilibrium, for example, of a parcel of water in the ocean relative to the atmosphere; (b) by interpreting the extent to which the inferred isotopic disequilibrium reflects each of the various radiocarbon ventilation processes that act to transfer atmospheric radiocarbon into the ocean interior (which may be categorized according to air-sea gas exchange-, transport time-, or mixing components—as well as their interaction with variable radiocarbon production); and (c) to isolate and interpret those radiocarbon “ventilation” processes that derive from ocean transport and mixing processes only. This three-step process, targeting information on ocean dynamics, presents a significant challenge. Future progress in the application of radiocarbon as a paleoceanographic dynamical tracer is likely to be met through the combination of radiocarbon measurements with other proxy measurements that are able to constrain a sub-set of those physical processes (e.g., water sourcing from Nd, relative transport rates from sediment grain sizes or Pa/Th, respiration from nutrient concentrations, stable carbon isotopes, or apparent oxygen utilization, etc.), in particular if deployed in combination with appropriate statistical techniques and numerical models (DeVries & Primeau, 2010).

3. Radiocarbon in Numerical Models

3.1. Process Comprehensiveness in Models

The percolation of radiocarbon from its atmospheric source throughout the carbon pools of the Earth's surface environment is convoluted by the three-dimensional circulation of the ocean and the passage of carbon through living organic matter and biogenic carbonate. When secular changes in production rate, and changes in ocean circulation are also considered, the resulting four-dimensional problem can become extremely complex. Models are therefore indispensable tools for quantitatively considering the suite of processes that influence the distribution of radiocarbon within the environment. Essentially, all such models calculate the input, output and internal decay of radiocarbon (either implicitly or explicitly) in discrete reservoirs, accounting for air-sea exchange and ocean circulation (some also include exchange with the biosphere). Because the ocean dominates the carbon pool (it contains approximately 95% of the ocean-atmosphere-biosphere carbon), it also dominates the radiocarbon pool, so that radiocarbon modeling is primarily concerned with the air-sea transfer of radiocarbon and its spatial distribution within the ocean.

The simplest models of radiocarbon consider a ^{14}C concentration per unit volume, in the atmosphere or in the ocean, as a tracer that decays according to the Cambridge half-life, and which in the surface ocean layer relaxes toward the atmospheric radiocarbon activity with a prescribed timescale. Often, the concentration of the ^{14}C tracer is scaled to convenient values, such as “100” for a pre-industrial atmosphere (e.g., Siegenthaler et al., 1980; Toggweiler et al., 1989). These simplified implementations are sufficient to provide a first-order estimate of the global air-sea-biosphere radiocarbon budget, and the effect of ocean circulation on radiocarbon distributions. For example, if the global atmospheric production of radiocarbon is Q , the decay rate is λ , the radiocarbon activity of

a reservoir per unit volume is R , the concentration of carbon in that reservoir is C , and the volume of the reservoir is V , then at steady state:

$$Q = \lambda \sum_{i=1}^n V_i C_i R_i \quad (17)$$

That is, at steady state, the production of radiocarbon is balanced by the decay of radiocarbon in all reservoirs. Because λ is constant, there is a unique sum of radiocarbon that can be present in all reservoirs for a given production rate, equal to Q/λ . If we simplify the system to just two reservoirs, atmosphere (a) and ocean (o),

$$\frac{Q}{\lambda} = V_a C_a R_a + V_o \overline{C_o R_o} \quad (18)$$

Since V_a and V_o are essentially fixed (V_o changed by $\sim 3\%$ over the last ~ 1 million years), this very simple model predicts a strong compensatory relationship between the radiocarbon inventories of the ocean and atmosphere, at steady state, for a given Q . Although the Earth system, and the ocean, are unlikely to ever be exactly at steady state, variations in radiocarbon production will rapidly be accommodated by changes in the radiocarbon content of the atmospheric reservoir, allowing the global radiocarbon inventory to come to equilibrium relatively quickly. The new radiocarbon inventory would then be redistributed to other carbon reservoirs, including the ocean, on their respective time-scales of equilibration (thus effectively rebalancing the terms on the right hand side of Equation 18). On the other hand, since the marine carbon inventory is much larger than that of the atmosphere ($C_o V_o \gg C_a V_a$), small changes in R_o will require large, opposite changes in R_a at steady state (Siegenthaler et al., 1980). These elementary principles illustrate the power of reservoir-based mass-balance calculations for understanding the global radiocarbon cycle. The approach can be scaled up to include hundreds of thousands of reservoirs, in the form of grid cells within a “general circulation model” (GCM), allowing the effect of ocean circulation to be estimated. Variants of this simple approach were introduced by Oeschger et al. (1975), Toggweiler et al. (1989), and Stocker and Wright (1996), and it has continued to be employed in many other simulations (e.g., Butzin et al., 2017; Meissner et al., 2003). The main advantages of the simple approach are that it is easy to implement and interpret, and requires only a single ocean tracer. However, this approach can often ignore the fact that air-sea exchange and associated isotopic fractionation is influenced by carbonate chemistry, biology (carbon uptake and remineralization) and physics (e.g., temperature, salinity, sea ice and wind-speed).

A second domain of comprehensiveness resolves the nuances of ocean carbon chemistry, for example, as exemplified by the protocol for the Ocean Carbon Modeling Intercomparison Project 2 (OCMIP2), often referred to as “abiotic” ^{14}C (Orr et al., 2000). The OCMIP2 approach requires including two tracers in the ocean model, DIC and DI^{14}C , where DIC is the sum of all dissolved inorganic carbon (dominated by ^{12}C and ^{13}C) and DI^{14}C is the concentration of dissolved inorganic ^{14}C . Typically, the numerical values of DI^{14}C are scaled by the natural abundance of $^{12}\text{C}/^{14}\text{C}$ in the model, so that they differ from the numerical values of DI^{12}C by less than 40%, rather than 12 orders of magnitude. This convention minimizes the impact of numerical round-off errors on the resulting isotopic ratios, and provides an approximation of $\Delta^{14}\text{C} = (\text{DI}^{14}\text{C}/\text{DIC} - 1) \times 1,000$ (in *permil* notation).

A defining feature of this approach is the representation of air-sea exchange as dependent on the dissolved CO_2 concentration. This results in a non-linear “buffering effect” of CO_2 dissolving in seawater, for example, with incrementally smaller adjustments in DIC occurring as air-sea exchange progresses (e.g., see Williams & Follows, 2011; Zeebe & Wolf-Gladrow, 2001). Carbon dioxide is an unusual gas in that it reacts with water predominantly to form two carbonate species (HCO_3^- and CO_3^{2-}), which greatly slows its equilibration relative to non-dissociative gases like O_2 , or inert gases like Xe. In general, as reviewed in depth by Sarmiento and Gruber (2006), models that consider carbon speciation calculate the air-sea flux of carbon (ϕ_{DIC}) at the ocean surface as something like:

$$\phi_{\text{DIC}} = k_w (\text{CO}_{2\text{sat}} - \text{CO}_{2\text{ocean}}) \quad (19)$$

In the above equation, k_w is the wind-speed dependent “piston velocity” that determines the rapidity of gas exchange, $\text{CO}_{2\text{sat}}$ is the concentration of CO_2 in the water at saturation or equivalently the atmospheric partial pressure of CO_2 , and $\text{CO}_{2\text{ocean}}$ is the actual concentration of CO_2 in the seawater, as defined by the DIC concentration, the alkalinity (usually provided by a third, interactive tracer), the salinity and the temperature of the seawater. The concentration of $\text{CO}_{2\text{ocean}}$ is determined at every time step of the model by a carbon system solver for

carbon speciation, such as $\text{CO}_{2\text{calc}}$ or CSYS (Zeebe & Wolf-Gladrow, 2001). Thus, the air-sea exchange includes the physical impacts of wind-speed, temperature and salinity, and the chemical impacts of carbon speciation. Biological impacts can also be included by accounting for particulate transport of radiocarbon and fractionation during biological uptake, although these effects tend to be small (<10% of the signal that arises from abiological processes, such as water transport) and are typically ignored (Fiadiero, 1982), hence the moniker “abiogenic.” The air-sea equilibration timescale is thus an emergent property of the model environment, and varies over a factor of roughly 2 across the modern ocean surface, as determined by the DIC buffer factor and therefore $d\text{DIC}/d\text{CO}_{2\text{ocean}}$ (e.g., Galbraith et al., 2015). The dependence of the equilibration time on the ratio of DIC to dissolved CO_2 is intuitive in the sense that the timescale will be longer if the DIC pool to equilibrate with is larger, and will be shorter to the extent that the dissolved CO_2 “window” (or “bottle neck”) through which the equilibration occurs is larger.

The air-sea exchange equation for radiocarbon is identical to that of ^{12}C , but uses the atmospheric partial pressure of ^{14}C (rather than total carbon) to calculate $^{14}\text{CO}_{2\text{sat}}$, and uses DI^{14}C to calculate $^{14}\text{CO}_{2\text{ocean}}$ (see Figure 1b). If we define R_{atm} and R_{ocean} as the $^{14}\text{C}/\text{C}$ ratios of the atmosphere and the ocean respectively, then the atmosphere to ocean radiocarbon flux is given by:

$$\phi_{\text{DI}^{14}\text{C}} = k_w(\alpha_{ao}R_{\text{atm}}\text{CO}_{2\text{sat}} - \alpha_{oa}R_{\text{ocean}}\text{CO}_{2\text{ocean}}) \quad (20)$$

where $\alpha_{oa} = 0.9897^2$ and $\alpha_{ao} = 0.9980^2$, which are the isotopic fractionation factors for ocean-atmosphere transfer and vice versa. Note therefore that net carbon fluxes are not equivalent to net radiocarbon fluxes: that is, there can be zero net exchange of carbon (i.e., $\text{CO}_{2\text{ocean}} = \text{CO}_{2\text{sat}}$) while there is still a net flux of radiocarbon into the ocean from the atmosphere (i.e., $\alpha_{ML-\text{atm}}^T < 1$).

Another important difference from CO_2 transfer is that the speciation of DI^{14}C is not dependent on DI^{14}C itself, but depends on the abundance of *total* carbon, or DIC. This apparent subtlety leads to a surprisingly large difference in the air-sea exchange timescale relative to DIC, increasing it by an order of magnitude relative to total carbon. As noted above (Section 2.4.1), the result is a relatively slow (decadal) equilibration timescale for radiocarbon, roughly 200 times slower than for O_2 (and roughly 10 times slower than for CO_2), and scaling with the ratio $\text{DIC}/\text{CO}_{2\text{ocean}}$ (Galbraith et al., 2015; D. C. Jones et al., 2014).

The OCMIP2 implementation (and closely related variants) are widely applied in models. However, they ignore one important process: mass-dependent fractionation. Because the mass of ^{14}C differs from ^{12}C , it is subject to mass-dependent fractionation in most reactions, with approximately twice the fractionation as experienced by ^{13}C . As described above, conventional measurements of radiocarbon are always corrected for the relative abundance of ^{13}C measured simultaneously, which inherently includes natural as well as analytical mass-dependent fractionation. The standard corrections (Stuiver & Polach, 1977) assume that a constant mass-dependent fractionation has been experienced by the sample, relative to the atmosphere, with the correction approximately calibrated for a terrestrial plant. Because air-sea exchange and biological cycling in the ocean introduce additional mass-dependent fractionations (see Figure 1b), different histories of air-sea exchange and biological cycling can in principle result in different *reported* “conventional radiocarbon ages” (due to different $\delta^{13}\text{C}$ -based mass-dependent fractionation corrections [Stuiver & Polach, 1977]), even for identical in situ radiocarbon activities in seawater. Thus, conventional radiocarbon dates obtained from marine biogenic carbonate samples are normalized, in principle, to the radiocarbon activity that a terrestrial plant would have if it sampled its radiocarbon from the same host reservoir. For a model to be accurately compared with conventional radiocarbon observations, it should therefore also simulate ^{13}C , and include mass-dependent fractionations for both ^{13}C and ^{14}C . Currently, there are relatively few examples of models that include this (e.g., Jahn et al., 2015). The results of Jahn et al. (2015) suggest that biology and mass-dependent fractionation may actually have quite a significant effect in simulations, both on the distribution of radiocarbon in the ocean-atmosphere system (biotic runs were linked to an overall more radiocarbon depleted ocean), and on the equilibration time for model runs. One area where neglecting mass-dependent fractionation corrections will definitely have a significant effect, is in the calculation of global radiocarbon inventories (e.g., Dinauer et al., 2020), for which “raw” uncorrected ratios must be used. The reason for this is that the very large marine carbon reservoir will appear to include less radiocarbon if it is “corrected” to what it would be if it obtained its carbon from the atmosphere through photosynthesis, as illustrated by a comparison of measured- and modeled bomb- ^{14}C inventories (Bard et al., 1988).

Table 1
Examples Radiocarbon-Enabled General Circulation Models That Have Been Used for Palaeoclimate Studies

Model name	Reference	Radiocarbon implementation	Representative palaeoclimate study	Simulated CO _{2-atm} ?
UVIC	Koeve et al. (2015)	As dissolved carbon (DI14C)	Muglia et al. (2018; LGM)	No
LOVECLIM	Mouchet (2013)	As a fraction	Menviel et al. (2017; LGM)	Yes
LSG	Butzin et al. (2005)	As a fraction	Butzin et al. (2017; 50 ka)	No
Bern3D + C	Müller et al. (2006)	As a fraction	Dinauer et al. (2020; 50 ka)	Yes
GENIE	Ridgwell et al. (2007)	As dissolved carbon (DI14C)	Singarayer et al. (2008; Younger Dryas)	No
CM2Mc	Galbraith et al. (2011)	As dissolved carbon (DI14C)	Galbraith and de Lavergne (2019; pseudo-LGM)	No
CLIMBER	Brovkin et al. (2002)	As dissolved carbon (DI14C)	Ganopolski and Brovkin (2017)	Yes

3.2. Physical Implementation of Radiocarbon in Models

Over the past few decades, a diverse array of approaches has been developed for modeling radiocarbon. The most simplified approaches make use of box-models, which typically prescribe the physical exchanges between a small number of reservoirs (usually between 2 and 20) in an ad hoc manner, with the only physical constraint being the conservation of mass between boxes. One way of avoiding the ad hoc prescription of physical exchanges is via the use of “isopycnal box models,” where the volumes of boxes representing individual density classes scale according to the advective and diffusive mass fluxes through them, and therefore with buoyancy forcing applied at the box model boundaries (e.g., Goodwin, 2012). Temporal discretization tends to be very coarse, on the order of 1 or more years, usually ignoring the seasonal cycle. These models have formed the backbone of radiocarbon research since the 1950s (e.g., Arnold & Anderson, 1957; Craig, 1957; Revelle & Suess, 1957; Siegenthaler, 1983; Toggweiler & Sarmiento, 1985) and continue to be extremely useful. Given the very slow equilibration of radiocarbon among reservoirs (order 10,000 years) and the long timescale of past changes in production rate, the computational speed of box models is a tremendous advantage.

General Circulation Models (GCMs), in contrast, calculate the physical exchanges between reservoirs from fundamental physical principles, based on governing equations of fluid dynamics, and typically supplemented with many empirically based parameterizations. GCMs range from highly simplified, “reduced-physics” models, such as CLIMBER 2 (Ganopolski & Brovkin, 2017) or GENIE (Ridgwell et al., 2007), to state-of-the-art (process-) comprehensive models that are used to project future climate change (e.g., C. D. Jones et al., 2016). An important defining characteristic of any GCM is the size of its grid cells (spatial resolution), since circulation features smaller than ~threefold the grid cell size cannot be explicitly resolved. For example, to resolve geostrophic flows 1,000 km across, grid cells of ~300 km across (i.e., ~3°) are required, while resolving mesoscale eddies of 30 km across requires grid cells on the order of 10 km or ~0.1°. The temporal discretization of the model is intimately linked to the spatial resolution, since each time-step must be short enough to prevent transports from crossing a grid cell in a single time-step. Time-steps range from days for highly simplified GCMS to minutes for extremely high resolution GCMs.

The short time-steps used in GCMs allow fast processes to be explicitly calculated, which is relevant for the air-sea exchange of radiocarbon. Processes such as seasonal cycles of sea ice and mixed layer depths, storms with elevated winds and reduced sea level pressure, and short bursts of deep convection can be simulated in GCMs, with potentially significant impacts on radiocarbon distributions. As a side effect of the higher spatiotemporal resolution of GCMs, their computational cost is orders of magnitude greater than for box models. Crucially, this makes it extremely difficult to reach equilibrium for radiocarbon, as a full GCM can require a full year of computation on a small computer cluster to complete a single run of 10,000 years. Amongst available GCMs, only a sub-set will include biogeochemistry modules, and further sub-set of these will also include the cycling of isotopes such as radiocarbon, or atmospheric CO₂ as a prognostic variable: the full treatment of the global carbon and radiocarbon cycles in GCMs is far from universal. Table 1 provides a list of GCMs that include radiocarbon, and that have been applied to paleoceanographic investigations.

A final type of model we discuss is a type of “hybrid” of box models and GCMs, which we call “matrix” solutions, or “transport matrix methods” (TMM; e.g., Khatiwala et al., 2005). The latter models use GCM-like grids, but do not calculate physical or chemical exchanges, instead relying on one among a number of techniques to

impose a matrix of transports (i.e., exchanges between grid cells) previously calculated from a steady-state GCM solution. These models combine computational speed with the spatial resolution of GCMs, allowing equilibrium radiocarbon distributions to be calculated for well-resolved, 3-dimensional oceans. Some matrix solution methods are used exclusively for steady state, and solve the biogeochemistry for the equilibrium using something like Newton's method (e.g., Kwon & Primeau, 2006). Because these methods provide analytical solutions, they can be extremely valuable for making statistical calculations, or for solving inverse problems (e.g., calculating ocean transport from radiocarbon observations [DeVries & Primeau, 2011]). Meanwhile others use a biogeochemical module similar to those embedded in GCMs and simply use a transport matrix for calculating the transport of biogeochemical tracers over discrete time-steps (Khatiwala et al., 2005, 2019). The latter approach is significantly more computationally costly than the analytical solutions, but allows the seasonal cycle and/or biogeochemical transients, such as changes in radiocarbon production, to be resolved. Matrix solutions are still relative newcomers in this field of research, and have not yet been widely applied. However, given the dual importance of long simulations for radiocarbon, and the need to resolve spatial patterns, they hold great promise for future advances (Bardin et al., 2014). One particularly enticing opportunity is the use of such methods for the inverse modeling of geochemical tracers, for example, to place tighter constraints on mass transports in the past ocean (LeGrand & Wunsch, 1995; Marchal & Curry, 2008). Although inverse modeling has been applied to radiocarbon (Gebbie & Huybers, 2012; Marchal, 2005), this technique has yet to be fully exploited in the paleoceanographic context.

4. Radiocarbon and the Marine Carbon Cycle

The ocean is guaranteed a key role as a potential trigger and modulator of atmospheric CO₂ change due to its magnitude (containing ~60 times more carbon than the atmosphere), its dynamism on a range of timescales, and its inherent connection to the atmosphere via air-sea gas-exchange. Indeed, air-sea gas exchange, along with the solubility and reactivity of CO₂ in seawater, ensures that the atmospheric and marine carbon pools remain coupled to some degree. The degree to which the marine and atmospheric carbon pools are equilibrated (i.e., with the same average CO₂ partial pressure [*p*CO₂], and the same average radiocarbon activity) is important, because atmospheric CO₂ will be drawn down to the extent that more of the marine carbon inventory is shifted away from regions of the ocean that are well-equilibrated with the atmosphere to regions that are not (and vice versa; Eggleston & Galbraith, 2018). The main vector for moving carbon out of the atmosphere-equilibrated carbon pool is the so-called biological carbon pump (Volk & Hoffert, 1985). This “pump” maintains chemical gradients between the surface ocean (which is relatively well-equilibrated with the atmosphere) and deep ocean interior (which is relatively poorly equilibrated with the atmosphere). This is achieved through the fixation of carbon in the photic zone and its subsequent remineralization at depth. The *efficiency* of this biological pump is a key determinant of the marine carbon cycle's impact on atmospheric CO₂, and can be defined in terms of the magnitude of the *p*CO₂ gradient that it maintains between the surface ocean and the deep ocean interior (Ito & Follows, 2005; Volk & Hoffert, 1985; where the latter is relatively poorly equilibrated with the atmosphere). The efficiency of this carbon sequestration process can be further enhanced via relatively poor air-sea exchange/equilibration in regions of the surface ocean with relatively high *p*CO₂ (given DIC, ALK, *T*, and *S*) (Ito & Follows, 2013). Such regions are typically the regions of the ocean that provide the main “leaks” in the biological carbon pump due to significant “upwelling” of deep water to the ocean surface (e.g., the Southern Ocean). Both of these marine carbon cycle determinants (i.e., biological carbon pump efficiency and air-sea equilibration efficiency) have a direct impact on marine radiocarbon activities, making radiocarbon a particularly useful carbon cycle metric.

The link between radiocarbon and marine carbon cycling can be illustrated by considering a conceptual model that divides the marine carbon pool into two components (e.g., following Williams and Follows [2011]): a “*performed*” carbon pool, and a “*remineralized*” carbon pool. The performed carbon pool can be further divided, conceptually, into “*equilibrium*” and “*disequilibrium*” components, that account respectively for: (a) the hypothetical amount of carbon that would reside in the ocean as determined by atmospheric CO₂ (given the ocean's circulation and surface T-S distribution, which together comprise the so-called “solubility pump” [Volk & Hoffert, 1985]) and (b) the deviation from this hypothetical amount that results from imperfect air-sea gas exchange (which could be an excess or a deficit on average):

$$I_o = I_{\text{pre}} + I_{\text{rem}} = (I_{\text{eq}} + I_{\text{dis}}) + I_{\text{rem}} \quad (21)$$

Above, I_o , I_{pre} , I_{rem} , I_{eq} , and I_{dis} , are respectively the total-, preformed-, respired/remineralized-, equilibrium-, and disequilibrium carbon inventories. If we consider the ocean and atmospheric carbon inventories as forming a closed system (which is reasonable for relatively short timescales), then any change in the atmospheric carbon inventory will be given by:

$$-\Delta I_{atm} = -M_a \Delta XCO_2 = \Delta I_o = \Delta I_{pre} + \Delta I_{rem} = (\Delta I_{eq} + \Delta I_{dis}) + \Delta I_{rem} \quad (22)$$

where ΔI_{atm} is the change in the atmospheric carbon inventory, M_a is the molar mass of the atmosphere, ΔXCO_2 is the change in the molar mixing ratio of CO_2 in the atmosphere, and other terms indicate changes in the respective carbon inventories of the ocean. The above equation can be simplified to:

$$-M_a \Delta XCO_2 = V_o (\overline{\Delta C_{eq}} + \overline{\Delta C_{dis}} + \overline{\Delta C_{rem}}) \quad (23)$$

where V_o is the volume of the ocean, and $\overline{\Delta C_{eq}}$, $\overline{\Delta C_{dis}}$, and $\overline{\Delta C_{rem}}$ are the changes in the global average concentrations of the equilibrium-, disequilibrium- and, remineralized/respired DIC pools. We can eliminate $\overline{\Delta C_{eq}}$ from the above expression by relating it to the atmospheric CO_2 mixing ratio (XCO_2), via the average DIC buffer factor (γ_{DIC}) of the equilibrated carbon pool (Williams & Follows, 2011). In addition, we can define the total “sequestered” carbon pool (with respect to the atmosphere) as comprising the remineralized- and disequilibrium carbon pools (i.e., $\overline{\Delta C_{seq}} = \overline{\Delta C_{dis}} + \overline{\Delta C_{rem}}$). A typical approach is to ignore any changes in disequilibrium, thereby eliminating $\overline{\Delta C_{dis}}$ from consideration (e.g., Kwon et al., 2011; Skinner et al., 2015). However, it is becoming increasingly clear that changes in the disequilibrium carbon pool may play a significant role in altering the partitioning of carbon between the ocean and atmosphere (Eggleston & Galbraith, 2018; Galbraith & Skinner, 2020; Ito & Follows, 2013; Khatiwala et al., 2019; Skinner, Muschitiello, & Scrivner, 2019).

It is notable that the two marine carbon reservoirs that constitute the total sequestered carbon inventory will both tend to scale in magnitude with their respective radiocarbon ventilation ages. Thus, $\overline{\Delta C_{dis}}$ will be related to changes in the average air-sea exchange efficiency, which can be seen as a function of how much older the surface ocean is, as compared to what is expected from changes in the average pCO_2 /DIC ratio of the equilibrium carbon pool (Galbraith et al., 2015). In addition, $\overline{\Delta C_{rem}}$ can be related to changes in the product of the average residence time of water below the mixed layer and the average remineralization rate of organic carbon in the ocean interior (i.e., average export productivity, B_c) (Eggleston & Galbraith, 2018). All else being equal, changes in the degree of radiocarbon depletion of the ocean, relative to the contemporary atmosphere, should therefore relate to changes in the total sequestered carbon inventory (i.e., the sum of the disequilibrium and respired carbon pools) of the ocean, and therefore changes in atmospheric pCO_2 .

In order to describe this relationship more explicitly, we can assume that any change in the inventory of the total sequestered carbon pool (i.e., the sum of the disequilibrium and remineralized pools) will be distributed between the atmosphere and the equilibrium carbon pool, as determined by an average Revelle “buffer factor” (γ_{DIC}) (Oeschger et al., 1975; Williams & Follows, 2011), such that:

$$\overline{\Delta C_{eq}} = \frac{\overline{C_{eq(i)}} \Delta XCO_2}{\gamma_{DIC} XCO_{2(i)}} \quad (24)$$

where $XCO_{2(i)}$ is the atmospheric CO_2 molar mixing ratio prior to any perturbation, and ΔXCO_2 is the change in the mixing ratio as a result of the perturbation. By substituting Equation 24 into Equation 23, and defining the sequestered carbon pool as the sum of the respired and disequilibrium carbon pools (i.e., $\overline{\Delta C_{seq}} = \overline{\Delta C_{dis}} + \overline{\Delta C_{rem}}$), we can write:

$$\Delta XCO_2 = \frac{-V_o \overline{\Delta C_{seq}}}{(M_a + V_o \overline{C_{eq(i)}} / (\gamma_{DIC} XCO_{2(i)}))} \quad (25)$$

In order to approximate the change in the total sequestered carbon inventory ($V_o \overline{\Delta C_{seq}}$), we can consider that a change in its equilibrium value will be given by the product of the change in the average “residence time” of carbon in the sequestered pool ($\Delta\tau$; equivalent to the change in average age of carbon leaving the sequestered pool, also called its “transit time” [Bolin & Rodhe, 1973]), and the net flux of carbon into/out of the sequestered

carbon pool (assumed constant). The latter might be approximated by the average organic carbon export rate (B_c), from the surface ocean mixed layer into the ocean, such that:

$$\overline{\Delta C_{\text{seq}}} = \frac{B_c \Delta \tau}{V_o} \quad (26)$$

By substituting Equation 26 into Equation 25, we can obtain a theoretical description of the link between changes in the atmospheric CO_2 concentration and changes in the ocean interior average residence time:

$$\Delta X\text{CO}_2 = \frac{-B_c \Delta \tau}{(M_a + V_o \overline{C_{\text{eq}(i)}} / (\gamma_{\text{DIC}} X\text{CO}_{2(i)}))} \quad (27)$$

where the subscripts (i) indicate initial values prior to the perturbation. If we further assume that the average residence time of carbon in the sequestered carbon pool, equivalent to the average age of carbon *leaving* the sequestered carbon pool, is the same as the average age of carbon *in* this pool (Bolin & Rodhe, 1973), then we can approximate $\Delta \tau$ as the change in the average radiocarbon age offset between the deep ocean and the atmosphere (i.e., the average $\Delta(\text{B-Atm})$), less any expected change in global average surface reservoir age due to equilibrium effects (i.e., determined by solubility and/or the surface ocean's $p\text{CO}_2/\text{DIC}$ ratio). While this assumption will be accurate for a “well mixed” reservoir (e.g., in a box model), it is likely to yield an underestimate of the average residence time ($\Delta \tau$) where we are dealing with an ocean reservoir that has modest transport velocities and a large spatial separation between the main sources and sinks of carbon in the reservoir (Bolin & Rodhe, 1973).

The above Equation 27 does not imply that *any* change in atmospheric CO_2 will be linked to a change in the ocean interior's radiocarbon activity. Instead, it serves to illustrate that a change in ocean turnover and/or gas exchange that reduces the radiocarbon activity of the ocean interior will also tend to reduce atmospheric CO_2 to an extent that depends on a few key factors: (a) the strength of the biological carbon pump (e.g., modulated by sub-surface or exogenous nutrient supply to the surface ocean); (b) average air-sea gas exchange efficiency (affecting the contribution of $\overline{C_{\text{dis}}}$ to $\overline{C_{\text{seq}}}$); and (c) the carbonate chemistry of the equilibrated carbon pool (affecting the link between $\overline{C_{\text{eq}}}$ and $p\text{CO}_2$). The latter will depend on any parallel changes in the efficiency of the *carbonate* pump, and in global ocean carbonate chemistry (e.g., due to carbonate compensation/dissolution; Hain et al., 2011). These considerations cohere with an alternative analysis, based on a large number of GCM simulations (Galbraith & de Lavergne, 2019), that describes marine carbon sequestration from the atmosphere as being primarily dependent on the product of the average age (i.e., transit time) of water in the ocean interior and the average export productivity, as well as the preponderance of water masses in the ocean interior with high levels of “disequilibrium DIC” (whereby the end-member values are influenced by air-sea gas exchange efficiency in the regions of deep water formation) (Galbraith & Skinner, 2020).

The general implication of the above analysis is that a more radiocarbon-depleted ocean is one that tends to sequester more CO_2 from the atmosphere, *if* biological export/remineralization and the ocean's carbonate chemistry are conducive to this. Of course, this does not apply to transient changes in ocean-atmosphere radiocarbon age offsets that arise from large/rapid changes in radiocarbon production that the ocean interior has not yet responded to. As shown in Figure 7, changes in atmospheric CO_2 (caused by variable overturning rates or gas exchange efficiency) scale with deep ocean radiocarbon ventilation age changes in a predictable manner that is consistent with the simple theory laid out above. It is encouraging that, without excessive “tuning,” good agreement can be obtained between the predictions of the simple inventory-based theory, and the outputs of 2- and 3 box model simulations, as well as the outputs of more complex general circulation models (Kwon et al., 2011; Tschumi et al., 2011). A link between atmospheric CO_2 and radiocarbon ventilation of the ocean interior is therefore clearly identifiable in biogeochemical ocean general circulation models (Kwon et al., 2011; Tschumi et al., 2011), and this link can be understood in terms of basic marine carbon cycle theory (e.g., as described by the equation above). However, as noted already, this same theory reminds us that the exact sensitivity of the link will be controlled by a number of auxiliary parameters that may be difficult to pin down, including in particular: ocean overturning rates, ocean-atmosphere gas exchange efficiency, and export productivity. Nevertheless, these considerations provide a useful backdrop for assessing the impact of ocean ventilation changes on past atmospheric CO_2 , based on marine radiocarbon reconstructions. Below we turn to an assessment of such reconstructions from the Last Glacial Maximum and the last deglaciation, as well as their potential implications for ocean dynamics and the carbon cycle.

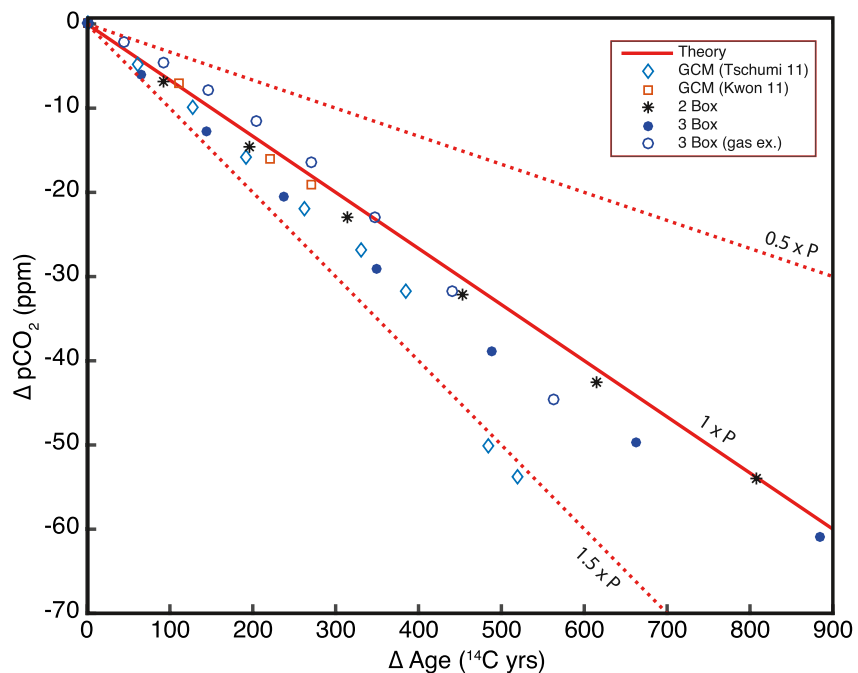


Figure 7. The link between deep ocean radiocarbon ventilation and atmospheric CO_2 change, predicted by theory and by numerical models. Inventory-based theory is shown by solid red line (assuming 13 PgC/yr organic carbon export productivity [P], as in Tschumi et al. [2011]); dashed red lines illustrate the effect of higher ($1.5 \times P$) and lower ($0.5 \times P$) export productivity, as labeled. Symbols indicate model outputs: blue open diamonds, Bern3D OGCM (Tschumi et al., 2011) (ages are for $>2 \text{ km}$ water depth); red open squares, OGCM and offline biogeochemistry model (Kwon et al., 2011) (ages are for the global average); simple two-box ocean model, black asterisks; and simple three-box ocean model, blue open/closed squares. The GCMs simulate atmospheric CO_2 as a function of changing ocean ventilation, driven by altered winds or ocean diffusivity (from a pre-industrial configuration); whereas the box models do so using directly altered mass overturning rates (or high-latitude gas-exchange efficiency in one suite of three-box model simulations; open circles). All of the data are plotted as anomalies in B-Atm age offsets and in atmospheric CO_2 , for perturbed states, relative to a relatively well-ventilated (“pre-industrial”) control state. Code for the box-models is available upon request.

5. The Record of Past Marine Radiocarbon Variability

5.1. The Last Glacial Maximum

The Last Glacial Maximum (LGM; $\sim 20 \text{ ka BP}$) provides an opportune target for the use of radiocarbon as a carbon cycle- or ocean circulation tracer. The LGM, like preceding glacials throughout the Quaternary, was characterized by a very different global carbon cycle, and ocean state, providing an excellent training ground for our understanding of chemical, biological and physical processes that interact to influence global climate (Galbraith & Skinner, 2020). Notably, atmospheric CO_2 at the LGM was $\sim 90 \text{ ppm}$ lower than pre-industrial levels (Monnin et al., 2001), associated with changes in the distribution of water masses (and possibly also their transport rates) (Adkins, 2013), as well as the conditions of air-sea gas exchange at high latitudes (e.g., due to altered sea ice distribution [Gersonde et al., 2003; Schüpbach et al., 2018], and upper ocean stratification [Francois et al., 1997]).

Understanding the nature and magnitude of large scale ocean dynamical changes between the LGM and the present, including their contribution to the evolution of atmospheric CO_2 , remains a long-standing challenge in paleo-oceanography, where radiocarbon has an important role to play. Paired calendar- and radiocarbon ages obtained for for example, coral, speleothem, and plant macrofossil samples, indicate that atmospheric $\Delta^{14}\text{C}$ was $\sim 400\%$ higher at the LGM (see Figure 4) (Reimer et al., 2020). As discussed further below, passive cosmogenic nuclide fluxes recorded in ice cores, and paleomagnetic field intensity reconstructions, further indicate that increased radiocarbon production at (and leading up to) the LGM can only partially account for the observed increased atmospheric radiocarbon activity (e.g., Bard, 1998; Broecker & Barker, 2007; Channell et al., 2018; Dinauer et al., 2020; Hain et al., 2014; Hughen, Lehman, et al., 2004; Köhler et al., 2005; Marchitto et al., 2007; Skinner et al., 2010). This would suggest a significant change in the partitioning of radiocarbon between the various

surface carbon reservoirs, including in particular an increase in the mean residence time of carbon in the ocean (e.g., Bard, 1998; Muscheler et al., 2004).

For negligible changes in radiocarbon production, an increase in the mean residence time of carbon in the ocean interior would lead to a reduction in the marine radiocarbon inventory, and would require a parallel increase in the atmospheric radiocarbon inventory, so that total radiocarbon decay is able to balance total radiocarbon production at equilibrium (see Section 3.1 above). Essentially, the radiocarbon production rate determines the global radiocarbon inventory, which is distributed between the various Earth carbon reservoirs: less radiocarbon in another carbon reservoir (e.g., due to a decrease in its total size, or an increase in its turn-over time), will require that more radiocarbon accumulates in the atmosphere, all else being equal. The magnitude of the marine radiocarbon inventory therefore provides an essential constraint for reconciling estimates of past atmospheric radiocarbon activity with estimates of past radiocarbon production, and with past carbon cycle change.

Efforts to determine if, and how, the LGM marine radiocarbon inventory differed from the pre-industrial have been ongoing for decades, stimulated to a large extent by the pioneering work of Wally Broecker (e.g., Broecker, 1989; Broecker et al., 1984, 1990). Initial efforts focused on the radiocarbon age offset between benthic and planktonic foraminifera (B-P offsets) (Broecker et al., 1984) (see Case D in Figure 6), which elegantly focused on the fact that the accuracy of such age offsets does not depend on the accuracy with which the “true” calendar age of the samples is known (e.g., see Section 2.4.2 above), but also relied on the assumption that the shallow sub-surface habitat in which the planktonic foraminifer lived remained more or less in equilibrium with the contemporary atmosphere (cf., Bard, 1988). This early work appeared to show only a very modest increase in the radiocarbon depletion of the LGM ocean as compared to today (Broecker et al., 1990; Broecker, Andree, Bonani, Wolfli, Oeschger, et al., 1988; Shackleton et al., 1988), which was hard to reconcile with existing reconstructions of altered nutrient distributions in the glacial ocean (Boyle & Keigwin, 1985, 1987; Broecker, 1989; Duplessy et al., 1988). Arguably, this early work was hampered to some extent by the use of relatively low sedimentation rate sediment cores (exacerbating differential bioturbation and preservation biases; see Section 2.2 above), and by the fact that surface ocean radiocarbon disequilibrium relative to the atmosphere has not been spatially or temporally constant (e.g., Bard, 1988; Sikes & Guilderson, 2016; Skinner, Muschitiello, & Scrivner, 2019), causing B-P offsets to differ from B-Atm offsets. Evidence for a significant increase in Pacific deep-water radiocarbon ventilation ages was first reported by Sikes et al. (2000), and although these ground-breaking results initially seemed difficult to reproduce in the wider Pacific (Broecker et al., 2007, 2008; Broecker, Barker, et al., 2004; Broecker, Clark, et al., 2004), evidence for significant B-P changes soon emerged from the Atlantic (Keigwin, 2004; Keigwin & Schlegel, 2002; Skinner & Shackleton, 2004).

The latter findings were consistent with new radiocarbon ventilation estimates derived from cold-water corals (e.g., Adkins et al., 1998; Robinson et al., 2005), dated using both radiocarbon and uranium-series decay (i.e., Case F in Figure 6). The use of U-series dated corals presented a means to overcome some of the impediments associated with the use of foraminifera (e.g., bioturbation, surface reservoir age variability), and provided direct estimates of the radiocarbon disequilibrium between deep-waters and the atmosphere. While the use of U-series dated corals has typically been limited to regions of the ocean that are relatively well ventilated (i.e., intermediate water depths, potentially due to oxygen requirements of the coral organisms), these studies have shown robustly that enhanced radiocarbon depletion indeed prevailed at the LGM in the northern- (Robinson et al., 2005), low latitude- (Chen et al., 2015), and southern Atlantic (Burke & Robinson, 2012), as well as the southern Pacific (Hines et al., 2015).

In the same vein, work using radiocarbon dated benthic foraminifera (prioritizing high-sedimentation rate cores, as advocated by for example, Shackleton et al., 1988) has increasingly aimed to reference benthic foraminiferal radiocarbon dates directly to the contemporary atmosphere (i.e., case C in Figure 6). Typically, this has been achieved through the use of co-deposited and independently dated tephra (e.g., Siani et al., 2001, 2013; Sikes & Guilderson, 2016; Sikes et al., 2000; Sikes, Cook, & Guilderson, 2016; Skinner et al., 2015), or chronostratigraphic constraints (e.g., Austin et al., 2011; Gottschalk et al., 2020; Marchitto et al., 2007; Peck et al., 2006; Skinner & Shackleton, 2004; Skinner et al., 2010, 2014), or indeed by the so-called “plateau tuning” approach (whereby inflections in planktonic radiocarbon time-series are matched to presumed counterparts in the atmospheric record) (Ausín et al., 2021; Balmer et al., 2016; Sarnthein et al., 2007, 2013, 2015; Umling & Thunell, 2017).

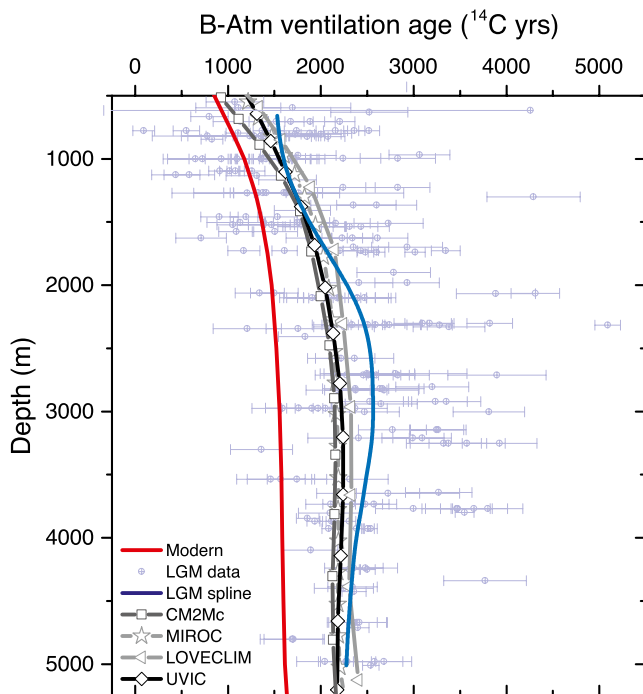


Figure 8. A compilation of Last Glacial Maximum (LGM) modeled global average radiocarbon activity (lines with open symbols; Chikamoto, Abe-Ouchi, et al., 2012; Chikamoto, Menviel, et al., 2012; Menviel et al., 2017; Muglia et al., 2018; Galbraith & de Lavergne, 2019) and reconstructed radiocarbon activity (light blue crossed circles, with 1 sigma error bars; Skinner et al., 2017), expressed relative to the atmosphere and as a function of water depth. A cubic spline fit to the proxy data (solid blue line), and the modern radiocarbon profile corrected for the influence of nuclear bomb testing in the twentieth century (solid red line; Key et al., 2004), are shown for comparison. The ocean is generally observed, and modeled, to have been more radiocarbon depleted at the LGM, relative to the contemporary atmosphere, as compared to modern, with generally good agreement between models despite a slight underestimation of simulated radiocarbon ventilation ages in the middepth ocean, where a “bulge” in ventilation ages is apparent (Burke et al., 2015; Skinner et al., 2017).

The accumulated evidence for the LGM (e.g., Skinner et al., 2017) now indicates that the ocean interior was clearly more radiocarbon-depleted versus the atmosphere than in pre-industrial times (see Figure 8). The data further suggest (albeit tentatively, since there remains a significant degree of scatter in the available observations) that this global average depletion represented the equivalent of at least $\sim 689 \pm 53$ ^{14}C yrs (Figures 8 and 11, where an updated value of $\sim 822 \pm 54$ ^{14}C yrs is suggested), resulting in a global average ocean radiocarbon “ventilation age” likely more than $\sim 2048 \pm 53$ ^{14}C yrs (Skinner et al., 2017). A similar global average increase has been proposed based on the “plateau tuning” methodology (Sarnthein et al., 2013).

5.2. Transport Time Versus Gas-Exchange Effects at the LGM

As illustrated in Figure 8, spatially resolved numerical model simulations of a putative “equilibrium LGM” state that include radiocarbon as a prognostic tracer (e.g., Chikamoto, Abe-Ouchi, et al., 2012; Chikamoto, Menviel, et al., 2012; Galbraith & de Lavergne, 2019; Kobayashi & Oka, 2018; Meissner et al., 2003; Menviel et al., 2017; Muglia et al., 2018), also typically produce an increase in ocean-atmosphere radiocarbon age offsets, relative to pre-industrial conditions, that is often only slightly smaller than suggested by the available observations. However, it is important to note that two simulations can obtain a similar magnitude of radiocarbon depletion in the “glacial” ocean interior for two very different reasons: (a) through an increase in the average turn-over time for water in the ocean interior (i.e., a reduction of transport rates); or (b) through a reduction in the efficiency of air-sea gas exchange, in particular in the regions of deep-water formation at high latitudes.

This is illustrated in Figure 9, where three (arbitrarily selected) model scenarios for the LGM circulation that all obtain an increase in average ocean radiocarbon depletion, nevertheless yield significantly different “preformed ages” (i.e., the radiocarbon depletion at the sea surface, prior to subduction). One simulation achieves an ocean interior “aging” primarily due to slower overturning, while the others do so primarily due to reduced gas exchange. This ambiguity reflects an inability, based on ocean interior radiocarbon depletion estimates alone, to distinguish between transport effects and air-sea gas-exchange effects (Koeve et al., 2015) (see Section 2.4.1 above), and highlights the need for data that constrain past variability in both surface- and deep-water radiocarbon disequilibria relative to the atmosphere.

An important question that remains to be resolved therefore concerns the relative contributions to CO_2 draw-down at the LGM, from air-sea gas exchange (e.g., Khatiwala et al., 2019) versus mass turn-over rates (e.g., Burke et al., 2015; Ferrari et al., 2014; Menviel et al., 2017; Watson et al., 2015). Arguments can be advanced to support a role for both of these contributing processes (Galbraith & Skinner, 2020). On the one hand, the existing LGM radiocarbon observations, indicating the most significant “aging” in the deep Atlantic and Southern Ocean (Skinner et al., 2017), appear to resolve a long-standing puzzle regarding the reconciliation of the deep ocean’s LGM radiocarbon- and nutrient distributions (Broecker, 1989), under the assumption that a reduced overturning rate in these basins allowed the accumulation of more respired nutrients (and respired carbon) (e.g., Siegenthaler & Wenk, 1984; Toggweiler, 1999; Toggweiler & Sarmiento, 1985). The role of respired carbon accumulation is tentatively supported by the fact that the aging of the deep ocean appears, in general, to have occurred in parallel with a drop in oxygenation (Anderson et al., 2019; de la Fuente et al., 2017; Gottschalk et al., 2016, 2020; Hoogakker et al., 2015, 2018; Jaccard & Galbraith, 2012; Skinner, Sadokov, et al., 2019; Umling & Thunell, 2018), an increase in nutrient concentrations (e.g., Curry & Oppo, 2005; Duplessy et al., 1988; Marchitto & Broecker, 2006; Peterson et al., 2014), and a (modest) drop in carbonate ion saturation (Anderson et al., 2019; de la Fuente et al., 2017; Umling & Thunell, 2018; Yu et al., 2014) (Figure 10). These associations could at face value reflect a longer residence time in the ocean interior, allowing more radiocarbon depletion,

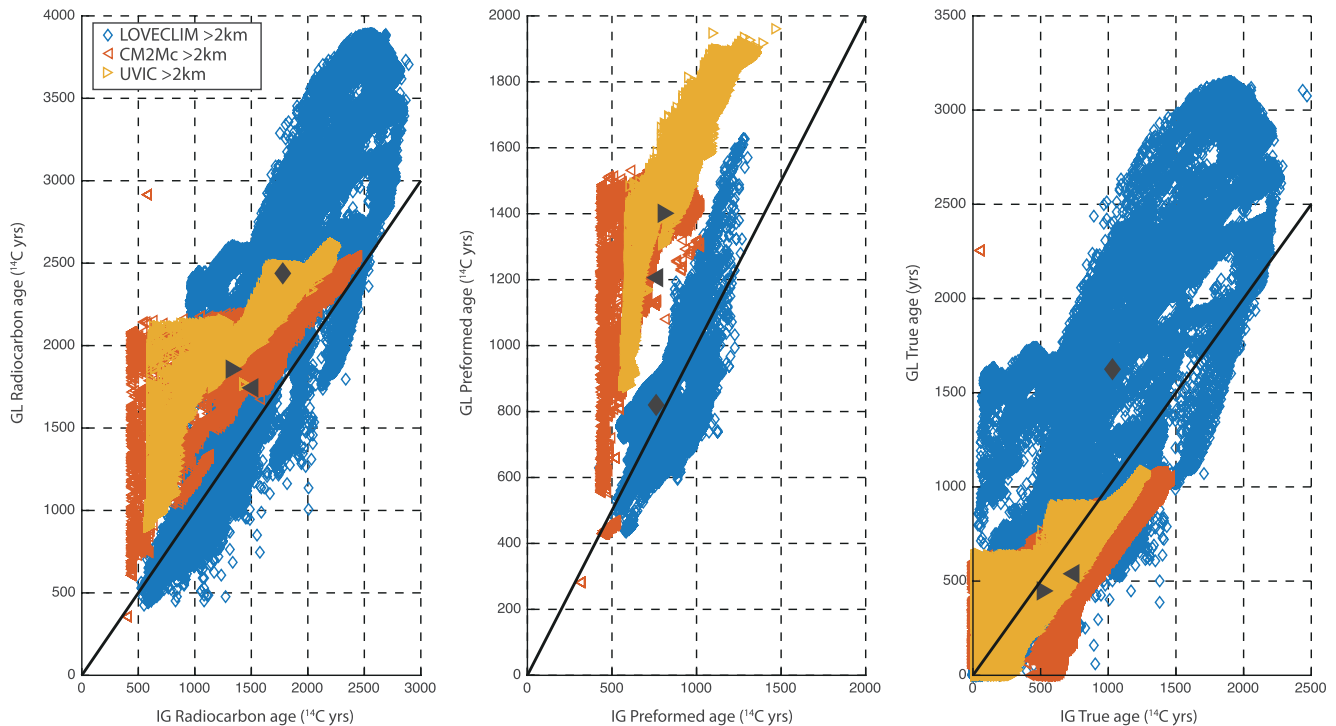


Figure 9. A comparison of model simulations yielding a more radiocarbon-depleted “glacial” ocean state, relative to the contemporary atmosphere, either primarily due to a more sluggish overturning, or primarily due to poor air-sea gas exchange (and a faster overturning). Left hand plot: cross-plot of in situ radiocarbon ventilation ages (expressed as radiocarbon age offsets from the atmosphere, for water depths >2 km) for “glacial” versus “interglacial” simulations, from a selection of numerical models (Galbraith & de Lavergne, 2019; Khatiwala et al., 2019; Menviel et al., 2017; Muglia et al., 2018). Middle plot: for the same model scenarios, a comparison of the average radiocarbon activity possessed by each parcel of water, relative to the contemporary atmosphere, before it was transported into the ocean interior (i.e., preformed radiocarbon ages) for “glacial” and “interglacial” climate states, demonstrating that some model scenarios obtain a significant portion of the relative ocean interior radiocarbon depletion via an increase in “preformed” ages, rather than slower overturning. Right hand plot: Comparison of the corresponding “true” ages (i.e., mean transport times, approximately equal to in situ ages minus preformed ages; Matsumoto, 2007), obtained for glacial- and interglacial climate states by the same models. Some models can produce a deep ocean that is more “poorly ventilated,” despite having a faster overturning (Galbraith & de Lavergne, 2019; Muglia et al., 2018). Solid black symbols in each plot show the whole-ocean average values for each numerical model scenario.

and more respired carbon/nutrient accumulation, while also consuming oxygen and lowering the carbonate ion concentration through the addition of respired CO_2 .

However, a fundamental ambiguity remains, since the patterns shown in Figure 10 could also be achieved in principle by unchanged mass turn-over rates combined with less effective gas exchange at the sea surface. Indeed, it would appear that oxygen concentrations can also exhibit significant disequilibrium effects, under very restricted conditions of gas-exchange, despite the much faster equilibration time for O_2 as compared to CO_2 (and especially $^{14}\text{CO}_2$; see Section 2.5.1) (Khatiwala et al., 2019). Therefore, the question arises: to what extent was the LGM ocean more “sluggish,” and to what extent was it more effectively “sealed off” from the atmosphere at high latitudes? This question remains a challenging one to resolve, and it bears directly on which climate-carbon cycle feedbacks tend to dominate under different climatic conditions (Galbraith & Skinner, 2020). Once again, this challenge underlines the need for improved observational constraints on past radiocarbon disequilibria relative to the atmosphere, from both the surface- and deep ocean.

As described above in Section 4, ocean interior radiocarbon can relate to ocean-atmosphere carbon partitioning through its link to the total “sequestered carbon pool,” regardless of its partitioning into respired- versus disequilibrium components (Galbraith & Skinner, 2020). The simple relationship between marine radiocarbon depletion and the sequestered carbon inventory proposed in Section 4 (see Equation 27) predicts an atmospheric draw down of more than 50 ppm for a 689 ^{14}Cyr “aging” of the ocean’s carbon pool (all else being equal) (Skinner et al., 2017). This very rough estimate is broadly in line with the contribution that is typically attributed to “ocean ventilation” processes in numerical model scenarios (Brovkin et al., 2012; Hain et al., 2014; Köhler et al., 2005). Note that such “ventilation processes” include those that influence the ocean’s total disequilibrium

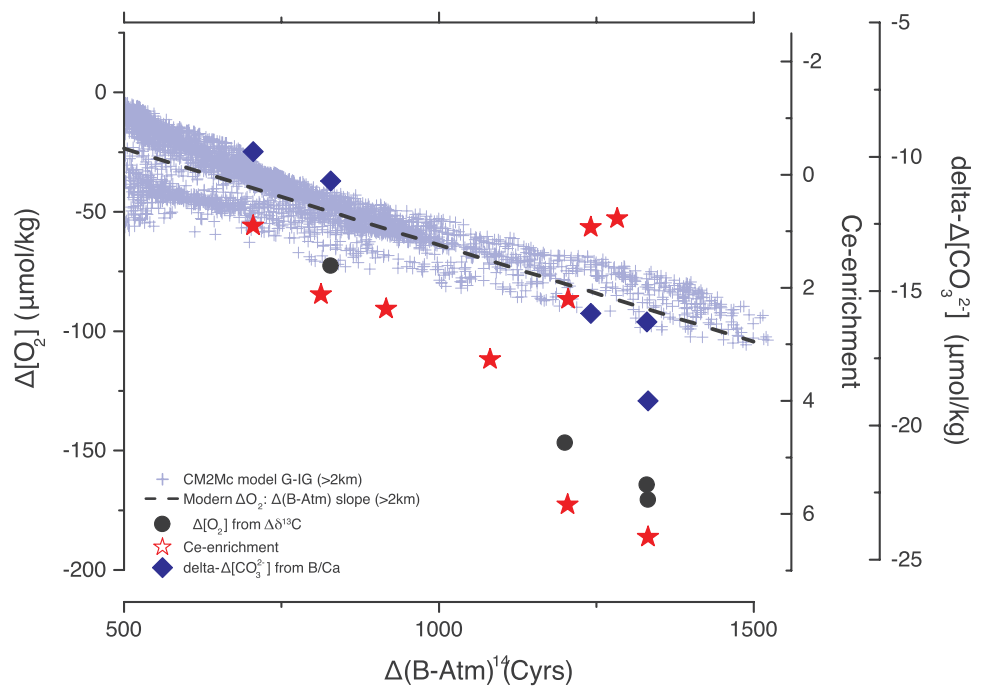


Figure 10. Deep-water radiocarbon ventilation (B-Atm) age offsets for the LGM ocean (Skinner et al., 2017), relative to the modern, plotted against: (1) paired quantitative oxygenation estimates based on epibenthic-endobenthic foraminifer $\delta^{13}\text{C}$ offsets (filled black circles), and qualitative oxygenation estimates based on “Ce-enrichment” (red filled stars; Skinner, Sadekov, et al., 2019) and (2) paired/proximal carbonate ion saturation estimates, based on B/Ca measurements in epibenthic foraminifera (filled blue diamonds). Also shown is the average spatial correlation between radiocarbon ventilation and oxygenation > 2 km in the modern ocean (dashed black line, offset by $-25 \mu\text{mol/kg}$ for ease of comparison) (Key et al., 2004), and modeled oxygenation changes in the ocean interior > 2 km, when shifting from an “interglacial” to a “glacial” climate state (Galbraith & de Lavergne, 2019) (blue crosses, offset by $-50 \mu\text{mol/kg}$ for ease of comparison). A broad correlation of respired carbon (illustrated for the modern ocean by the dashed line); however, restricted gas exchange can also contribute (as illustrated by the model results, indicated by the blue crosses). Note that the y-axes are arbitrarily scaled to each other. Proxy data used for this figure, and the relevant data sources, are included in Table S1.

carbon inventory (e.g., Khatiwala et al., 2019; Muglia et al., 2018) (i.e., sea-ice, wind speeds and gas exchange “piston velocities” etc.), as well as those that influence the ocean’s total respired carbon inventory (e.g., Menviel et al., 2017). Therefore, the inferred impact on marine carbon sequestration from the atmosphere may not depend strongly on the variable contributions of transport- versus air-sea gas exchange effects alluded to above (and illustrated in Figures 7 and 9). While there remains the significant challenge of attributing marine radiocarbon anomalies at the LGM to the effects of ocean transport versus gas-exchange, models and data tend to converge in suggesting that ocean ventilation processes have played a significant role in glacial-interglacial atmospheric CO_2 change (Siegenthaler & Wenk, 1984; Sigman et al., 2010; Toggweiler, 1999), specifically where these ventilation processes are broadly defined as including *both* gas-exchange and mass transport effects (Galbraith & Skinner, 2020) (e.g., see Section 2.4.2).

5.3. Radiocarbon Ventilation Patterns at the LGM

Despite the emerging clarity regarding marine carbon cycling at the LGM (Galbraith & Skinner, 2020), major challenges remain to be addressed insofar as radiocarbon is concerned. One outstanding challenge is to narrow the scatter in marine radiocarbon ventilation age estimates for the LGM, and in particular to better constrain their spatial patterns. To some extent this is a question of improving high-quality data coverage, allowing for example, vertical-, intra- and inter-basin gradients to be constrained with greater precision. Figure 11 shows a global spatial interpolation of available radiocarbon data, following Skinner et al. (2017), indicating a significant “aging” >2,000 m, particularly in the deep Atlantic and Southern Ocean, but also extending into the Indo-Pacific. It is notable that the shallow/intermediate depth Atlantic (<2,000 m) was less radiocarbon depleted than the deepest

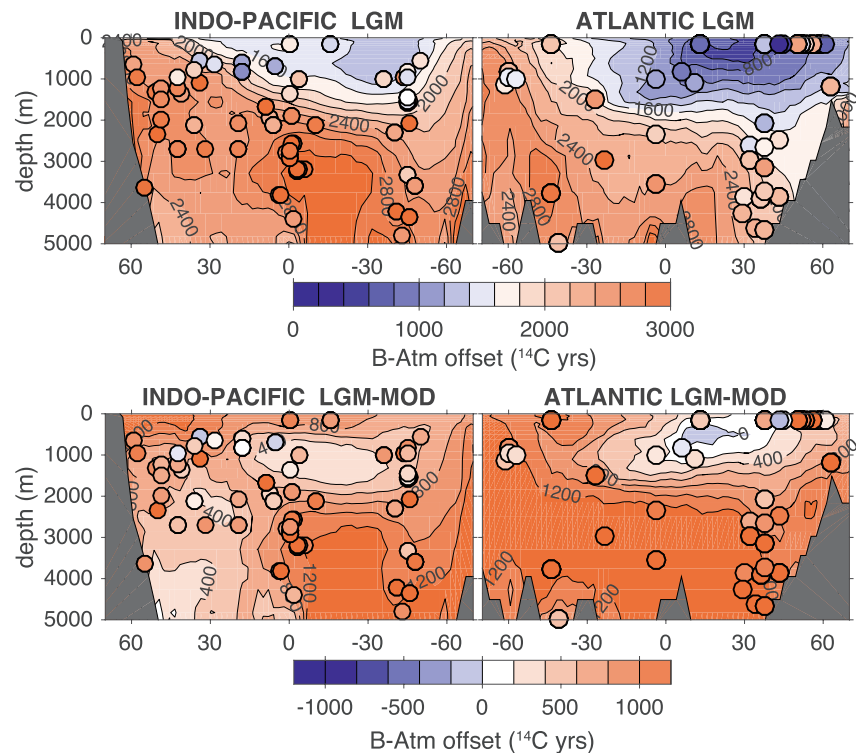


Figure 11. Meridional sections of B-Atm radiocarbon ventilation ages at the LGM (top panels), and offsets from modern bomb-corrected GLODAP data (Key et al., 2004) (bottom panels). Sections are based on zonally averaged global interpolations, after Skinner et al. (2017), incorporating more recent data (Chen et al., 2020; Dai et al., 2021; Gottschalk et al., 2020; Hines et al., 2019; Li et al., 2020; Ronge et al., 2019; Shao et al., 2019; Skinner et al., 2021; Skinner, Muschitiello, & Scrivner, 2019; Zhao et al., 2018). In this interpolation, the global average offset from modern at the LGM is 822 ± 54 ^{14}C yrs, slightly higher than 689 ± 53 ^{14}C yrs estimated by Skinner et al. (2017).

Atlantic at the LGM (e.g., Chen et al., 2020), suggesting an active, if shoaled, North Atlantic overturning cell (Freeman et al., 2015; Lippold et al., 2012; Skinner et al., 2017, 2021). In showing a modest aging of intermediate waters, as compared to modern (and as compared to the deepest Atlantic), these data fail to support the proposal of enhanced ventilation at the LGM in the deep North Atlantic reaching down to 3,500 m, as inferred from “plateau tuned” radiocarbon data (Sarnthein et al., 2020). The collected radiocarbon data (Skinner et al., 2017) very tentatively support the existence of a middepth “bulge” in radiocarbon ventilation ages in the Southern Ocean at the LGM (Burke et al., 2015), which could indicate altered buoyancy forcing in the Southern Ocean, resulting in a reduced residual overturning circulation (Ferrari et al., 2014). The latter would be conducive to an increased disequilibrium/respired carbon inventory at the LGM, with implications for atmospheric CO_2 (Watson et al., 2015).

Overall therefore, a familiar picture emerges of a relatively “poorly equilibrated” marine carbon pool in the bottom half of the LGM ocean, resonating with other lines of paleoceanographic evidence suggesting something of a “hydrographic divide” $\sim 2,000$ m water depth (e.g., Boyle, 1988; Lund, Adkins, & Ferrari, 2011; Lund, Mix, & Southon, 2011; Marchitto & Broecker, 2006), notwithstanding the radiocarbon evidence for active overturning and deep-water export in the North Atlantic and abyssal Southern Ocean (e.g., Burke et al., 2015; Skinner et al., 2021). Beyond this general picture, much of the detail of the LGM radiocarbon hydrography remains to be elucidated, for example, regarding the possibility of an east-west ventilation gradient in the Atlantic basin (Menviel et al., 2020; Ng et al., 2018; Skinner et al., 2021), or the patterns of ventilation across the Southern Ocean (Sikes et al., 2017; Sikes, Elmore, et al., 2016), and in the Indian basin in particular (Gottschalk et al., 2020; Ronge et al., 2020).

5.4. Extreme Radiocarbon Ventilation Ages at the LGM

One important aspect of the spatial variability in LGM radiocarbon ventilation ages that has yet to be completely resolved, is the observation of extreme radiocarbon depletions (i.e., the equivalent of more than 4,000–10,000 ^{14}C yrs offset from the contemporary atmosphere). These offsets have been observed in foraminifera from a handful of locations, primarily at intermediate water depths, off Galapagos and in the southern Pacific in particular (Bova et al., 2018; Ronge et al., 2016; Stott et al., 2009, 2019). The same challenge arises in accounting for “extreme” marine radiocarbon depletion anomalies that have been observed at a few locations subsequent to the LGM, across the last deglaciation (in both benthic and planktonic foraminifera), again primarily at intermediate water depths in the low-latitude eastern Pacific (Lindsay et al., 2015; Marchitto et al., 2007; Rafter et al., 2018, 2019), but also the South Pacific (Ronge et al., 2016, 2019), and Arabian Sea (Bryan et al., 2010). These extreme radiocarbon depletions reflect statistical “outliers” in the global LGM and deglacial datasets, in the sense that they differ significantly from the global population (Skinner et al., 2017); however, they cannot be ignored and currently defy straightforward explanation and integration into a complete theory of LGM and deglacial carbon cycle change. We return to these extreme observations when discussing the last deglaciation, below.

5.5. Balancing the Global Radiocarbon Budget

A further issue that arises is the difficulty of reconciling reconstructions of past radiocarbon production rates with estimates of the atmospheric- and marine radiocarbon and carbon inventories, as these have evolved over time from the last glacial period to the present. A major source of difficulty in this respect derives from uncertainties regarding past radiocarbon production rates (Dinauer et al., 2020): these diverge significantly depending on how they are derived and the age-scales that are attributed to them (Channell et al., 2018; Frank et al., 1997; Guyodo & Valet, 1999; Laj et al., 2004; Muscheler et al., 2005), as well as the cosmogenic radiocarbon production model that is employed (Kovaltsov et al., 2012; Masarik & Beer, 1999). Thus, depending on the radiocarbon production history and the model that is adopted, between $\sim 350\%$ (Bard, 1998; Bard et al., 1990), $\sim 180\text{--}240\%$ (Bard, 1998; Hain et al., 2014; Muscheler et al., 2004; Skinner et al., 2010), $\sim 146\%$ (Dinauer et al., 2020), or perhaps as little as $\sim 0 \pm 50\%$ (Channell et al., 2018), of the observed $\sim 400\%$ drop in atmospheric radiocarbon activity since the LGM can be accounted for in the absence of any carbon cycle changes (see Figure 12a). Accordingly, the above estimates leave anything from ~ 50 to $\sim 500\%$ atmospheric radiocarbon activity change to be accounted for by factors other than production, such as carbon cycle changes or even observational biases (Dinauer et al., 2020) (see residuals in Figure 12d). It is notable that the portion of the atmospheric radiocarbon record that cannot be accounted for by radiocarbon production rate changes shares some features with the atmospheric $p\text{CO}_2$ record, strongly suggesting the involvement of carbon cycle change (Figure 12d; Channell et al., 2018; Muscheler et al., 2004).

A complete explanation of the evolution of the global radiocarbon budget is a long-standing puzzle. The generation of marine sedimentary ^{10}Be records, as a complement to ice-core ^{10}Be and paleomagnetic reconstructions, represents a useful development in this regard (Frank et al., 1997; Ménébréaz et al., 2014; Simon et al., 2020). The combination of such records, from a range of latitudes, with numerical modeling of the production and spread of cosmogenic isotopes in the atmosphere and ocean, could in principle be used to assess the degree to which ice-core ^{10}Be and ^{36}Cl records provide an accurate picture of the global geomagnetic dipole moment variations, and therefore radiocarbon production rates. This would be aided by the fact that the relative geomagnetic modulation of cosmogenic isotope production is maximum at the equator, while the solar modulation (i.e., independent of geomagnetism) is maximum at the poles. Although most cosmogenic isotope production occurs in the stratosphere (Masarik & Beer, 1999), which is characterized by intense horizontal mixing and a residence time of a few years (Delaygue et al., 2015; Waugh & Hall, 2002), any deviation from a completely homogenous atmospheric (troposphere) mixing would affect the relative amplitudes of the geomagnetic and solar signals embedded in ^{10}Be and ^{36}Cl records. These considerations provide a glimmer of hope for disentangling the disparate geomagnetic and solar impacts on cosmogenic isotope production, and therefore also for assessing the accuracy of radiocarbon production rate estimates based on ^{10}Be fluxes near the poles or relative paleomagnetic intensity. Here, a key challenge for ice core reconstructions will be to improve our ability to reconstruct atmospheric fluxes of ^{10}Be or ^{36}Cl , from concentrations or accumulation rates recorded in ice. For sedimentary reconstructions, the primary challenge will similarly be to accurately relate measured sedimentary ^{10}Be concentrations (normalized

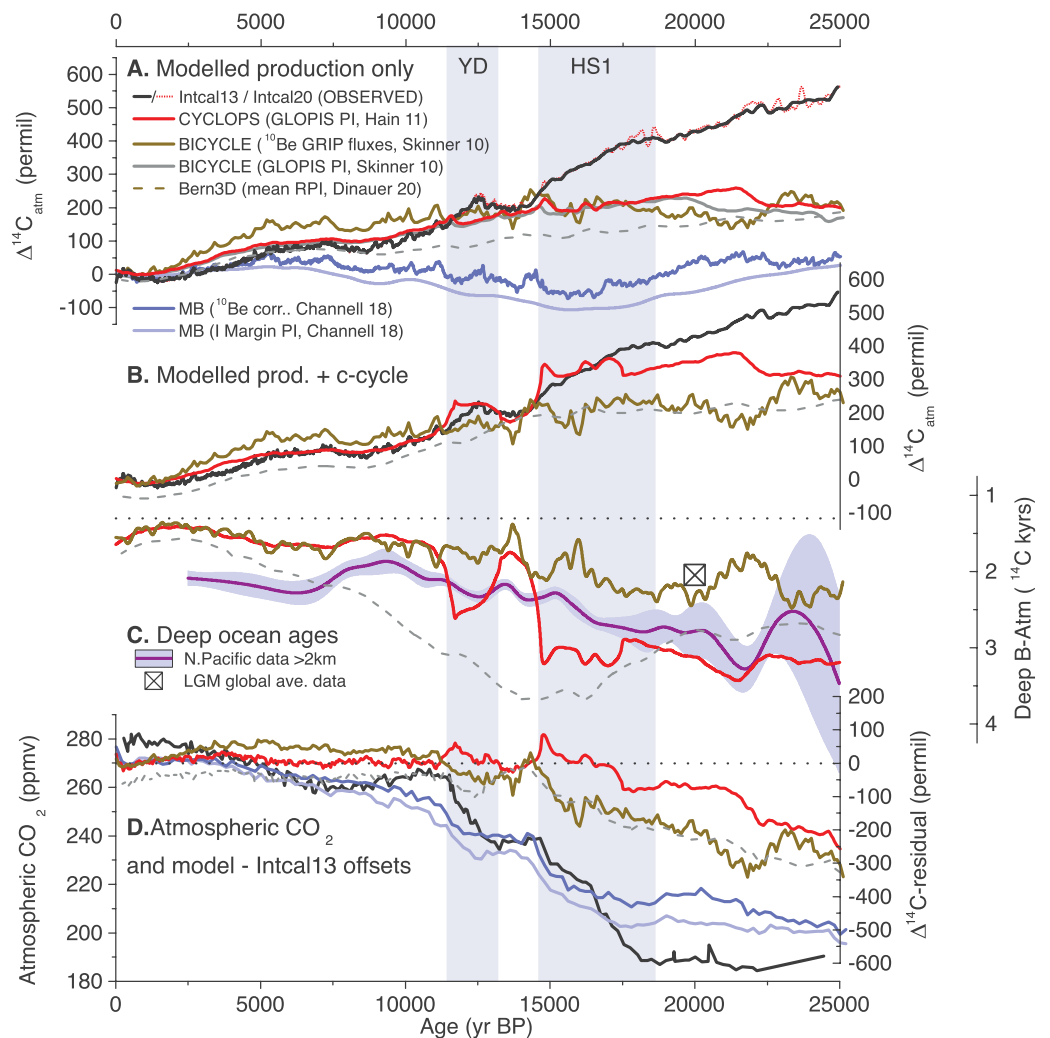


Figure 12. Modeling atmospheric $\Delta^{14}\text{C}$ ($\Delta^{14}\text{C}_{\text{atm}}$) based on evolving radiocarbon production rates, and carbon cycle change. (a) Observed $\Delta^{14}\text{C}_{\text{atm}}$ (solid black line, Intcal13 [Reimer et al., 2013]; dashed red line, Intcal20 [Reimer et al., 2020]), compared with modeled $\Delta^{14}\text{C}_{\text{atm}}$ based on different reconstructions of evolving radiocarbon production rates only (red line [Hain et al., 2014]; olive line [Köhler et al., 2006]; dashed gray line [Dinauer et al., 2020], blue lines [Channell et al., 2018]). (b) As for plot (a), but with model scenarios that also included carbon cycle changes (lines as for plot [a]). (c) B-Atm radiocarbon age offsets, generated by the model scenarios shown in plot (b) (lines as for plots [a] and [b]), compared with cubic spline fit to available B-Atm data from the North Pacific >2 km (solid blue line and shaded 95% confidence interval, [Cook & Keigwin, 2015; Galbraith et al., 2007; Gorbarenko et al., 2000; Keigwin & Lehman, 2015; Lund, Adkins, & Ferrari, 2011; Lund, Mix, & Southon, 2011; Max et al., 2014; Mix et al., 1999; Murayama et al., 1992; Okazaki et al., 2012; Zhao et al., 2018]), and an LGM global average estimate based on observations (Skinner et al., 2017); horizontal dashed line indicates the modern average B-Atm for reference. (d) Atmospheric CO_2 (Monnin et al., 2001), compared with offsets between observed $\Delta^{14}\text{C}_{\text{atm}}$ (i.e., Intcal13, Reimer et al., 2013) and the model scenarios shown in plot B, which involve carbon cycle changes (red line [Hain et al., 2014]; olive line [Köhler et al., 2006]; and dashed gray line [Dinauer et al., 2020]), as well as two scenarios from plot A that ignore any carbon cycle change (blue lines; Channell et al., 2018). All model results are referenced to Intcal13.

^{9}Be or ^{230}Th) to atmospheric fluxes, taking into account the complex effects of ocean transport, sea-water sediment interactions and “boundary scavenging” associated with vertical sedimentary particle fluxes.

In addition to past radiocarbon production changes, a number of carbon cycle changes are known to have occurred across the last deglaciation, and each will have had its own distinct, positive or negative, contribution to atmospheric radiocarbon activity (Köhler et al., 2006). For example, the well constrained atmospheric carbon inventory increase since the LGM (i.e., inferred from $p\text{CO}_2$) will have contributed to an atmospheric radiocarbon activity drop of $\sim 25\%$, if the total radiocarbon budget remained constant (Bard, 1998). The contributions from changes

in for example, carbonate sedimentation, terrestrial biosphere magnitude, marine biological export productivity, and a variety of ocean “ventilation” processes (such as North Atlantic overturning, Southern Ocean overturning, sea-ice influenced gas-exchange etc.), might each have been of comparable magnitudes that remain difficult to quantify from observations (Dinauer et al., 2020; Köhler et al., 2006).

As a starting point, under constant radiocarbon production, it can be shown that an increase in the average marine surface-to-deep radiocarbon gradient (i.e., the age gradient between the sequestered- and equilibrated carbon pools) of ~ 439 ^{14}C yrs, as previously proposed for the LGM (Skinner et al., 2017), might be expected to raise atmospheric radiocarbon activity by the equivalent of only $\sim 50\%$ (Bard, 1998). Larger changes in atmospheric $\Delta^{14}\text{C}$ between the LGM and the pre-industrial can be obtained for larger changes in the marine radiocarbon inventory (as required by mass balance; see Section 3.1 above), with broadly similar sensitivities emerging from box-models (e.g., Hain et al., 2014) and comprehensive Earth system models (e.g., Dinauer et al., 2020; see Figure 12). The available observations indicate a significant but modest change in the marine radiocarbon inventory at the LGM (Skinner et al., 2017; see Figure 12c), suggesting that neither radiocarbon production (as currently estimated), nor ocean ventilation, can account for the elevated atmospheric $\Delta^{14}\text{C}$ of the last glacial period (Broecker & Barker, 2007), either “single handedly” or in combination (Dinauer et al., 2020). This presents us with something of a puzzle that has yet to be resolved: how can we balance the global carbon/radiocarbon budgets across the last glacial cycle?

Based on a set of plausible estimates for a wider range of carbon cycle changes (including ocean ventilation, as well as carbonate sedimentation, terrestrial biosphere changes etc.), it has been proposed tentatively that as much as $\sim 100\%$ (i.e., 25%) of the atmospheric $\Delta^{14}\text{C}$ drop since the LGM can be accounted for by the combined (and partly compensating) effects of the various carbon cycle changes (Köhler et al., 2006) (see Figure 12). When further combining these carbon cycle changes with a selection of radiocarbon production scenarios (Laj et al., 2004; Muscheler et al., 2005), this same study was able to predict atmospheric $\Delta^{14}\text{C}$ as high as $\sim 224 \pm 150\%$ at the LGM, in parallel with an increase in the average marine radiocarbon ventilation age of ~ 690 ^{14}C yrs, both of which are reasonably close to current observations (Reimer et al., 2020; Skinner et al., 2017). As shown in Figure 12c, the deglacial evolution of average marine radiocarbon ages simulated by (Köhler et al., 2006) is not extremely different from that reconstructed here for the deep North Pacific. While this convergence is encouraging, it may be fortuitous, and would need to be revisited in light of revised estimates of radiocarbon production based on both geomagnetic “paleointensity” and cosmogenic nuclide (e.g., ^{10}Be) flux reconstructions, some of which now suggest that production changes may have contributed very little to increased atmospheric $\Delta^{14}\text{C}$ at the LGM (Channell et al., 2018). A recent study, applying a range of radiocarbon production scenarios in a comprehensive Earth system model (Dinauer et al., 2020), found that atmospheric $\Delta^{14}\text{C}$ as high as observed during the last glacial could only be reproduced if extreme (and likely implausible) changes in air-sea gas exchange were employed. This study thus reiterated the difficulty of reconciling observations of atmospheric- and marine radiocarbon, with available radiocarbon production rate scenarios, particularly when ocean ventilation is the only “control knob” that is manipulated (and when millennial-scale changes in ocean ventilation across the last deglaciation are not incorporated). Taken together with the earlier idealized scenarios of (Köhler et al., 2006), one further implication may be that increased attention should be focused on other contributing processes, such as marine sedimentation for example (Jeltsch-Thömmes & Joos, 2020). An alternative implication is that existing estimates of tropospheric radiocarbon input rates (i.e., production, and transfer from the stratosphere) might need to be revisited.

The project of reconciling deglacial radiocarbon- and carbon surface reservoir inventory changes, while taking into account emerging marine and atmospheric carbon isotope data (i.e., both $\Delta^{14}\text{C}$ and $\delta^{13}\text{C}$) (Bauska et al., 2016), as well as emerging estimates of terrestrial biosphere (Ciais et al., 2012), marine organic carbon/carbonate sedimentation (Cartapanis et al., 2018), and volcanism (Huybers & Langmuir, 2009), remains a major challenge to be met in future. Addressing this challenge will represent a major step forward in the long-standing goal of identifying and quantifying the contributors to global carbon cycle change across the last glacial cycle.

5.6. Deglacial Change: “Ventilation Seesaws” and “Mode Shifts”

The drop in atmospheric radiocarbon activity across the last deglaciation was not smooth; rather it was punctuated by at least two millennial-scale steps that were each accompanied by an acceleration of atmospheric CO_2 rise (see Figure 12). The *prima facie* implication of these millennial features would be that they represent the pulsed release of radiocarbon-depleted carbon dioxide into the atmosphere (Marchitto et al., 2007). Notably, these two

intervals of accelerated atmospheric change also coincide with cold events (stadials) in the North Atlantic region and over Greenland (Heinrich Stadial 1, HS1, and the Younger Dryas, YD [Björck et al., 1998]), as well as activations of the so-called “thermal bipolar seesaw” (EPICA Community Members, 2006; Stocker & Johnsen, 2003) (Figure 12). Although millennial-scale fluctuations in atmospheric radiocarbon are resolved with difficulty prior to the last deglaciation (Gottschalk et al., 2016), similar associations between the activation of the thermal bipolar seesaw and pulses in atmospheric CO₂ are also apparent on previous deglaciations (Barker et al., 2019), and during previous glacial cycles (Gottschalk et al., 2019; Nehrbass-Ahles et al., 2020). Millennial carbon cycle perturbations are thus persistent phenomena in the climate system that could play an important role in longer-term climate dynamics (Barker et al., 2019; Wolff et al., 2009).

It has been argued that the available deglacial radiocarbon database exhibits sufficient scatter to preclude the unequivocal identification of any trends in global average ocean-atmosphere disequilibrium across the last deglaciation (Zhao et al., 2018). However, there may be several possible explanations for a set of marine radiocarbon dates (including diagenetic, taphonomic or habitat biases), in addition to the hydrographic influences we are typically seeking to reconstruct (see Section 2.2 above). Therefore, some disagreement between observations need not imply the refutation of a null hypothesis that is premised on a high level of agreement between samples that are interpreted a priori be drawn from a population of estimates of a single parameter (Zhao et al., 2018). Furthermore, while the combination of all available radiocarbon data into a single time-series may yield no discernable deglacial trend (Zhao et al., 2018), clear patterns in the distribution of marine radiocarbon do emerge when well-resolved records are grouped together according to their locations and the water masses that they were likely bathed in.

This is shown in Figure 13, where three broad associations of deglacial radiocarbon ventilation change are proposed for: (a) the intermediate depth (900–2,000 m) North Pacific (Figure 13b); (b) the deep (>2 km) Southern Ocean and EEP (Figure 13c); and (c) the North Atlantic, including high-latitude North Atlantic “reservoir ages” (Figure 13d), the intermediate (900–2,000 m) equatorial Atlantic (Figure 13d), and the deep (>2 km) Atlantic outside of the Southern Ocean (Figure 13e). Figure 13 gives a sense of the global coverage and diversity of deglacial B-Atm time-series that exist, while also illustrating the coherent signals that emerge in three key regions of the ocean interior that are intimately connected to the three main areas of ocean-atmosphere buoyancy exchange: the Southern Ocean, the North Atlantic, and the North Pacific (Primeau, 2005). For simplicity, Figure 13 does not illustrate uncertainty estimates associated with the B-Atm data; however, analytical uncertainties typically amount to a few centuries (~200 years on average). This level of analytical uncertainty effectively sets the minimum signal amplitude that can be interpreted with confidence in the deglacial time-series. As discussed in Section 2.2, the most significant source of uncertainty in the collected deglacial B-Atm time-series is probably not analytical, but instead derives from potential biases resulting from bioturbation, diagenesis, calendar age-control, reservoir age corrections etc. Arguably therefore, in this context, an indication of B-Atm time-series accuracy, and signal character/amplitude, may be derived from the coherence of multiple independent time-series. It is notable that, despite all the challenges potential biases associated with B-Atm reconstructions, Figure 13 demonstrates quite consistent regional patterns.

Although the compilation of data in Figure 13 is not exhaustive, it does include the bulk of available time-series that span the last deglaciation. One notable omission from detailed consideration here, is a set of records produced using the “plateau tuning” approach (Ausín et al., 2021; Sarnthein et al., 2007, 2013, 2015, 2020). As for a handful of other records/locations (e.g., Cleroux et al., 2011; Davies-Walczak et al., 2014; Lund et al., 2015; Rae et al., 2014; Sortor & Lund, 2011), these sometimes derive from locations (e.g., the South China Sea) that are not easily slotted into the three dominant hydrographic associations proposed in Figure 13 (i.e., the North Atlantic, the shallow/deep Southern Ocean and Eastern Equatorial Pacific, and the intermediate North Pacific). A further difficulty is that the analysis of “plateau tuned” radiocarbon data has generally focused on restricted time-slices, such as the LGM or HS1 (Sarnthein et al., 2020), rather than time-series that span the last deglaciation. This makes it difficult to compare most of the “plateau tuning” results with those shown in Figure 13. However, where B-Atm (and reservoir age) time-series can be reconstructed from the plateau tuning control points, they often differ significantly from other reconstructions for proximal locations. For example, using the plateau tuning approach, (Ausín et al., 2021) propose very muted change in B-Atm offsets across the last deglaciation at 2,646 m water depth on the Iberian Margin (with lower radiocarbon ventilation ages at the LGM). This contrasts starkly with B-Atm records from several other cores in the same area (often within hundreds of meters) (Freeman

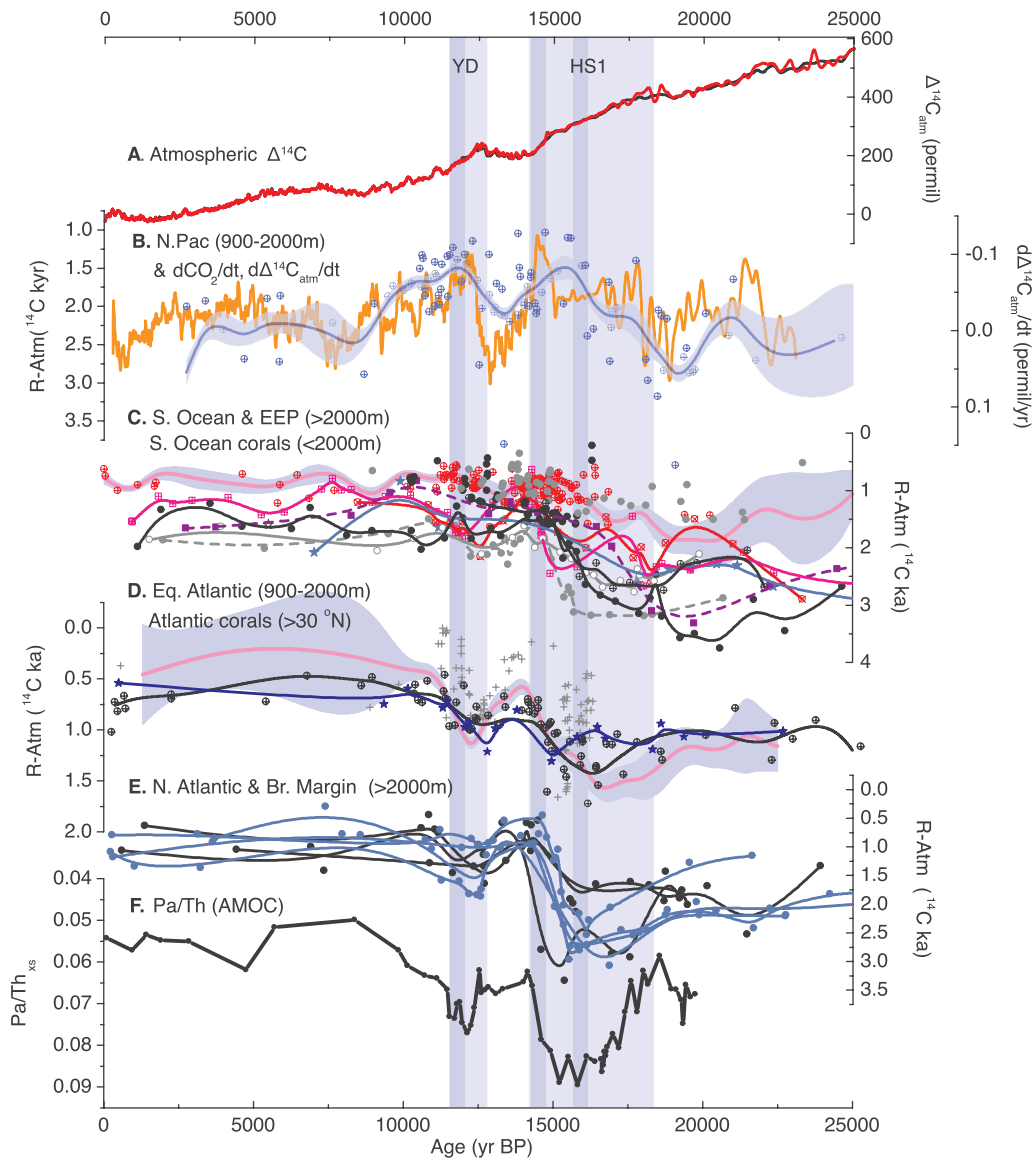


Figure 13.

et al., 2016; Skinner & Shackleton, 2004; Skinner et al., 2014, 2021). The latter records (blue lines in Figure 13e) are highly coherent, and track local reconstructions of epibenthic $\delta^{13}\text{C}$ (Freeman et al., 2016; Skinner & Shackleton, 2004), as well as B-Atm offsets from U-series dated corals in the western and equatorial Atlantic (Chen et al., 2015; Robinson et al., 2005) (Figure 13d), and reconstructions of AMOC strength (McManus et al., 2004) (Figure 13f). Similar contrasts from “plateau tuned” records arise in other regions (e.g., Broecker et al., 2008; Ezat et al., 2017; Kennett & Ingram, 1995; Thornalley et al., 2011, 2015; Wan & Jian, 2014). It should be underlined that, to a large extent, these discrepancies simply represent contrasting approaches to the development of calendar age-models for the various sediment cores. Like other chronostratigraphic methods, the “plateau tuning” approach commendably seeks to overcome problems associated with assuming a priori knowledge of past surface reservoir age offsets. However, it is particularly prone to the nexus of foraminifer abundance variability and bioturbation (Costa et al., 2017), due to its dependence on fluctuations in the observed radiocarbon age-depth relationship (e.g., Sarnthein et al., 2013). Furthermore, its accuracy and universal applicability have been questioned on theoretical grounds (Bard & Heaton, 2021). For example, the inference of surface reservoir age offsets >2 kyr (Sarnthein et al., 2020) is inconsistent with plateau tuning’s premise of perfect equilibrium and synchrony between the atmosphere and the surface ocean habitat of planktonic foraminifera, while the sparsity and scatter

in atmospheric and marine data can be shown to lead to ambiguous matching of plateaus, and therefore equivocal marine chronologies and reservoir age offsets (Bard & Heaton, 2021). Regardless of the proposed (de)merits of the plateau tuning approach, the conflicting results of Ausín et al. (2021) and for example, Skinner et al. (2021) indicate that plateau tuning is not always reconcilable with alternative chronostratigraphic methods, even where both avoid making assumptions regarding past surface reservoir age variability. Nevertheless, we emphasize that any records that are not included in Figure 13 are not “rejected” as invalid; rather, they may demand a more nuanced sedimentary, regional or intra-basin analysis/interpretation than is permitted by the body of existing data currently at our disposal.

In the interest of brevity, we also omit from detailed consideration the Mediterranean and the Nordic Seas, both of which make relatively small volumetric contributions to the global ocean, but are nonetheless hydrographically unique and important regions. The deglacial radiocarbon ventilation history of the Mediterranean remains relatively poorly constrained, though its degree of radiocarbon ventilation was likely not constant (McCulloch et al., 2010; Siani et al., 2001). The deglacial radiocarbon history of the Norwegian Seas exhibits some ambiguity. It has been proposed to include the influence of a “stagnant” Arctic Mediterranean feeding extreme radiocarbon depletions into the North Atlantic at times of reduced AMOC (Thornalley et al., 2011, 2015); however other reconstructions point to the possible influence of benthic foraminiferal “biases” as the source of at least some of the extreme radiocarbon depletions (Ezat et al., 2017), and ventilation records from the Fram Strait appear to rule out the delivery of extremely aged waters from the Arctic to the Nordic Seas (Ezat et al., 2019; Telesiński et al., 2021). As noted above, radiocarbon ventilation ages derived using the “plateau tuning” approach (Sarnthein et al., 2015) suggest a slightly different ventilation history in the Nordic Seas, particularly prior HS1. Nevertheless, most of the existing data are consistent with a pattern of lower B-Atm offsets during the B-A, as compared to HS1 and the YD (Muschitiello et al., 2019), broadly consistent with the wider North Atlantic (Figure 13e). The Mediterranean and the Arctic are both regions of particular environmental sensitivity, and both play important roles in determining the heat and salt budgets of the Atlantic. Fully elucidating the ventilation histories of the Norwegian and Mediterranean Seas, and their contribution to past climate and carbon cycle change therefore remains an important target for future work.

Finally, it is important to note that the hydrographic/regional groupings shown in Figure 13 do not include a set of intriguing records, many of which exhibit “extreme” radiocarbon depletions equivalent to 4,000–10,000 ^{14}C -years offset from the contemporary atmosphere (a magnitude that is not observed anywhere in the modern ocean). These records derive primarily from the shallow/intermediate (<1,000 m water depth) eastern low-latitude Pacific (Bova et al., 2018; Marchitto et al., 2007; Rafter et al., 2018; Stott et al., 2009), though similar signals have been proposed in the Arabian Sea (Bryan et al., 2010) and the deep equatorial- and South Pacific (Bova et al., 2018; Ronge et al., 2016). This group of records is sufficiently perplexing that we treat them separately in Section 5.7.

Figure 13. Summary of deglacial time-series of ocean interior radiocarbon ventilation (B-Atm), grouped according to regional and water depth associations. (a) Atmospheric radiocarbon activity, $\Delta^{14}\text{C}_{\text{atm}}$ (black line, Intcal13 [Reimer et al., 2013]; red line Intcal20 [Reimer et al., 2020]). (b) Collected intermediate-depth (900–2,000 m) North Pacific B-Atm data (blue crossed circles (Ahagon et al., 2003; Cook & Keigwin, 2015; Duplessy et al., 1989; Gorbarenko et al., 2000; Ikehara et al., 2006, 2011; Max et al., 2014; Mix et al., 1999; Okazaki et al., 2012, 2014), with cubic spline fit to all data shown by solid blue line, with shaded 95% confidence interval), compared with the rate of change of atmospheric $\Delta^{14}\text{C}_{\text{atm}}$ (orange line, time derivative of Intcal20 600-year moving average). (c) Southwest Pacific foraminifer data (2,314 m), filled blue stars and solid line (Skinner et al., 2015, 2017); Southwest Pacific coral data (1,400–1,900 m), gray solid circles (Hines et al., 2015); Drake Passage coral data <1,500 m, red crossed circles (Burke & Robinson, 2012; Chen et al., 2015; Li et al., 2020); Drake Passage coral data >1,500 m, filled black circles (Burke & Robinson, 2012; Chen et al., 2015; Li et al., 2020); South Atlantic, black crossed circles and solid line (Barker et al., 2010) (4,981 m), and black filled circles and solid line (Skinner et al., 2010) (3,770 m); Eastern Equatorial Pacific, purple filled squares and dashed line (de la Fuente et al., 2015; Skinner et al., 2017) (2,921 m), and filled gray circles and dashed line (Umling & Thunell, 2017) (2,730 m). Compiled Southern Ocean surface reservoir ages (which include shallow Drake Passage coral data) are shown for comparison (solid pink line, and shaded 95% confidence interval) (Skinner, Muschitiello, & Scrivner, 2019). (d) North Atlantic (>30°N) coral data (gray crosses; Adkins et al., 1998; Cao et al., 2007; Eltgroth et al., 2006; Robinson et al., 2005; Schroder-Ritzrau et al., 2003; Thiagarajan et al., 2014; Wilson et al., 2014), compared with equatorial Atlantic records from intermediate depths (900–2,000 m), including compiled coral data (black crossed circles and line, Chen et al., 2015), and a benthic foraminifer record from 1,000 m on the Brazil margin (filled blue stars and line; Freeman et al., 2015). Compiled high-latitude North Atlantic surface reservoir age offsets are also shown for comparison (pink solid line and shaded 95% confidence interval) (Skinner, Muschitiello, & Scrivner, 2019). (e) North Atlantic and Brazil Margin records >1 km, including: compiled deep Northwest Atlantic foraminifer data (black filled circles and solid line, Keigwin & Schlegel, 2002; Keigwin et al., 2005; Robinson et al., 2005); Northeast Atlantic data from >2 km water depth on the Iberian Margin (filled blue circles and solid lines; Skinner et al., 2021); and Brazil Margin data from >2 km water depth (filled black circles and dashed lines; Skinner et al., 2021). (f) North Atlantic overturning strength, based on Pa/Th ratios (McManus et al., 2004). Vertical light blue shaded bars indicate the approximate timing of Heinrich Stadial 1 (HS1) and the Younger Dryas (YD), and darker shaded bars indicate the approximate timing of centennial scale jumps in atmospheric CO_2 . All ventilation ages have been “corrected” from the original published results or from those given by Zhao et al. (2018) according to the difference between the Intcal20 and Intcal13 atmospheric radiocarbon curves, without changing the proposed reservoir ages or chronology basis.

Based on a survey of the existing radiocarbon data spanning the last deglaciation (and the data grouped together in Figure 13), we tentatively propose four principal “modes” of deglacial radiocarbon ventilation change that appear to have consistent regional/hydrographic associations:

1. *Transient ventilation pulses during HS1 and the YD*, that broadly coincide with two millennial scale accelerations in atmospheric- $\Delta^{14}\text{C}$ drop (Reimer et al., 2020) and CO_2 rise (Monnin et al., 2001) (see Figure 13a). Note that these millennial features are distinguished from the centennial “jumps” apparent within HS1, and at the end of HS1 and the YD (see below). These periods of ocean interior rejuvenation, when the North Pacific and Southern Ocean may have become a stronger source of radiocarbon to the deep ocean than the North Atlantic (Menviel et al., 2018; Skinner et al., 2013, 2014), are most clearly identified in the intermediate depth (900–2,000 m) North Pacific (Ahagon et al., 2003; Duplessy et al., 1989; Ikehara et al., 2006; Max et al., 2014; Okazaki et al., 2012, 2014) (Figure 13b).
2. An “*HS1 mode-shift*,” affecting the radiocarbon ventilation of the deep Southern Ocean in particular (and tentatively also the deep eastern equatorial Pacific, EEP), and representing the earliest onset of deep ocean rejuvenation broadly coincident with the initiation of HS1 and deglacial atmospheric CO_2 rise (see Figure 13c). Records that exhibit this pattern of deglacial radiocarbon ventilation change may also exhibit a second, smaller increase in radiocarbon ventilation across the YD (Burke & Robinson, 2012; Skinner et al., 2010). In contrast to the transient radiocarbon ventilation pulses seen in the intermediate depth North Pacific (where radiocarbon ventilation remained only slightly different from modern at the LGM; see Figure 13b), this pattern of deglacial ventilation likely reflects the initiation of a “mode shift” in the mean radiocarbon ventilation state of the global ocean (i.e., from a glacial mode to an interglacial mode). Based on the collected data, it seems to have been mostly complete by the B-A, ~15 ka BP. Although this deglacial pattern is best expressed in records from the deep Southern Ocean (>2,000 m) (e.g., Gottschalk et al., 2020; Sikes et al., 2000; Sikes, Cook, & Guilderson, 2016; Skinner et al., 2010, 2015), evidence for early rejuvenation from the beginning of HS1 is also apparent in some data from the deep EEP (de la Fuente et al., 2015; Umling & Thunell, 2017), and in coral data from areas of the Drake Passage that are bathed in Upper Circumpolar (UCDW) (Burke & Robinson, 2012). It is also notable that the same pattern of change is seen in reconstructions of Southern Ocean shallow sub-surface reservoir age offsets (Skinner, Muschitiello, & Scrivner, 2019) (Figure 13c). However, surface reservoir ages show a smaller amplitude of change across the deglaciation than their deep ocean counterparts (Sikes & Guilderson, 2016; Skinner et al., 2015), indicating that a significant portion, *but not all*, of the post-LGM shift in deep ocean radiocarbon ventilation might be accounted for by changes in air-sea gas exchange, rather than ocean interior mixing or transport rates (Galbraith & Skinner, 2020; Skinner et al., 2021; Skinner, Muschitiello, & Scrivner, 2019). Note that while the gradual shift in radiocarbon ventilation across HS1 is distinguished here from a second “mode shift” in ventilation that occurred at the onset of the B-A (see below), it seems likely that it may simply represent the combined influences of a transient ventilation pulse during HS1 sourced from the Southern Ocean and North Pacific (noted above; Menviel et al., 2018), and a particularly strong ventilation pulse immediately after this, during the B-A, sourced primarily from the North Atlantic (Barker et al., 2010).
3. A *Bølling-Allerød (B-A) ventilation surge*, broadly tracking deglacial Atlantic Meridional Overturning Circulation (AMOC) reconstructions (McManus et al., 2004) (Figures 13d–13f), and characterized primarily by a strong pulse of ventilation associated with the B-A interstadial (Barker et al., 2010; Skinner et al., 2013, 2021), which occurred between two periods of reduced radiocarbon ventilation during HS1 and the YD. As with the early rejuvenation observed in the deep Southern Ocean across HS1, the B-A surge in ventilation seems to have represented a distinct (and more rapid) “mode shift” toward the modern ventilation state, that was only partially and temporarily reversed during the YD. This trend is well expressed in the deep- and intermediate North Atlantic foraminifer and coral data (>900 m) (Adkins et al., 1998; Cao et al., 2007; Eltgroth et al., 2006; Keigwin & Schlegel, 2002; Robinson et al., 2005; Schroder-Ritzrau et al., 2003; Skinner & Shackleton, 2004; Skinner et al., 2014, 2021; Thiagarajan et al., 2014), and the intermediate depth (900–2,000 m) equatorial Atlantic (Chen et al., 2015; Freeman et al., 2015; Skinner et al., 2021). Evidence for a ventilation pulse during the B-A (as compared to HS1 and the YD) is also seen in areas of the Drake Passage influenced by UCDW (Burke & Robinson, 2012), and the deep South Atlantic (Barker et al., 2010; Skinner et al., 2010), as well as the deep North Pacific (e.g., Galbraith et al., 2007), the intermediate/deep South Pacific (Hines et al., 2015), and perhaps also the EEP thermocline and deep ocean (Bova et al., 2018; Umling & Thunell, 2017). It is notable that high-latitude North Atlantic shallow sub-surface “reservoir age” reconstructions (Skinner,

Muschitiello, & Scrivner, 2019; Stern & Lisiecki, 2013) show broadly the same pattern as their deep ocean counterparts, and appear to track both the pattern and the amplitude of changes seen in the deep *western* North Atlantic and equatorial intermediate Atlantic (but not the deep eastern North Atlantic; Figures 13d and 13e). This likely indicates a dominant influence of air-sea gas exchange (rather than transport) on the radiocarbon activity of water exported along the pathway of the deep western boundary current (and suggests continuous export of deep water from the North Atlantic since the last glacial period) (Bradtmiller et al., 2014; Freeman et al., 2015; Lippold et al., 2012; Skinner et al., 2021).

4. *Centennial-scale ventilation jumps*, coinciding with at least two out of three abrupt CO₂ jumps that occurred during deglaciation (Marcott et al., 2014) (see darker vertical bars in Figure 13), have been identified in coral data from the equatorial Atlantic (Chen et al., 2015) and the Drake Passage (Burke & Robinson, 2012; Chen et al., 2015; Li et al., 2020) (see below), and possibly also in data with less precise chronological control from the North Atlantic and North Pacific (Keigwin & Schlegel, 2002; Rae et al., 2014; Robinson et al., 2005; Skinner & Shackleton, 2004; Skinner et al., 2014, 2021; Thornalley et al., 2011) (Figure 13d).

Of course, as alluded to above, the global hydrography is far too complex and varied to slot entirely into the framework suggested above and illustrated in Figure 13. However, this framework does provide a “zero-order” sketch of some key features that can be identified in the majority of deglacial marine radiocarbon time-series, and that may deserve closer attention. Based on a substantial body of paleoceanographic research, tentative explanations for most of these key features can be advanced, as discussed further in the following sections.

5.6.1. Ventilation Pulses During HS1 and the YD

A possible explanation of the transient “*HS1/YD ventilation pulses*” and the “*HS1 mode-shift*” is that they reflect the operation of two different “ventilation see-saws.” This is supported by the observation that radiocarbon ventilation ages in the North Pacific and Southern Ocean sub-surface gradually dropped, in time with periods of increased ventilation ages in the deep North Atlantic, during HS1 and the YD (see Figure 14). One of these “seesaws” would have operated in the Atlantic, characterized by an alternating dominance of deep convection (with accompanying ocean heat- and CO₂ loss) in the North Atlantic versus the Southern Ocean (Broecker, 1998; Menviel et al., 2015; Skinner et al., 2013, 2014) (and with a direct link to the “thermal bi-polar seesaw” [EPICA Community Members, 2006; Pedro et al., 2018; Skinner, Muschitiello, & Scrivner, 2019; Stocker & Johnsen, 2003]; Figure 14). The link between the thermal bi-polar seesaw and Southern Ocean convection is likely to have operated via impacts on Southern Ocean sea-ice (Rae et al., 2018; Skinner et al., 2013; Skinner, Muschitiello, & Scrivner, 2019), winds (Menviel et al., 2018; Sikes, Elmore, et al., 2016), and/or buoyancy forcing (Ferrari et al., 2014; Hines et al., 2019; Watson et al., 2015). A further coupling with the North Pacific is evident in the approximately anti-phase character of North Atlantic and North Pacific radiocarbon ventilation records (particularly from intermediate depths, 900–2,000 m, in the North Pacific), as illustrated in Figure 14. These relationships have been interpreted to reflect the development of a Pacific meridional overturning circulation (PMOC) at times of reduced AMOC (Chikamoto, Abe-Ouchi, et al., 2012; Chikamoto, Menviel, et al., 2012; Freeman et al., 2015; Menviel et al., 2014; Okazaki et al., 2010, 2012). The emergence of a PMOC appears to have been linked to altered freshwater balance in the Pacific basin (Menviel et al., 2014), possibly influenced by reduced moisture transports across the Isthmus of Panama during North Atlantic stadials (Leduc et al., 2007). The depth to which the putative PMOC would have reached remains a contentious issue (Rae et al., 2014), though the records assembled by Zhao et al. (2018) indicate a rather muted and lagged response in the deep North Pacific, with ventilation increasing late in the HS1 and YD stadials, suggesting a PMOC with limited direct impact on depths >2,000 m.

Acting together, the two putative (North Atlantic/Southern Ocean and North Atlantic/North Pacific) “ventilation seesaws” may have been effective in ventilating a particularly large volume of the ocean interior, converting its sequestered carbon inventory to equilibrium carbon, and pushing up atmospheric CO₂. The potential integrated effects of these two seesaws on atmospheric CO₂ has been attested to by numerical model simulations (Menviel et al., 2018), though the physical basis for their coordination arguably remains to be fully analyzed. The likely importance of ventilating the intermediate ocean, via these putative “seesaws,” is underlined by the fact that the deepest ocean (>2,000 m) appears to have achieved a ventilation state broadly commensurate with the Holocene by the onset of the B-A (see Figure 13), whereas only ~56% of the deglacial CO₂ rise had been achieved at this time. The proposed transient pulses of marine carbon release, during HS1 and the YD (as well as their associated centennial “jumps”—see below) may therefore have been the most instrumental component of the proposed ocean ventilation contribution to deglacial atmospheric CO₂ rise, as is suggested by a close link to the rate of

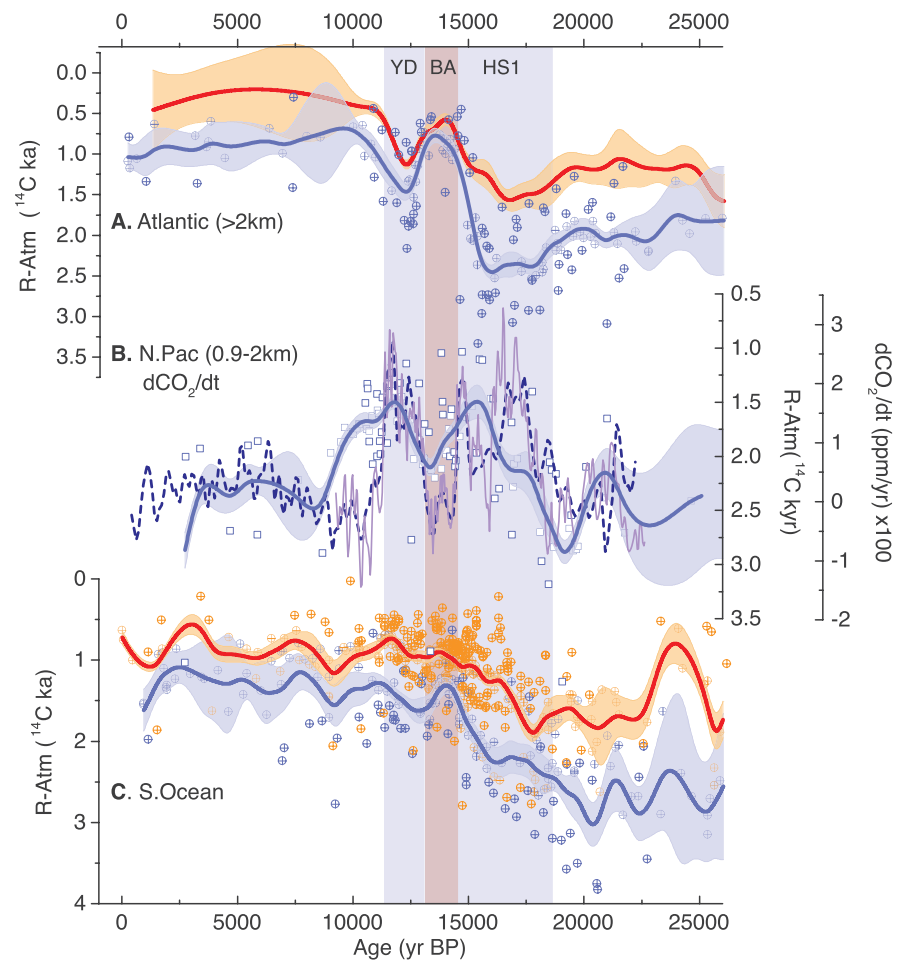


Figure 14. Suggested “ventilation seesaws” between the North Atlantic and both the intermediate depth North Pacific, and the Southern Ocean. (a) Compiled high-latitude surface reservoir ages (Skinner, Muschitiello, & Scrivner, 2019) (solid red line and shaded 95% confidence interval), and compiled deep Atlantic (>2 km) B-Atm offsets (blue crossed circles, and cubic spline fit shown by solid blue line with shaded 95% confidence intervals, Keigwin & Schlegel, 2002; Keigwin & Swift, 2017; Keigwin et al., 2005; Robinson et al., 2005; Skinner & Shackleton, 2004; Skinner et al., 2021; Zhao et al., 2018). (b) Comparison of: collected intermediate-depth (900–2,000 m) North Pacific B-Atm data (blue open squares [Ahagon et al., 2003; Cook & Keigwin, 2015; Duplessy et al., 1989; Gorbarenko et al., 2000; Ikehara et al., 2006, 2011; Max et al., 2014; Mix et al., 1999; Okazaki et al., 2012, 2014], with cubic spline fit shown by solid blue line and shaded 95% confidence intervals); the rate of change of atmospheric CO_2 (dashed blue line, EDC time-derivative of 500-year moving average [Monnin et al., 2001]; solid purple line, WAIS time-derivative of 600-year moving average [Marcott et al., 2014]). (c) Comparison of: compiled Southern Ocean data from <2 km water depth, including surface reservoir age offsets (orange crossed circles, and cubic spline fit shown by solid red line and shaded 95% confidence intervals, [Burke & Robinson, 2012; Chen et al., 2015; Gottschalk et al., 2020; Hines et al., 2015; Li et al., 2020; Ronge et al., 2020; Shao et al., 2019; Siani et al., 2013; Sikes & Guilderson, 2016; Sikes, Cook, & Guilderson, 2016; Skinner et al., 2010, 2015]); and compiled Southern Ocean data from >2 km water depth excluding 3 “extreme” values >4000 ^{14}C yrs equivalent (crossed blue circles with cubic spline fit shown by solid blue line and shaded 95% confidence intervals, Barker et al., 2010; Dai et al., 2021; Gottschalk et al., 2020; Ronge et al., 2016, 2020; Sikes, Cook, & Guilderson, 2016; Skinner et al., 2010, 2015). Vertical light blue shaded bars indicate the approximate timing of Heinrich Stadial 1 (HS1) and the Younger Dryas (YD); light red shaded bar indicates the approximate timing of the Bølling-Allerød (B-A). All ventilation ages have been “corrected” from the original published results or from those given by Zhao et al. (2018) according to the difference between the Intcal20 and Intcal13 atmospheric radiocarbon curves.

atmospheric radiocarbon- and CO_2 change (see Figures 13b and 14b). A corollary is that only a portion of deglacial CO_2 rise, yet to be accurately quantified, could be accounted for by ocean ventilation processes (Brovkin et al., 2012).

5.6.2. The “B-A Ventilation Surge”

The “B-A ventilation surge” coincides with what has been interpreted to reflect an intensification (Gherardi et al., 2005; McManus et al., 2004), and possibly also an “extreme deepening” or “overshoot,” of the AMOC (Barker et al., 2010; Skinner et al., 2013). A clear association is thus apparent between the rapid rejuvenation of the deep (and shallow sub-surface) North Atlantic, the reinvigoration of the AMOC, and the abrupt warming over Greenland that marks the onset of the B-A, and that coincides with warming and sea-ice loss in the North Atlantic region. This is entirely consistent with the standard account of the AMOC's role in the thermal bi-polar seesaw (Barker et al., 2009). However, it is intriguing that the bulk of the collected B-Atm records from the deep North Atlantic, shown in Figure 13e, appear to suggest that rejuvenation may have preceded the abrupt B-A onset by several centuries. While this may simply reflect signal smoothing due to bioturbation, or limitations in chronology precision, it is intriguing that a similar lead has been substantiated for the analogous transition that occurred at the end of the YD (Muschitiello et al., 2019).

While the influence of an AMOC during the B-A surge might be expected to reach downstream into the deep- and intermediate South Atlantic within centuries (Barker et al., 2010; Skinner et al., 2010), the time required to advect this signal to the deep EEP, and subsequently the deep North Pacific, would be >1000 years (Primeau & Deleersnijder, 2009). Nevertheless, it has been proposed by Umling and Thunell (2017) that a pulse of radiocarbon ventilation at ~2,700 m in the deep EEP was essentially synchronous with the B-A surge observed in the North Atlantic at ~14.8 ka BP, yet was delayed with respect to the earlier rejuvenation initiated in the Southern Ocean and intermediate Atlantic (which represents an interface between northern and southern sourced waters [Freeman et al., 2015]). The deep EEP B-Atm ventilation pulse inferred by Umling and Thunell (2017) at ~14.8 ka BP is not clearly expressed in B-P ¹⁴C-age offsets at this site. As concluded by Umling and Thunell (2017), this would require that the radiocarbon ventilation of the thermocline- and deep EEP were affected in synchrony by a presumed southern source. This could be achieved in principle by rapid changes in Southern Ocean surface reservoir ages at ~14.8 ka BP (i.e., air-sea gas exchange, influencing Antarctic mode- and deep waters transported to the EEP thermocline) (de la Fuente et al., 2015; Skinner et al., 2015). While Southern Ocean surface reservoir ages appear not to support this (exhibiting a gradual decline across HS1, in asynchrony with the North Atlantic) (Skinner, Muschitiello, & Scrivner, 2019) (Figures 13c and 14c), an abrupt centennial ventilation pulse ~14.8 ka BP does seem to have affected the shallow sub-surface of the Drake Passage (Li et al., 2020) and Galapagos (Chen et al., 2020) (see below). Alternatively, the North Pacific may have contributed, alongside the AMOC, to a surge in deep Pacific ventilation during the B-A (Gray et al., 2018). There is a great deal of scatter in the collected data, though there does appear to be a slight decrease in ventilation ages, on average, just prior to the B-A in the deep (>2 km) North Pacific. Nevertheless, this trend appears to be reversed during the B-A, in keeping with an anti-phased relationship between PMOC and AMOC intensity (Chikamoto, Abe-Ouchi, et al., 2012; Chikamoto, Menviel, et al., 2012; Max et al., 2014; Menviel et al., 2014; Mix et al., 1999; Okazaki et al., 2010, 2012). In light of the foregoing discussion, it is fair to say that a host of interesting and puzzling observations from the Pacific basin currently defy a tidy explanation, particular in relation to the B-A. Their elucidation represents an important target for future work, particularly as this bears on the distinct roles of convection and air-sea exchange in the high latitudes of each hemisphere.

A further puzzle emerges when considering that the AMOC surge across the B-A appears to have had little impact on atmospheric CO₂, whereas an acceleration of ocean ventilation via renewed deep convection would be expected to reduce the ocean's respired carbon content and push up atmospheric CO₂ (Sarmiento & Toggweiler, 1984). Instead, CO₂ declined slightly across the B-A (Marcott et al., 2014), though notably far more slowly than during previous D-O interstadials of the last glacial (Wolff et al., 2009). Indeed, D-O interstadials of the last glacial period (which were all characterized by a relatively strong AMOC [Gottschalk et al., 2015; Henry et al., 2016]) were consistently associated with *declining* atmospheric CO₂ (Ahn & Brook, 2008; Bauska et al., 2021), unlike during the B-A. The nearly stable CO₂ levels across the B-A therefore suggest an additional source of carbon (or a missing carbon sink) as compared to preceding D-O interstadials (Skinner et al., 2013, 2021).

Part of the explanation for nearly stable atmospheric CO₂ during the BA may be that the AMOC has a limited ability to affect the ocean's total respired carbon content (Hain et al., 2014), both due to its limited volumetric influence (Johnson, 2008; Primeau, 2005), and relative to the overwhelming impacts of countervailing changes in ventilation occurring in the Southern Ocean and North Pacific during D-O interstadials (Anderson et al., 2009; Freeman et al., 2015; Menviel et al., 2014, 2015; Okazaki et al., 2012; Skinner et al., 2020). Therefore, from a

marine CO₂ release perspective, the B-A may have simply been an intermission between stronger pulses of CO₂ release during HS1 and the YD, while from an atmospheric radiocarbon perspective, the onset of the B-A may have been the more significant event (Hain et al., 2014). In this respect it is worth noting that the net fluxes of radiocarbon and CO₂ across the air-sea interface do not have to be correlated (see Section 3.1 above). Taken together, these considerations may suggest that deglacial AMOC changes associated with the “thermal bipolar seesaw” primarily influenced atmospheric CO₂ through far-field impacts during periods of reduced AMOC (Cheng et al., 2009), in particular in the Southern Ocean (Anderson et al., 2009; Skinner et al., 2014), and perhaps also the North Pacific (Menviel et al., 2014; Okazaki et al., 2010) (Figure 14). Accordingly, pulses of ocean interior ventilation during HS1 and the YD might be seen as the main enablers for deglacial CO₂ rise: metaphorically, “punctures” that produced a leak in the biological pump and thus deflated the ocean’s overall sequestered carbon inventory (Anderson et al., 2009; Marchitto et al., 2007). While this canonical view of the AMOC contribution to deglacial carbon cycle dynamics is supported by many available observations and model simulations (e.g., Anderson et al., 2009; Cheng et al., 2009; Marchitto et al., 2007; Menviel et al., 2014, 2018; Okazaki et al., 2010; Skinner et al., 2014), it is now clear that it can only represent a partial explanation for deglacial CO₂ change as it ignores the possible contribution of shorter lived centennial events that occurred within stadial periods and at stadial-interstadial transitions (Bauska et al., 2021; Marcott et al., 2014). These are taken up next.

5.6.3. Centennial “Jumps”

Highly resolved CO₂ reconstructions from the WAIS Divide ice-core demonstrate that millennial-scale perturbations linked to the thermal bipolar seesaw can only account for a portion of deglacial CO₂ rise: at least ~40% of the total deglacial rise was achieved during separate centennial scale CO₂ jumps that were far more short-lived than HS1 and the YD (Marcott et al., 2014). Three main abrupt CO₂ jumps have been identified: in the middle of HS1 (16.3 ka BP), at the end of HS1 (and the onset of the B-A; 14.8 ka BP), and at the end of the YD (11.7 ka BP) (Marcott et al., 2014). Although evidence for marine radiocarbon ventilation pulses coinciding with each of these CO₂ jumps is hard to identify in the bulk of the available marine radiocarbon data (mostly foraminifer-based; see Figure 13), some tentative evidence for an association between ocean ventilation and centennial atmospheric CO₂ (and atmospheric $\Delta^{14}\text{C}$) jumps does exist. This is shown in Figure 15d, where rather subtle pulses in radiocarbon ventilation are apparent at ~12, 15, and 16 ka BP in collected coral-based data from both the Drake Passage in the Southern Ocean (in particular <1 km water depth) (Burke & Robinson, 2012; Chen et al., 2015; Li et al., 2020), and the Galapagos Plateau (~600 m water depth) (Chen et al., 2020). These regions are plausibly linked hydrographically by the influence of southern sourced intermediate-depth mode water.

The coincidence of the subtle ventilation pulses shown in Figure 15d with periods of rapid atmospheric CO₂ rise (Figure 15b) is probably not spurious, due to the accuracy of U-series dating performed on the corals. However, it is likely that the expression of ventilation pulses that coincided with the atmospheric CO₂ jumps may have been obscured to some degree (particularly in the Drake Passage data) due to the scatter of coral samples in space and time, which precludes the observation of varying conditions at a single location over time. While foraminifer-based radiocarbon ventilation data have the advantage of providing consistently ordered observations at a single location over time (in the absence of sedimentary disturbance), they are more difficult to date with centennial precision, and are typically affected by the smoothing and potentially biasing effects of bioturbation (see Section 2.2 above). Nevertheless, a few foraminifer-based radiocarbon ventilation reconstructions, for example, from the Brazil Margin (similarly influenced by southern-sourced water to some degree), provide rather tentative circumstantial evidence for declining B-Atm ventilation ages ~12, 15, and 16ka BP (see Figure 15e).

Two of the CO₂ jumps (at the end of HS1 and the YD) coincide with well-documented intervals of rapid intensification of the AMOC (McManus et al., 2004), and associated radiocarbon ventilation via the intermediate- (Chen et al., 2015) and deep Atlantic (Robinson et al., 2005; Skinner et al., 2014, 2021; Figures 13d and 13e). A link with North Atlantic convection is also suggested by rapid radiocarbon ventilation pulses that have been reconstructed in the North Atlantic south of Iceland (Thornalley et al., 2011). Tentatively therefore, the ventilation pulses seen in the Southern Ocean, and downstream in the equatorial Pacific (see Figure 15), may have originated in the North Atlantic. Indeed, it has been proposed, on the basis of pH reconstructions (Rae et al., 2018), that the CO₂ jumps at ~11.7 and 14.8 ka BP may have been linked to carbon loss from the Southern Ocean due to the “excavation” of respired carbon from the deep Atlantic basin by rapid AMOC intensification at the onset of interstadial conditions in the North Atlantic, which was made possible by Antarctic sea-ice loss during the preceding “swing” of the thermal bipolar seesaw that warmed the South Atlantic (Rae et al., 2018).

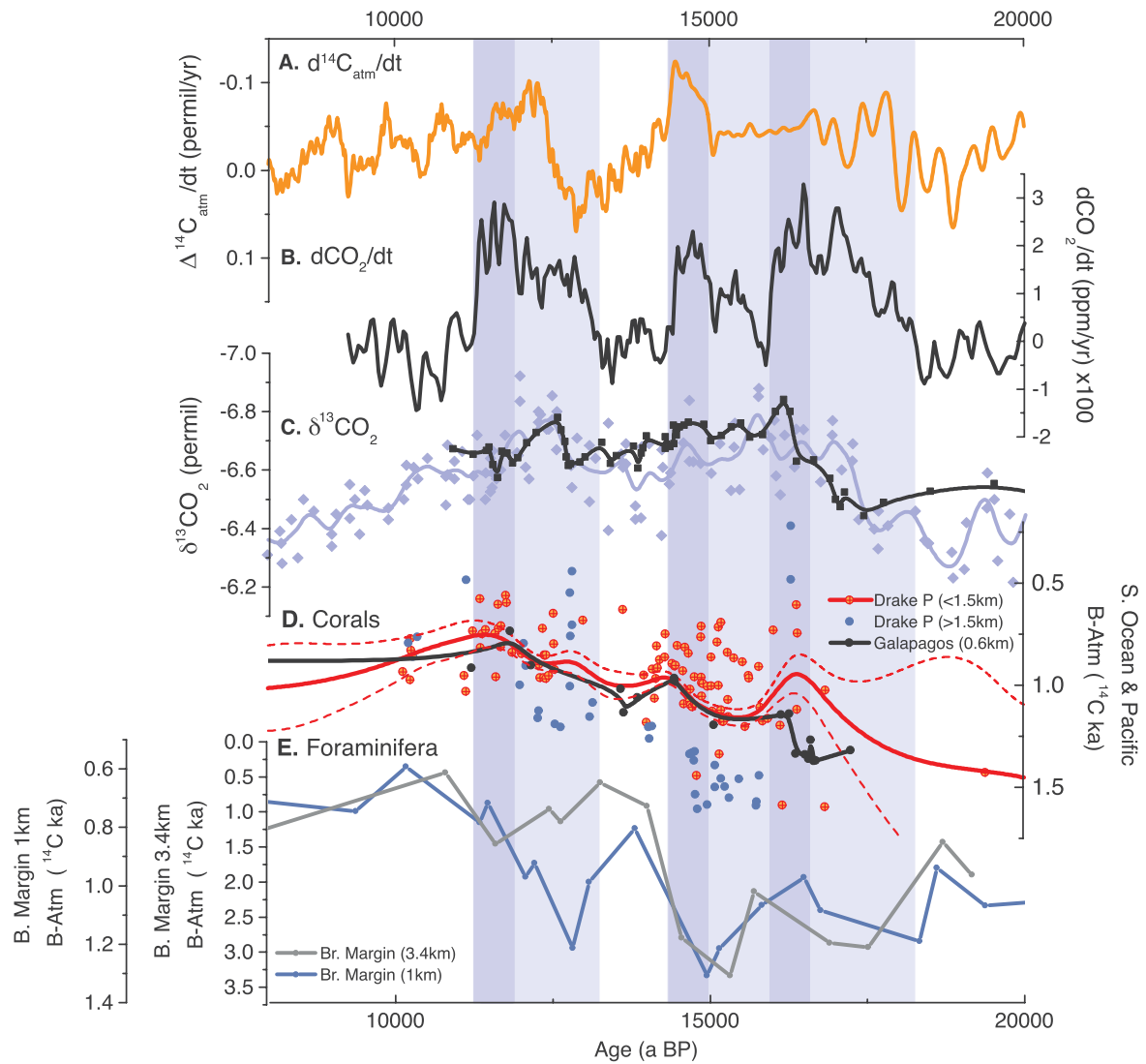


Figure 15. Illustration of centennial-scale CO_2 changes and associated marine radiocarbon ventilation anomalies. (a) Time-derivative of 600-year moving average of Intcal20 atmospheric $\Delta^{14}\text{C}_{\text{atm}}$ (Reimer et al., 2020). (b) time-derivative of 500-year moving average of WAIS Divide atmospheric CO_2 (Marcott et al., 2014). (c) Atmospheric $\delta^{13}\text{CO}_2$, based on: compiled measurements from a suite of Antarctic ice cores (Schmitt et al., 2012) (light blue filled circles and cubic spline); and based on measurements in Taylor Glacier ice (Bauska et al., 2016) (black filled squares and line). (d) Coral radiocarbon ventilation (B-Atm) data: from the Drake Passage (filled blue circles are data >1,500 m water depth; orange filled circles are data <1,500 m water depth; solid and dashed red lines show cubic spline through all data, with 95% confidence range; Burke & Robinson, 2012; Chen et al., 2015; Li et al., 2020); from 627 m water depth off Galapagos (black filled circles and line, Chen et al., 2020). (e) Foraminifer-based B-Atm data from 1,000 m (filled gray circles and line) and 3,400 m (filled blue circles and line), on the Brazil Margin (Skinner et al., 2021). Vertical shaded bars indicate the approximate timing of HS1 and the YD, with darker bars indicating the timing of three centennial CO_2 pulses. All ventilation ages have been “corrected” by the difference between the Intcal20 and Intcal13 atmospheric radiocarbon curves.

The temporal resolution of measurements in the latter study (Rae et al., 2018) was too low to rule in or out a similar dynamic for the third CO_2 jump at ~ 16.3 ka BP, and other evidence has previously been advanced that would tentatively link the mid-HS1 CO_2 pulse to a millennial ventilation anomaly in the North Pacific instead (Rae et al., 2014). However, if it is hypothesized that all three of the main centennial CO_2 jumps during the last deglaciation were linked to the same mechanism, it is not obvious that a reinvigoration of the AMOC was at the center of it, mainly because a mid-HS1 AMOC pulse has so far not been identified (McManus et al., 2004). Nevertheless, the emerging radiocarbon evidence for a mid-HS1 ventilation pulse in the South Atlantic and equatorial Pacific (Figure 15), and perhaps also the North Atlantic (Thornalley et al., 2011), suggests that a marine role in the deglacial centennial CO_2 jumps should not yet be ruled out. Indeed, even if a mid-HS1 AMOC surge has not yet been identified, a change in the geometry of the AMOC is apparent within HS1, when comparing Pa/Th

reconstructions of ocean transports in the western and eastern North Atlantic basins (Gherardi et al., 2005; Ng et al., 2018).

The existence of two distinct phases during the HS1 chronozone has long been apparent in a range of archives, including: atmospheric CO₂ (Marcott et al., 2014; Monnin et al., 2001; Figure 15b); atmospheric δ¹³C_{CO₂ (Bauska et al., 2016; Figure 15c); atmospheric methane (Rhodes et al., 2015); low latitude hydrological cycling (Wang et al., 2001); North American Great Plains hydrology (Broecker et al., 2009); ice-rafted debris deposition in the North Atlantic (Bard et al., 2000); and surface temperature variability on the Iberian Margin (Pailler & Bard, 2002; Skinner & Elderfield, 2005; Skinner & Shackleton, 2006). Piecing these lines of evidence together into a coherent mechanistic framework remains a difficult challenge to address (Broecker & Putnam, 2012), and is one that appears to be intimately connected to an elucidation of the mechanisms behind the centennial CO₂ jumps of the last deglaciation (Bauska et al., 2021).}

Despite the plausibility of an ocean ventilation role in at least some of the deglacial centennial CO₂ jumps (Bauska et al., 2016, 2021), and the emerging support for this role from some observations (Figure 15; Chen et al., 2015, 2020; Li et al., 2020; Rae et al., 2018), other explanations for these rapid carbon cycle perturbations have also been advanced. It has been proposed for example, that the atmospheric CO₂ pulse at ~14.8 ka BP may have resulted from northern hemisphere permafrost thawing, possibly as a knock-on effect of abrupt AMOC intensification and North Atlantic warming (Köhler et al., 2014). Indeed, it is possible that each of the centennial pulses involved the activation of different carbon sources, of either terrestrial or marine origin (Bauska et al., 2016; Chen et al., 2015; Köhler et al., 2014; Winterfeld et al., 2018), leaving open the possibility that (regardless of an ocean ventilation contribution) the correct mix of sources for all three of the deglacial pulses has yet to be identified.

Independent of their explanation, these abrupt CO₂ jumps, and the slower millennial increases across HS1 and the YD, emphasize the important role of rapid adjustments in the deglacial processes: deglacial carbon cycle evolution was clearly by “by jerks, *and* by creeps.” An important next step, for our understanding of the process of deglaciation and the involvement of the carbon cycle, will surely be to identify the origins of (and possible synergies between) events that occurred on a range of timescales: abrupt centennial jumps that were dispersed throughout the deglacial period; millennial anomalies that were coordinated by the bipolar seesaw; and longer term “mode shifts” (which may have been completed already half-way through the deglaciation).

5.7. Extreme Deglacial Anomalies: Fly in the Ointment or Red Herring

As noted above, there is a final grouping of deglacial radiocarbon ventilation records that resists integration into the canonical narrative of ocean circulation change and deglacial marine carbon release to the atmosphere, or indeed the general framework described above. These records derive primarily from the intermediate-depth eastern low-latitude Pacific (Baja California, California Margin, Galapagos), and exhibit a diversity of deglacial signatures. Some, from Baja California, exhibit well-expressed transient millennial-scale radiocarbon depletions that appear to coincide with the North Atlantic stadials HS1 and the YD (Lindsay et al., 2016; Marchitto et al., 2007). Others, mainly from just outside of the Gulf of California, exhibit a broad (and rather noisy) “extreme” radiocarbon anomaly that straddles the entire deglacial period, from the onset of HS1 to the end of the Pre-boreal period ~10 ka BP (Rafter et al., 2018, 2019). Yet others, from Galapagos, exhibit an extreme radiocarbon depletion that developed well before the LGM and was eliminated by the onset of the Holocene, ~10 ka BP (Bova et al., 2018; Stott et al., 2009). Similarly large amplitude radiocarbon depletions have also been reported at two sites in the South Pacific (Ronge et al., 2016), and a site in the Arabian Sea (Bryan et al., 2010) (the latter bearing a passing resemblance to the signal observed off Baja California) (Lindsay et al., 2016; Marchitto et al., 2007).

Suspensions that these observations reflect diagenetic overprinting, bioturbation, turbidites, or inaccurate age-models, have been argued against on the basis of the apparent consistency between sites within specific regions (Bova et al., 2018; Lindsay et al., 2016; Marchitto et al., 2007; Rafter et al., 2019; Stott et al., 2009), and due to a lack of evidence for sedimentary disturbance, secondary calcite phases, or age-differences between foraminifera of different species or of different degrees of preservation (Rafter et al., 2019; Stott et al., 2009). Nevertheless, high resolution radiocarbon dating has shown that at least one of the two South Pacific sites that exhibit “extreme” radiocarbon depletion (Ronge et al., 2016) has indeed been affected by a sedimentation hiatus and bioturbation (Ronge et al., 2019). Depositional hiatuses and age-reversals are also apparent in a set of cores from the

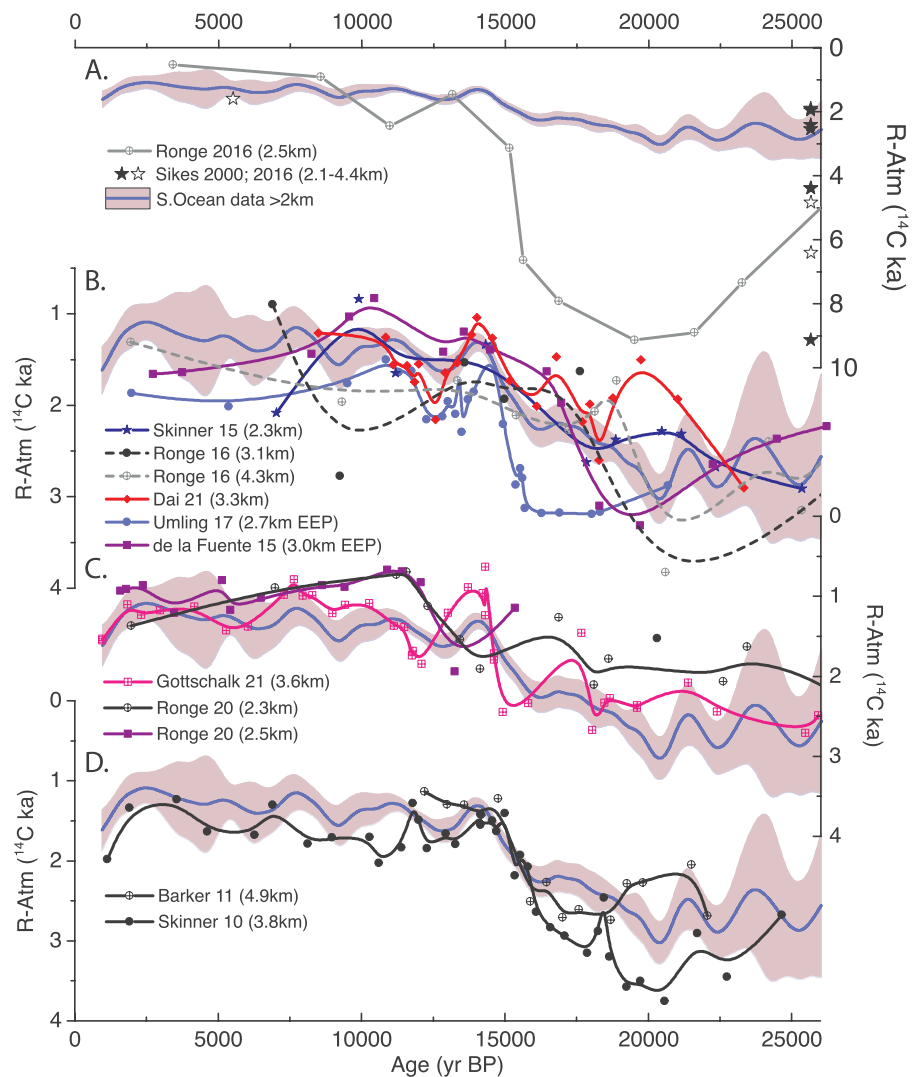


Figure 16. Southern Ocean radiocarbon ventilation data, south of 40°S and >2 km water depth. (a) Comparison of southwest Pacific B-Atm offsets from core PS75/100–4 (gray crossed circles and solid line, Ronge et al., 2016), B-Atm associated with tephra deposited off New Zealand (black open stars [Sikes et al., 2000], and black filled stars [Sikes, Cook, & Guilderson, 2016]), and spline fit to Southern Ocean data >2 km water depth shown in plots B to D (solid blue line and 95% shaded confidence interval). (b) Deep South Pacific and EEP B-Atm offsets (Dai et al., 2021; de la Fuente et al., 2015; Ronge et al., 2016; Skinner et al., 2015; Umling & Thunell, 2017). (c) Deep South Indian B-Atm offsets (Gottschalk et al., 2020; Ronge et al., 2020). (d) Deep South Atlantic B-Atm offsets (Barker et al., 2010; Diz & Barker, 2015; Skinner et al., 2010). All ventilation ages have been “corrected” according to the difference between the Intcal20 and Intcal13 atmospheric radiocarbon curves.

southern Indian Ocean presented by Ronge et al. (2020), further underlining the challenges that can arise (Costa et al., 2017), and that can often go undetected in some sedimentary contexts (Stott, 2020).

It is worth noting that additional observations of B-Atm offsets ranging from ~1,600 up to 6,800 ^{14}C years have also been reconstructed off New Zealand in association with the Kawakawa tephra, at $25,650 \pm 40$ kaBP (Sikes et al., 2000; Sikes, Cook, & Guilderson, 2016) (see Figure 16a). These results indicate a consistent “aging” of deep waters in the South Pacific during the last glacial period, consistent with numerous other reconstructions from the across the South Pacific water column (Hines et al., 2015; Shao et al., 2019; Siani et al., 2013), as well as from the Atlantic (Barker et al., 2010; Skinner et al., 2010), Indian (Gottschalk et al., 2020; Ronge et al., 2020),

and Pacific sectors of the deep (>2 km) Southern Ocean (Dai et al., 2021; Skinner et al., 2015; see Figure 16). However, the large degree of scatter exhibited in the results obtained for a single time horizon also suggests that individual observations (which may be subject to bioturbational biases above/below tephra [Sikes, Cook, & Guilderson, 2016]) are probably less representative of regional ventilation ages than their average. On this basis, only a single record from south of New Zealand (Ronge et al., 2016) would appear to deviate from a significant body of fairly consistent evidence from across the deep Southern Ocean (Barker et al., 2010; Dai et al., 2021; Gottschalk et al., 2020; Shao et al., 2019; Sikes, Cook, & Guilderson, 2016; Skinner et al., 2010, 2015, 2017), and indeed the deep EEP (de la Fuente et al., 2015; Umling & Thunell, 2017) (see Figure 16). It is probably fair to say that the current balance of evidence does not support the widespread prevalence of extremely aged *deep-water* radiocarbon signatures (i.e., >4,000 ¹⁴Cyrs equivalent) in the South Pacific at the LGM or during deglaciation.

Off Baja California (see Figure 17d), marked radiocarbon anomalies during HS1 and the YD have been reproduced from a range of intermediate water depths, 430–1,270 m (Lindsay et al., 2016; Marchitto et al., 2007), and these are tracked by similar anomalies in obligate surface dwelling (i.e., algal symbiont bearing) planktonic foraminifera (red/orange symbols and lines in Figure 17d). The amplitude of the planktonic radiocarbon anomalies is ~50% of the benthic anomalies, and has been interpreted to reflect upwelling of “aged” intermediate waters sourced from the Southern Ocean (Lindsay et al., 2015). This interpretation has drawn circumstantial support from surface water *p*CO₂ reconstructions (Martinez-Boti et al., 2015), and some surface water “reservoir age” reconstructions from the EEP (de la Fuente et al., 2015; Umling & Thunell, 2017). However, all of these studies appear to be inconsistent with surface reservoir ages derived from radiocarbon dating of allochthonous wood detritus in a marine core from the Columbian Margin (Zhao & Keigwin, 2018).

In the modern ocean, intermediate waters off Baja California are primarily sourced from the North Pacific, with a thin wedge of Antarctic Intermediate Water (AAIW) beneath this (Fiedler & Talley, 2006). Although a North Pacific origin for extreme radiocarbon anomalies in the shallow eastern low-latitude Pacific has been proposed (Bova et al., 2018), radiocarbon ventilation ages in the deep North Pacific were apparently never >2,500 ¹⁴Cyrs since the LGM (Galbraith et al., 2007; Lund, Adkins, & Ferrari, 2011; Lund, Mix, & Southon, 2011; Mix et al., 1999; Okazaki et al., 2010, 2012; Rae et al., 2014) (see Figure 17e), making it difficult to account for the observed radiocarbon anomalies off Baja California with a northern source. Moreover, a southern source is also problematic, as intermediate depth sites in the Southern Pacific and Drake Passage do not record evidence for AAIW as old as implied by the Baja California anomalies (Burke & Robinson, 2012; De Pol-Holz et al., 2010; Hines et al., 2015; Siani et al., 2013; see Figure 17e). Furthermore, no evidence currently exists for B-Atm radiocarbon ventilation ages >3000 ¹⁴Cyrs anywhere in the deep ocean after the B-A (see Figure 13), making it hard to account for the Baja California anomalies observed during the YD, even by appealing to an abyssal ocean source.

An alternative, and speculative, proposal might be that the radiocarbon anomalies observed off Baja California represent the influence of a radiocarbon-depleted sedimentary/geological carbon source, delivered to pore-waters during HS1 and the YD. Indeed, this hypothesis has been advanced to account for the far more “extreme” radiocarbon anomalies observed off Galapagos and the Gulf of California (Bova et al., 2018; Rafter et al., 2018, 2019; Stott et al., 2009). The proposal of a geological carbon source that supplemented the deep ocean's respired/disequilibrium dissolved inorganic carbon pool from as early as ~25 ka BP until approximately the end of the YD (Rafter et al., 2019; Ronge et al., 2016; Stott et al., 2019) is intriguing, and raises something of a carbon cycle puzzle. There are three key aspects to this conundrum: (a) the reconciliation of carbon isotope-, carbonate chemistry- and carbon cycle impacts across the last deglaciation; (b) the explanation of the different timing and patterns of various putative “smoking gun/volcano” records; and (c) the implications for long-term ocean-atmosphere carbon budget evolution across recurring glacial cycles.

The first of these items requires that the proposed addition of geological carbon, directly to the deep ocean, was sufficient to alter the deep ocean's radiocarbon signature, while leaving its δ¹³C signature unaffected (Rafter et al., 2019; Stott et al., 2019), and while also leaving sea floor carbonate sediment preservation unaffected (Marchitto et al., 2007; Rafter et al., 2019). The latter requirement stems from the fact that the addition of CO₂ to the deep ocean would be expected to lower pH and shift the dissolved carbonate system equilibria away from carbonate ion, causing carbonate sediments to dissolve wherever carbonate ion concentrations dropped below carbonate saturation levels (they are close to saturation throughout the modern deep Pacific [Key et al., 2004]).

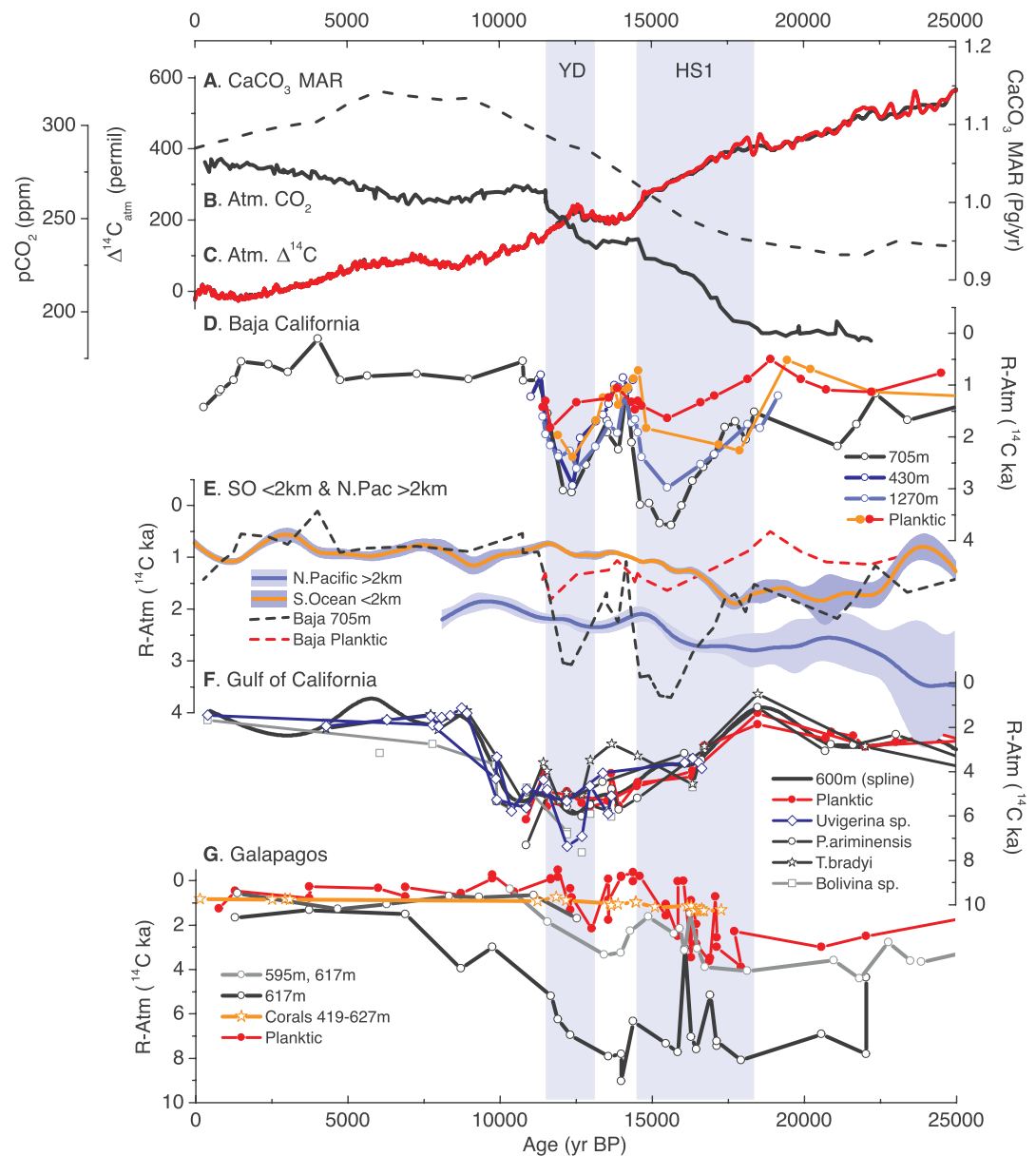


Figure 17. Marine radiocarbon ventilation records that exhibit evidence for extreme radiocarbon depletion, potentially suggestive of for example, localized “geological” carbon sources to the sedimentary environment, or diagenetic overprinting. (a) Global average carbonate sediment mass accumulation rates (Cartapanis et al., 2018). (b) Atmospheric CO₂ (Monnin et al., 2001). (c) Atmospheric radiocarbon activity (black line, Intcal13 (Reimer et al., 2013); red line Intcal20 [Reimer et al., 2020]). (d) Baja California records (Lindsay et al., 2015, 2016; Marchitto et al., 2007), exhibiting two transient radiocarbon depletions, during HS1 and the YD. (e) Cubic spline fits (with shaded 95% confidence interval) for data from the deep North Pacific (>2 km, see caption for Figure 11), and the upper Southern Ocean (<2 km, see caption for Figure 13), compared with planktonic and benthic records from Baja California. (f) Gulf of California records based on several different benthic foraminifer species and based on planktonic foraminifera (Rafter et al., 2018, 2019). (g) Galapagos foraminifer-based records (red filled circles, planktonic foraminifera [Stott et al., 2009]; open circles and lines, benthic foraminifera [Bova et al., 2018; Stott et al., 2009]); compared with coral-based data from the Galapagos Plateau (orange open stars and line) that show no extreme depletions (Chen et al., 2020). Vertical shaded bars indicate the approximate timing of Heinrich Stadial 1 (HS1) and the Younger Dryas (YD). All ventilation ages have been “corrected” according to the difference between the Intcal20 and Intcal13 atmospheric radiocarbon curves.

However, there is no evidence for significant carbonate dissolution at any of the eastern Pacific sites (Lindsay et al., 2015; Marchitto et al., 2007; Ortiz et al., 2004; Rafter et al., 2019; Stott et al., 2009). Globally, and across the Pacific, carbonate mass accumulation rates actually increased during the last deglaciation (Cartapanis et al., 2018; Figure 17a), as did carbonate ion concentrations in the deep Pacific (Allen et al., 2015, 2020; Marchitto et al., 2005; Yu et al., 2013). This would mean that significant and widespread geological CO₂ neutralization, either in the water column or at the sediment/sea-water interface, probably did not occur during deglaciation. Furthermore, if geological CO₂ neutralization by carbonate sediment dissolution did occur, it would cause ocean alkalinity to increase, and average ocean pCO₂ to decrease, thus counteracting deglacial CO₂ rise on a multi-millennial timescale.

To get around these “carbonate system” problems, a metamorphic source of bicarbonate ion has been hypothesized (Rafter et al., 2019). Similarly, if geological CO₂ was supplied in the ocean via deep sedimentary/metamorphic seeps in the south Pacific (Stott et al., 2019), with vertical fluid flow occurring over several hundred meters or more, one might also expect geological CO₂ to be neutralized by carbonate dissolution occurring deep in the sediment column, far below the sea floor. This workaround could potentially reconcile the radiocarbon observations from Galapagos (Bova et al., 2018; Stott et al., 2009) and the Gulf of California (Rafter et al., 2018, 2019) (and maybe the South Pacific [Ronge et al., 2016]) with records of deglacial carbonate chemistry and carbonate preservation (Allen et al., 2015, 2020; Cartapanis et al., 2018; Marchitto et al., 2005; Yu et al., 2013). However, it would also render them somewhat irrelevant to deglacial atmospheric CO₂ change (Rafter et al., 2019). This is because the supply of carbon in the form of bicarbonate would increase deep ocean DIC and ALK in a 1:1 ratio, thus decreasing the pCO₂ of the affected seawater only very slightly (Zeebe & Wolf-Gladrow, 2001). On a multi-millennial timescale, when this radiocarbon-dead bicarbonate-enriched water was transported to the sea surface by the overturning circulation, the “geological” contribution to reduced pH and increased pCO₂ in upwelling regions would therefore be negligible.

If they existed, submarine geological carbon sources (in the form of bicarbonate) could therefore be important for certain deglacial radiocarbon records, and perhaps for global carbon budgets over long time-spans via impacts on alkalinity, but not for deglacial atmospheric CO₂ change. The suggestion that a local volcanic input may be detected in sea floor sediments, and indeed seawater, without this input representing a major influence on the global radiocarbon distribution and budget, is hinted at by high resolution and high precision hydrographic measurements from the modern East Pacific rise (Jenkins et al., 2018). Such geological sources of carbon to the ocean interior are surely important for refining our understanding of the chemical inventories of the ocean; but they are too small to leave their mark on the global pattern of radiocarbon ventilation ages in the modern ocean (Broecker & Peng, 1982; Key et al., 2004). The latter are overwhelmingly controlled by air-sea gas exchange at the sea surface, and transports in the ocean interior (Koeve et al., 2015).

Accounting for the timing of the proposed volcanic contributions presents a further puzzle, since deglacial ice-volume and sea level changes (which were initiated ~19 ka BP [Lambeck & Chappell, 2001]) could not have triggered the submarine volcanic/metamorphic CO₂ release that are proposed to have occurred well before the LGM, and at least as early as 25 ka BP in some places (Ronge et al., 2016; Stott et al., 2019). Indeed, increased submarine volcanism would not be triggered by glacioeustatic sea level rise at all, but rather by glacioeustatic sea level *fall* (in opposition to subaerial volcanism) (Huybers & Langmuir, 2017). Any geological carbon release related to submarine volcanism during deglaciation would therefore need to reflect a rather auspiciously delayed response to sea level drop during the onset of glaciation before the LGM (Huybers & Langmuir, 2017), perhaps ~32 ka BP (Grant et al., 2012), or ~22 ka BP (Yokoyama et al., 2018). An alternative to the volcanic mechanism is the proposal of a CO₂-hydrate “capacitor,” possibly regulated by deep water temperature change (since increasing sea-level and pressure would on the contrary stabilize clathrates during deglaciation) (Stott et al., 2019). Although the details of this purely hypothetical mechanism have yet to be worked out, it would have the advantage of allowing geological carbon release to be linked more directly to local deglacial climatic/hydrographic triggers, rather than global glacioeustatic sea level.

The identification of extreme radiocarbon depletions at various locations and at various times between ~25 and 10 ka BP, might be taken to represent a “fly in the ointment” for the canonical account of deglacial marine radiocarbon change as primarily a story of evolving ocean circulation and air-sea gas exchange. Given the great efforts that have gone into assessing and replicating the evidence at various locations (e.g., Lindsay et al., 2015, 2016; Marchitto et al., 2007; Rafter et al., 2019), and in trying to place some of these results into an explicit geological

context (e.g., Stott et al., 2019), the evidence cannot be cast aside lightly. Indeed, a “geological” contribution to deglacial radiocarbon evolution in the marine *sedimentary* environment appears to be an incontrovertible conclusion at a few locations (Bova et al., 2018; Rafter et al., 2019; Stott et al., 2009, 2019). However, the further inference of a significant contribution from geological carbon sources to the ocean's dissolved inorganic carbon pool, seems more difficult to defend. This conclusion is supported in respect of the “global ocean” by the bulk of available data from the LGM (e.g., Skinner et al., 2017), and assembled here for the last deglaciation (Figures 13, 14, and 16). In respect of intermediate waters in the eastern low-latitude Pacific, it is further supported by U-series dated corals, from 627 m water depth on the Galapagos plateau (Chen et al., 2020), which show no evidence for extreme radiocarbon depletion in a region that is currently influenced by AAIW (stars in Figure 17f). As shown in Figure 15, these data exhibit a similar trend to coral data from the Southern Ocean (Burke & Robinson, 2012; Chen et al., 2015; Li et al., 2020), consistent with the expected preponderance of southern sourced mode waters in both of these locations, as in the modern ocean (Fiedler & Talley, 2006). The collected evidence therefore suggests that extreme radiocarbon depletion observed in benthic and planktonic foraminifera at several locations at the LGM and across the last deglaciation most likely reflects the influence of geological carbon sources on the *sedimentary* environment in which the foraminifera lived or were deposited, rather than the ocean interior per se.

Even if perceived as a “red herring,” as far as the main controls on deglacial carbon cycle evolution are concerned, the issue of geological carbon sources and their contribution to extreme radiocarbon depletion during deglaciation may yet serve as a useful tonic for our canonical account of Pleistocene carbon cycle dynamics. In this regard, it is interesting to note that glacial-interglacial variation of (subaerial) volcanic CO₂ flux, equivalent to ~30% of long-term average global emission rate, has emerged as an important “tuning parameter” (i.e., one that is adjusted to keep the surface carbon budgets balanced over time) in numerical model simulations of glacial-interglacial CO₂ that are forced only by insolation pacing of Earth system feedbacks (Ganopolski & Brovkin, 2017). The importance of sedimentation and sediment-seawater/pore-water interactions has also been underlined in modeling studies that implement sediment-modules and treat the joint ocean-atmosphere carbon reservoir as an “open” system (e.g., Tschumi et al., 2011). Something of a “geological turn” in emerging accounts of glacial-interglacial carbon cycle change is therefore apparent (Broecker et al., 2015; Ganopolski & Brovkin, 2017), and is arguably warranted, since the ocean-atmosphere system does not form a “closed” carbon budget on timescales longer than a few millennia (Jeltsch-Thömmes & Joos, 2020). Nevertheless, it seems clear that glacial-interglacial CO₂ and deglacial marine radiocarbon evolution is not either a simple story of solid Earth dynamics: the submarine (as opposed to sub-aerial) “geological” contribution to deglacial atmospheric CO₂ rise seems particularly challenging to explain when consideration is given to carbonate chemistry constraints, as well as the precise timing and structure of CO₂ changes. This includes their consistent link with the interhemispheric “bipolar seesaw” pattern, and associated changes in the AMOC, sea ice and ocean interior oxygenation for example (Gottschalk et al., 2016, 2019; Henry et al., 2016; Jaccard et al., 2016; Schüpbach et al., 2018). Identifying a “geological” contribution to global radiocarbon- and carbon cycle changes across glacial cycles, acting in parallel with the already well-defined (if also poorly quantified) contribution from the biological pump and air-sea gas exchange (Galbraith & Skinner, 2020), remains a further challenge for the future. Progress in addressing this challenge will benefit from a more detailed elucidation of the spatial and temporal evolution of seawater and sedimentary/authigenic-phase radiocarbon activities since the late glacial, in particular as a means of constraining isotope enabled numerical model scenarios that include carbonate chemistry and sedimentary fluxes.

6. Summary and Outlook

Radiocarbon is a particularly useful tool for the geosciences, applicable as a diagnostic carbon cycle tracer in paleoceanographic studies and in numerical models, and under certain circumstances as a radiometric dating tool extending to ~50 ka BP. A radiocarbon measurement performed on a single fossil entity can be used for one of three purposes (assuming that the fossil was in equilibrium with its parent reservoir at the time of formation):

1. to determine the radiocarbon activity of the fossil's parent reservoir at the time it formed, requiring knowledge of the true calendar age of the fossil entity;
2. to determine the time of formation of the fossil entity (i.e., its calendar age), requiring knowledge of the radiocarbon activity of its parent reservoir, and how it evolved over time;

3. to determine the extent of disequilibrium between the fossil entity's parent reservoir, at the time of the fossil entity's formation, relative to another contemporaneous reservoir (e.g., the ocean relative to the atmosphere at 19 ka BP, etc.).

The use of radiocarbon as a dating tool is severely limited by: past radiocarbon production changes; past changes in the exchange rates between the various Earth surface reservoirs; and variability within reservoirs, such as the ocean in particular. Uncertainty regarding past “marine reservoir ages” currently represents a major impediment to accurate calendar age dating of marine fossils using radiocarbon.

A further significant challenge that has been emphasized by the development of gas-source AMS capable of measuring very small carbon samples, is the elucidation of life-habit and taphonomic biases that may affect all fossil entities in the geological record. In this context, a pragmatic balance must be struck between cognizance of the distracting noise and bias that may plague radiocarbon data, versus the underlying signals that are informative, where “noise” and “signal” will always be defined relative to a particular question of interest.

Reliable (proxy) measurements of the radiocarbon activity of a parcel of water in the ocean interior will reflect the combined effects of variable radiocarbon production, the radiocarbon distribution at the sea surface and the transport trajectories and transit times for water moving through the ocean interior (Koeve et al., 2015), with minor contributions from newly remineralized (“old”) DOC and (“young”) organic carbon and biogenic carbonate (Walker et al., 2016). Marine radiocarbon activity therefore includes primarily the combined effects of air-sea gas exchange, ocean transport, and mixing; it does not provide a straightforward and immediate measure of water transit times.

Through its link to the ocean's disequilibrium- and respired carbon inventories (both relatively depleted in radiocarbon as compared to the atmosphere), marine radiocarbon maintains an intimate link with ocean-atmosphere carbon partitioning, and therefore the ocean's potential role in atmospheric CO₂ change. A larger sequestered carbon inventory in the ocean will typically imply a more radiocarbon depleted marine carbon reservoir, though this link will be modulated by ocean carbonate chemistry and marine biology.

Understanding and interpreting marine radiocarbon as a carbon cycle tracer still has much to gain from the implementation of this isotope in numerical models. Particularly promising areas of development are in the use of “offline” or “transport matrix” methods for efficiently resolving equilibrium solutions that would otherwise require very long integration times (Bardin et al., 2014; Khatiwala et al., 2005), as well as the development of “inverse methods” for application to radiocarbon in combination with other independent tracers (LeGrand & Wunsch, 1995). Due to the relatively short half-life of radiocarbon, its use in paleoceanography is restricted to the latter half of the last glacial cycle. In this context, most work has so far focused on the LGM and the last deglaciation. The analytically challenging, yet potentially rewarding, investigation of marine radiocarbon prior to the LGM represents an apparent gap to be filled. Similarly, detailed studies of marine radiocarbon evolution across the Holocene remain sparse, particularly for the deep ocean.

The great bulk of work looking at the distribution of radiocarbon in the past ocean has focused on the LGM (~20 ka BP), when atmospheric CO₂ was ~90 ppm lower than pre-industrial, and a very different climate state prevailed. The accumulated results demonstrate a significant “aging” of the ocean interior relative to the contemporary atmosphere (especially >2,000 m water depth, and by perhaps more than ~600 ¹⁴C yrs equivalent on average [Skinner et al., 2017]), thus supporting a role for ocean “ventilation” in CO₂ drawdown at the LGM, where ventilation is defined as including impacts on *both* disequilibrium- and respired carbon (i.e., gas exchange and ocean overturning rates [Galbraith & Skinner, 2020]). Although contributions to CO₂ drawdown at the LGM due to gas-exchange and ocean overturning are both supported by existing observations, determining their relative contributions remains a key challenge to address. The use of numerical models to this end will require that emphasis is placed on assessing changes in the “preformed” radiocarbon signatures of water in the ocean interior, in order to separate gas-exchange versus transport influences on radiocarbon and carbon sequestration (Eggleston & Galbraith, 2018). Surface reservoir age offsets, thus emerge as a particularly important target for reconstruction (Skinner, Muschitiello, & Scrivner, 2019), and for simulation (Butzin et al., 2017).

A long-standing overarching challenge remains to fully reconcile past atmospheric radiocarbon variability with reconstructed changes in radiocarbon production rates, and evolving marine radiocarbon activity (Dinauer et al., 2020). This challenge provides a stringent test, and an excellent training ground, for our understanding

of global carbon cycle evolution over the last glacial cycle, as it requires accurate and consistent descriptions of radionuclide production, ocean ventilation, terrestrial biomass evolution, and marine sedimentation. The eventual reconciliation of marine- and atmospheric radiocarbon change across the last deglaciation (since ~20 ka BP), has a direct bearing on the causes of natural atmospheric CO₂ variability, including 10–40 ppm centennial/millennial scale “jumps,” and the longer-term drift of CO₂ across recurrent glacial cycles that might arise from “open system” effects (Chalk et al., 2017; Hönlisch et al., 2009).

Existing marine radiocarbon data suggest that the ocean's role in atmospheric CO₂ rise across the last deglaciation involved a pair of “ventilation seesaws” (between the North Atlantic and Southern Ocean [Broecker, 1998; Menviel et al., 2018; Skinner et al., 2014], and between the North Atlantic and North Pacific [Freeman et al., 2015; Max et al., 2014; Menviel et al., 2014; Okazaki et al., 2010]), as well as a pair of “mode changes” (in Southern Ocean convection from the onset of HS1 [Skinner et al., 2010], and in the AMOC from the onset of the B-A [Barker et al., 2010; Chen et al., 2015; Robinson et al., 2005; Skinner et al., 2013]). These “ventilation seesaws” and “step changes” were intimately connected to AMOC perturbations, through the thermal bipolar seesaw and its globally distributed impacts. The Pacific, and especially the Indian basin, stand out as major observational gaps to fill. Intermediate depths (900–2,000 m) in these basins may deserve special attention as potentially the primary locus for enhanced ocean-atmosphere equilibration and the exchange of carbon, and heat, during periods of “bipolar seesaw” activation (Baggenstos et al., 2019; Skinner et al., 2020).

A further major challenge that stands out in the context of deglacial radiocarbon evolution is an elucidation of the origin and carbon cycle implications of “extreme” radiocarbon depletions that have been observed between ~25 and ~10 ka BP at a number of sites. A dominant theory is that these represent radiocarbon-dead “geological” carbon injection at different times and at various locations on the sea floor (Rafter et al., 2019; Stott et al., 2019). However, the reconciliation of such a carbon source with marine carbonate preservation constraints seems to ensure that, even if it existed, it would have made little contribution to deglacial CO₂ rise. Furthermore, emerging coral radiocarbon data strongly question the validity of the foraminifer-based reconstructions as representative of ocean interior, as opposed to sedimentary/pore-water, phenomena (Chen et al., 2020). It therefore seems likely that the extreme radiocarbon depletions, at best, represent the impacts of “isotopic smoking guns” associated with small and localized geological carbon sources. Such radiocarbon-dead geological carbon sources can be observed, albeit with difficulty, in the modern ocean (Jenkins et al., 2018). Nevertheless, the apparent variability of such geological carbon sources, and their coordination with glacial-interglacial hydrographic and/or glacioeustatic change, underlines the importance of “open system” effects for the evolving alkalinity, carbon and radiocarbon budgets of the ocean-atmosphere system across recurrent glacial cycles.

In the 60 years since Willard Libby was awarded the Nobel Prize in chemistry “for his method to use carbon-14 for age determination in archeology, geology, geophysics, and other branches of science”, radiocarbon has proven to be far more useful than as just a dating tool. Far from having already borne its most significant intellectual fruits, radiocarbon is arguably a geochemical tracer that is poised to yield transformative progress throughout the geosciences. Annually resolved records of atmospheric radiocarbon are changing our understanding of solar dynamics (Miyake et al., 2013), and helping to improve even our best chronologies (Adolphi et al., 2018); novel analytical techniques are opening up new possibilities for high-resolution component/micro-analysis (Fagault et al., 2019; Wacker et al., 2013); a diversity of proposals regarding past radiocarbon production changes (Channell et al., 2018), as well as new reconstructions of past atmospheric radiocarbon (Cheng et al., 2018), have reset the stage for understanding the geodynamo and the biogeochemical influence of evolving sedimentary carbon fluxes; and ongoing careful data collection continues to shine new light on the multi-faceted role of the ocean as a regulator of atmospheric CO₂, emphasizing its physical transports as well as its climatically sensitive exchanges with both the atmosphere and the solid Earth. Much has yet to be learned about the Earth system through the use of this unique radio-isotope.

Data Availability Statement

No new data were used in the review article, which is based on existing data from previously published sources. The sources of the published data used in the figures, and included in supplementary Table S1, are detailed in the relevant figure captions.

Acknowledgments

The authors are deeply indebted to many colleagues who have helped improve this review, through comments and discussion, and who have made available their data and model outputs for inclusion in figures. The authors are grateful for the inspiration provided, in different ways, by the late Nick Shackleton and the late Wally Broecker. Tom Marchitto, Piet Grootes, and two anonymous reviewers are thanked for their insightful and critical comments, which helped to improve an earlier draft of this review. The authors are indebted to Eric Galbraith and Francois Primeau for input on numerical modeling of radiocarbon, as well as Laurie Menviel, Peter Köhler, Mathis Hain, Ayako Abe-Ouchi, Megumi Chikamoto, Fortunat Joos, Andreas Schmittner, Juan Muglia, Samar Khattiwala, Ashley Dinauer, Andy Ridgwell, Guillaume Soulet, Maria de la Fuente, and a great number of other paleoceanographer colleagues for the provision of model outputs, data, and discussion. This review benefited from stimulating discussions during INQUA IPODS, PAGES OC3, and Lcal marine working group meetings. L. C. Skinner acknowledges funding from the Royal Society, the Isaac Newton Trust, and NERC grant NE/L006240/1, which supported data collection that has informed this review. E. Bard is supported at CEREGE by EQUIPEX ASTER-CE-REGE and ANR MARCARA.

References

- Adkins, J. F. (2013). The role of deep ocean circulation in setting glacial climates. *Paleoceanography*, 28, 539–561. <https://doi.org/10.1002/palo.20046>
- Adkins, J. F., & Boyle, E. A. (1997). Changing atmospheric $\Delta^{14}\text{C}$ and the record of deep water paleoventilation ages. *Paleoceanography*, 12(3), 337–344. <https://doi.org/10.1029/97pa00379>
- Adkins, J. F., Cheng, H., Boyle, E. A., Druffel, E. R. M., & Edwards, R. L. (1998). Deep-sea coral evidence for rapid change in ventilation of the deep North Atlantic 15,400 years ago. *Science*, 280, 725–728. <https://doi.org/10.1126/science.280.5364.725>
- Adolphi, F., Bronk Ramsey, C., Erhardt, T., Edwards, R. L., Cheng, H., Turney, C. S., et al. (2018). Connecting the Greenland ice-core and U/Th timescales via cosmogenic radionuclides: Testing the synchronicity of Dansgaard–Oeschger events. *Climate of the Past*, 14(11), 1755–1781. <https://doi.org/10.5194/cp-14-1755-2018>
- Ahagon, N., Ohkushi, K., Uchida, M., & Mishima, T. (2003). Mid-depth circulation in the northwest Pacific during the last deglaciation: Evidence from foraminiferal radiocarbon ages. *Geophysical Research Letters*, 30(21). <https://doi.org/10.1029/2003gl018287>
- Ahn, J., & Brook, E. J. (2008). Atmospheric CO_2 and climate on millennial time scales during the last glacial period. *Science*, 322, 83–85. <https://doi.org/10.1126/science.1160832>
- Allen, K. A., Sikes, E. L., Anderson, R. F., & Rosenthal, Y. (2020). Rapid loss of CO_2 from the South Pacific Ocean during the last glacial termination. *Paleoceanography and Paleoclimatology*, 35(2), e2019PA003766. <https://doi.org/10.1029/2019PA003766>
- Allen, K. A., Sikes, E. L., Honisch, B., Elmore, A. C., Guilderson, T. P., Rosenthal, Y., & Anderson, R. F. (2015). Southwest Pacific deep water carbonate chemistry linked to high southern latitude climate and atmospheric CO_2 during the Last Glacial Termination. *Quaternary Science Reviews*, 122, 180–191. <https://doi.org/10.1016/j.quascirev.2015.05.007>
- Anderson, R. F., Ali, S., Bradtmiller, L. I., Nielsen, S. H. H., Fleisher, M. Q., Anderson, B. E., & Burckle, L. H. (2009). Wind-driven upwelling in the Southern Ocean and the deglacial rise in atmospheric CO_2 . *Science*, 323, 1443–1448. <https://doi.org/10.1126/science.1167441>
- Anderson, R. F., Sachs, J. P., Fleisher, M. Q., Allen, K. A., Yu, J., Koutavas, A., & Jaccard, S. L. (2019). Deep-sea oxygen depletion and ocean carbon sequestration during the last ice age. *Global Biogeochemical Cycles*, 33(3), 301–317. <https://doi.org/10.1029/2018gb006049>
- Arnold, J. A., & Anderson, E. C. (1957). The distribution of carbon-14 in nature. *Tellus*, 9(1), 28–32. <https://doi.org/10.1111/j.2153-3490.1957.tb01850.x>
- Ausin, B., Haghypour, N., Wacker, L., Voelker, A. H. L., Hodell, D., Magill, C., et al. (2019). Radiocarbon age offsets between two surface dwelling planktonic foraminifera species during abrupt climate events in the SW Iberian margin. *Paleoceanography and Paleoclimatology*, 34(1), 63–78. <https://doi.org/10.1029/2018pa003490>
- Ausin, B., Sarnthein, M., & Haghypour, N. (2021). Glacial-to-deglacial reservoir and ventilation ages on the southwest Iberian continental margin. *Quaternary Science Reviews*, 255, 106818. <https://doi.org/10.1016/j.quascirev.2021.106818>
- Austin, W. E. N., Telford, R. J., Ninnemann, U. S., Brown, L., Wilson, L. J., Small, D. P., & Bryant, C. L. (2011). North Atlantic reservoir ages linked to high Younger Dryas atmospheric radiocarbon concentrations. *Global and Planetary Change*, 79(3), 226–233. <https://doi.org/10.1016/j.gloplacha.2011.06.011>
- Baggenstos, D., Häberli, M., Schmitt, J., Shackleton, S. A., Birner, B., Severinghaus, J. P., et al. (2019). Earth's radiative imbalance from the Last Glacial Maximum to the present. *Proceedings of the National Academy of Sciences*, 116(30), 14881–14886. <https://doi.org/10.1073/pnas.1905447116>
- Balmer, S., Sarnthein, M., Mudelsee, M., & Grootes, P. M. (2016). Refined modeling and ^{14}C plateau tuning reveal consistent patterns of glacial and deglacial ^{14}C reservoir ages of surface waters in low-latitude Atlantic. *Paleoceanography*, 31(8), 1030–1040. <https://doi.org/10.1002/2016PA002953>
- Bard, E. (1988). Correction of accelerator mass spectrometry ^{14}C ages measured in planktonic foraminifera: Paleoceanographic implications. *Paleoceanography*, 3(6), 635–645. <https://doi.org/10.1029/pa003i006p00635>
- Bard, E. (1998). Geochemical and geophysical implications of the radiocarbon calibration. *Geochimica et Cosmochimica Acta*, 62(12), 2025–2038. [https://doi.org/10.1016/s0016-7037\(98\)00130-6](https://doi.org/10.1016/s0016-7037(98)00130-6)
- Bard, E., Arnold, M., Duprat, J., Moyes, J., & Duplessy, J.-C. (1987). Reconstruction of the last deglaciation: Deconvolved records of $\delta^{18}\text{O}$ profiles, micropalaeontological variations and accelerator mass spectrometric ^{14}C dating. *Climate Dynamics*, 1, 101–112. <https://doi.org/10.1007/bf01054479>
- Bard, E., Arnold, M., Hamelin, B., Tisnerat-Laborde, N., & Cabioche, G. (1998). Radiocarbon calibration by means of mass spectrometric $^{230}\text{Th}/^{234}\text{U}$ and ^{14}C ages of corals: An updated database including samples from Barbados, Mururoa and Tahiti. *Radiocarbon*, 40(3), 1085–1092. <https://doi.org/10.1017/s0033822200019135>
- Bard, E., Arnold, M., Mangerud, J., Paterne, M., Labeyrie, L., Duprat, J., et al. (1994). The North Atlantic atmosphere-sea surface ^{14}C gradient during the Younger Dryas climatic event. *Earth and Planetary Science Letters*, 126, 275–287. [https://doi.org/10.1016/0012-821x\(94\)90112-0](https://doi.org/10.1016/0012-821x(94)90112-0)
- Bard, E., Arnold, M., Östlund, H. G., Maurice, P., Monfray, P., & Duplessy, J.-C. (1988). Penetration of bomb radiocarbon in the tropical Indian Ocean measured by means of accelerator mass spectrometry. *Earth and Planetary Science Letters*, 87(4), 379–389. [https://doi.org/10.1016/0012-821x\(88\)90002-7](https://doi.org/10.1016/0012-821x(88)90002-7)
- Bard, E., Hamelin, B., Fairbanks, R. G., & Zindler, A. (1990). Calibration of the ^{14}C timescale over the past 30,000 years using mass spectrometric U-Th ages from Barbados corals. *Nature*, 345, 405–410. <https://doi.org/10.1038/345405a0>
- Bard, E., & Heaton, T. J. (2021). On the tuning of plateaus in atmospheric and oceanic ^{14}C records to derive calendar chronologies of deep-sea cores and records of ^{14}C marine reservoir age changes. *Climate of the Past Discussions*, 2021, 1–36. <https://doi.org/10.5194/cp-2020-164>
- Bard, E., Ménot, G., Rostek, F., Licari, L., Böning, P., Edwards, R. L., et al. (2013). Radiocarbon calibration/comparison records based on marine sediments from the Pakistan and Iberian margins. *Radiocarbon*, 55(4), 1999–2019. https://doi.org/10.2458/azu_js_rc.55.17114
- Bard, E., Rostek, F., & Menot-Combes, G. (2004). A better radiocarbon clock. *Science*, 303, 178–179. <https://doi.org/10.1126/science.1091964>
- Bard, E., Rostek, F., Turon, J.-L., & Gendreau, S. (2000). Hydrological impact of Heinrich events in the subtropical Northeast Atlantic. *Science*, 289(5483), 1321–1324. <https://doi.org/10.1126/science.289.5483.1321>
- Bard, E., Tuna, T., Fagault, Y., Bonvalot, L., Wacker, L., Fahrni, S., & Synal, H.-A. (2015). AixMICADAS, the accelerator mass spectrometer dedicated to ^{14}C recently installed in Aix-en-Provence, France. *Nuclear Instruments and Methods in Physics Research Section B: Beam Interactions with Materials and Atoms*, 361, 80–86. <https://doi.org/10.1016/j.nimb.2015.01.075>
- Bardin, A., Primeau, F., & Lindsay, K. (2014). An offline implicit solver for simulating prebomb radiocarbon. *Ocean Modelling*, 73, 45–58. <https://doi.org/10.1016/j.ocemod.2013.09.008>
- Barker, S., Broecker, W., Clark, E., & Hajdas, I. (2007). Radiocarbon age offsets of foraminifera resulting from differential dissolution and fragmentation within the sedimentary bioturbated zone. *Paleoceanography*, 22, 1–11. <https://doi.org/10.1029/2006pa001354>

- Barker, S., Diz, P., Vautravers, M., Pike, J., Knorr, G., Hall, I. R., & Broecker, W. (2009). Interhemispheric Atlantic seesaw response during the last deglaciation. *Nature*, 457, 1097–1102. <https://doi.org/10.1038/nature07770>
- Barker, S., Knorr, G., Conn, S., Lordsmith, S., Newman, D., & Thornalley, D. (2019). Early interglacial legacy of deglacial climate instability. *Paleoceanography and Paleoclimatology*, 34(8), 1455–1475. <https://doi.org/10.1029/2019pa003661>
- Barker, S., Knorr, G., Vautravers, M., Diz, P., & Skinner, L. C. (2010). Extreme deepening of the Atlantic overturning circulation during deglaciation. *Nature Geoscience*, 3, 567–571. <https://doi.org/10.1038/NGEO921>
- Bauska, T. K., Baggenstos, D., Brook, E. J., Mix, A. C., Marcott, S. A., Petrenko, V. V., et al. (2016). Carbon isotopes characterize rapid changes in atmospheric carbon dioxide during the last deglaciation. *Proceedings of the National Academy of Sciences*, 113(13), 3465–3470. <https://doi.org/10.1073/pnas.1513868113>
- Bauska, T. K., Marcott, S. A., & Brook, E. J. (2021). Abrupt changes in the global carbon cycle during the last glacial period. *Nature Geoscience*, 14(2), 91–96. <https://doi.org/10.1038/s41561-020-00680-2>
- Beer, J., Siegenthaler, U., Bonani, G., Finkel, R. C., Oeschger, H., Suter, M., & Wölfli, W. (1988). Information on past solar activity and geomagnetism from ^{10}Be in the Camp Century ice core. *Nature*, 331(6158), 675–679. <https://doi.org/10.1038/331675a0>
- Bella, F., Alessio, M., & Fratelli, P. (1968). A determination of the half-life of ^{14}C . *Il Nuovo Cimento B (1965–1970)*, 58(1), 232–246. <https://doi.org/10.1007/bf02711792>
- Björck, S., Walker, M. J. C., Cwynar, L. C., Johnsen, S., Knudsen, K.-L., Lowe, J. J., & Wohlfarth, B. (1998). An event stratigraphy for the Last Termination in the North Atlantic region based on the Greenland ice-core record: A proposal by the INTIMATE group. *Journal of Quaternary Science*, 13(4), 283–292.
- Bolin, B., & Rodhe, H. (1973). A note on the concepts of age distribution and transit time in natural reservoirs. *Tellus*, 25(1), 58–62. <https://doi.org/10.1111/j.2153-3490.1973.tb01594.x>
- Bova, S. C., Herbert, T. D., & Altabet, M. A. (2018). Ventilation of northern and southern sources of aged carbon in the eastern equatorial Pacific during the Younger Dryas rise in atmospheric CO_2 . *Paleoceanography and Paleoclimatology*, 33(11), 1151–1168. <https://doi.org/10.1029/2018pa003386>
- Boyle, E. A. (1988). The role of vertical fractionation in controlling late Quaternary atmospheric carbon dioxide. *Journal of Geophysical Research*, 93(C12), 15701–15714. <https://doi.org/10.1029/jc093ic12p15701>
- Boyle, E. A., & Keigwin, L. D. (1985). Comparison of Atlantic and Pacific paleochemical records for the last 215,000 years: Changes in deep ocean circulation and chemical inventories. *Earth and Planetary Science Letters*, 76, 135–150. [https://doi.org/10.1016/0012-821x\(85\)90154-2](https://doi.org/10.1016/0012-821x(85)90154-2)
- Boyle, E. A., & Keigwin, L. D. (1987). North Atlantic thermohaline circulation during the last 20,000 years linked to high latitude surface temperature. *Nature*, 330, 35–40. <https://doi.org/10.1038/330035a0>
- Bradtmiller, L. I., McManus, J. F., & Robinson, L. F. (2014). $^{231}\text{Pa}/^{230}\text{Th}$ evidence for a weakened but persistent Atlantic meridional overturning circulation during Heinrich Stadial 1. *Nature Communications*, 5, 5817. <https://doi.org/10.1038/ncomms6817>
- Brazunias, T., Fung, I. Y., & Stuiver, M. (1995). The preindustrial atmospheric $^{14}\text{CO}_2$ latitudinal gradient as related to exchanges among atmospheric, oceanic, and terrestrial reservoirs. *Global Biogeochemical Cycles*, 9(4), 565–584.
- Broecker, W., Andree, M., Bonani, G., Wolfli, W., Klas, M., Mix, A., & Oeschger, H. (1988). Comparison between radiocarbon ages obtained on coexisting planktonic foraminifera. *Paleoceanography*, 3(6), 647–657. <https://doi.org/10.1029/pa003i006p00647>
- Broecker, W., Andree, M., Bonani, G., Wolfli, W., Oeschger, H., Klas, M., et al. (1988). Preliminary estimates for the radiocarbon age of deep water in the glacial ocean. *Paleoceanography*, 3(6), 659–669. <https://doi.org/10.1029/pa003i006p00659>
- Broecker, W., & Barker, S. (2007). A 190 permil drop in atmosphere's $\Delta^{14}\text{C}$ during the "Mystery Interval" (17.5 to 14.5 kyr). *Earth and Planetary Science Letters*, 256, 90–99. <https://doi.org/10.1016/j.epsl.2007.01.015>
- Broecker, W., Barker, S., Clark, E., Hajdas, I., Bonani, G., & Stott, L. (2004). Ventilation of glacial deep Pacific Ocean. *Science*, 306, 1169–1172. <https://doi.org/10.1126/science.1102293>
- Broecker, W., & Clark, E. (2011). Radiocarbon-age differences among coexisting planktic foraminifera shells: The Barker effect. *Paleoceanography*, 26(2). <https://doi.org/10.1029/2011PA002116>
- Broecker, W., Clark, E., & Barker, S. (2008). Near constancy of the Pacific Ocean surface to mid-depth radiocarbon-age difference over the last 20 kyr. *Earth and Planetary Science Letters*, 274, 322–326. <https://doi.org/10.1016/j.epsl.2008.07.035>
- Broecker, W., Clark, E., Barker, S., Hajdas, I., Bonani, G., & Moreno, E. (2007). Radiocarbon age of late glacial deep water from the equatorial Pacific. *Paleoceanography*, 22, 1–6. <https://doi.org/10.1029/2006pa001359>
- Broecker, W., & Peng, T.-H. (1974). Gas exchange rates between air and sea. *Tellus*, 26(1–2), 21–35. <https://doi.org/10.3402/tellusa.v26i1-2.9733>
- Broecker, W., & Putnam, A. E. (2012). How did the hydrologic cycle respond to the two-phase mystery interval? *Quaternary Science Reviews*, 57, 17–25. <https://doi.org/10.1016/j.quascirev.2012.09.024>
- Broecker, W. S. (1989). Some thoughts about the radiocarbon budget for the glacial Atlantic. *Paleoceanography*, 4(2), 213–220. <https://doi.org/10.1029/pa004i002p00213>
- Broecker, W. S. (1998). Palaeocean circulation during the last deglaciation: A bipolar seesaw? *Paleoceanography*, 13, 119–121. <https://doi.org/10.1029/97pa03707>
- Broecker, W. S., Clark, E., Hajdas, I., & Bonani, G. (2004). Glacial ventilation rates for the deep Pacific Ocean. *Paleoceanography*, 19. <https://doi.org/10.1029/2003pa000974>
- Broecker, W. S., McGee, D., Adams, K. D., Cheng, H., Edwards, R. L., Oviatt, C. G., & Quade, J. (2009). A Great Basin-wide dry episode during the first half of the Mystery Interval? *Quaternary Science Reviews*, 28(25), 2557–2563. <https://doi.org/10.1016/j.quascirev.2009.07.007>
- Broecker, W. S., Mix, A., Andree, M., & Oeschger, H. (1984). Radiocarbon measurements on coexisting benthic and planktonic foraminifera shells: Potential for reconstructing ocean ventilation times over the past 20,000 years. *Nuclear Instruments & Methods in Physics Research, Section B*, 5, 331–339. [https://doi.org/10.1016/0168-583x\(84\)90538-x](https://doi.org/10.1016/0168-583x(84)90538-x)
- Broecker, W. S., & Peng, T. H. (1982). *Tracers in the sea* (p. 690). Eldigio Press.
- Broecker, W. S., Peng, T. H., Trumbore, S., Bonani, G., & Wolfli, W. (1990). The distribution of radiocarbon in the glacial ocean. *Global Biogeochemical Cycles*, 4, 103–117. <https://doi.org/10.1029/gb004i001p0103>
- Broecker, W. S., Yu, J., & Putnam, A. E. (2015). Two contributors to the glacial CO_2 decline. *Earth and Planetary Science Letters*, 429, 191–196. <https://doi.org/10.1016/j.epsl.2015.07.019>
- Bronk Ramsey, C., Staff, R. A., Bryant, C. L., Brock, F., Kitagawa, H., van der Plicht, J., et al. (2012). A complete terrestrial radiocarbon record for 11.2 to 52.8 kyr B.P. *Science*, 338(6105), 370–374. <https://doi.org/10.1126/science.1226660>
- Brovkin, V., Bendtsen, J., Claussen, M., Ganopolski, A., Kubatzki, C., Petoukhov, V., & Andreev, A. (2002). Carbon cycle, vegetation, and climate dynamics in the Holocene: Experiments with the CLIMBER-2 model. *Global Biogeochemical Cycles*, 16(4), 86–18620. <https://doi.org/10.1029/2001GB001662>

- Brovkin, V., Ganopolski, A., Archer, D., & Munhoven, G. (2012). Glacial CO₂ cycle as a succession of key physical and biogeochemical processes. *Climate of the Past*, 8, 251–264. <https://doi.org/10.5194/cp-8-251-2012>
- Bryan, S. P., Marchitto, T. M., & Lehman, S. J. (2010). The release of ¹⁴C-depleted carbon from the deep ocean during the last deglaciation: Evidence from the Arabian Sea. *Earth and Planetary Science Letters*, 298(1–2), 244–254. <https://doi.org/10.1016/j.epsl.2010.08.025>
- Burke, A., & Robinson, L. F. (2012). The Southern Ocean's role in carbon exchange during the last deglaciation. *Science*, 335, 557–561. <https://doi.org/10.1126/science.1208163>
- Burke, A., Stewart, A. L., Adkins, J. F., Ferrari, R., Jansen, M. F., & Thompson, A. F. (2015). The glacial mid-depth radiocarbon bulge and its implications for the overturning circulation. *Paleoceanography*, 30(7), 1021–1039. <https://doi.org/10.1002/2015pa002778>
- Butzin, M., Köhler, P., & Lohmann, G. (2017). Marine radiocarbon reservoir age simulations for the past 50,000 years. *Geophysical Research Letters*, 44(16), 8473–8480. <https://doi.org/10.1002/2017GL074688>
- Butzin, M., Prange, M., & Lohmann, G. (2005). Radiocarbon simulations for the glacial ocean: The effects of wind stress, Southern Ocean sea ice and Heinrich events. *Earth and Planetary Science Letters*, 235, 45–61. <https://doi.org/10.1016/j.epsl.2005.03.003>
- Cao, L., Fairbanks, R. G., Mortlock, R. A., & Risk, M. J. (2007). Radiocarbon reservoir age of high latitude North Atlantic surface water during the last deglacial. *Quaternary Science Reviews*, 26(5), 732–742. <https://doi.org/10.1016/j.quascirev.2006.10.001>
- Capano, M., Miramont, C., Guibal, F., Kromer, B., Tuna, T., Fagault, Y., & Bard, E. (2017). Wood ¹⁴C dating with AixMICADAS: Methods and application to tree-ring sequences from the Younger Dryas Event in the southern French Alps. *Radiocarbon*, 60(1), 51–74. <https://doi.org/10.1017/RDC.2017.83>
- Capano, M., Miramont, C., Shindo, L., Guibal, F., Marschal, C., Kromer, B., et al. (2019). Onset of the Younger Dryas recorded with ¹⁴C at annual resolution in French subfossil trees. *Radiocarbon*, 62(4), 901–918. <https://doi.org/10.1017/RDC.2019.116>
- Cartapanis, O., Galbraith, E. D., Bianchi, D., & Jaccard, S. L. (2018). Carbon burial in deep-sea sediment and implications for oceanic inventories of carbon and alkalinity over the last glacial cycle. *Climate of the Past*, 14(11), 1819–1850. <https://doi.org/10.5194/cp-14-1819-2018>
- Chalk, T. B., Hain, M. P., Foster, G. L., Rohling, E. J., Sexton, P. F., Badger, M. P. S., et al. (2017). Causes of ice age intensification across the Mid-Pleistocene Transition. *Proceedings of the National Academy of Sciences*, 114(50), 13114–13119. <https://doi.org/10.1073/pnas.1702143114>
- Channell, J. E. T., Hodell, D. A., Crowhurst, S. J., Skinner, L. C., & Muscheler, R. (2018). Relative paleointensity (RPI) in the latest Pleistocene (10–45 ka) and implications for deglacial atmospheric radiocarbon. *Quaternary Science Reviews*, 191, 57–72. <https://doi.org/10.1016/j.quascirev.2018.05.007>
- Channell, J. E. T., Xuan, C., & Hodell, D. A. (2009). Stacking paleointensity and oxygen isotope data for the last 1.5 Myr (PISO-1500). *Earth and Planetary Science Letters*, 283(1–4), 14–23. <https://doi.org/10.1016/j.epsl.2009.03.012>
- Chen, T., Robinson, L. F., Burke, A., Claxton, L., Hain, M. P., Li, T., et al. (2020). Persistently well-ventilated intermediate-depth ocean through the last deglaciation. *Nature Geoscience*, 13(11), 733–738. <https://doi.org/10.1038/s41561-020-0638-6>
- Chen, T., Robinson, L. F., Burke, A., Southon, J., Spooner, P., Morris, P. J., & Ng, H. C. (2015). Synchronous centennial abrupt events in the ocean and atmosphere during the last deglaciation. *Science*, 349(6255), 1537–1541. <https://doi.org/10.1126/science.aac6159>
- Cheng, H., Edwards, R. L., Broecker, W. S., Denton, G. H., Kong, X. G., Wang, Y. J., et al. (2009). Ice age terminations. *Science*, 326(5950), 248–252. <https://doi.org/10.1126/science.1177840>
- Cheng, H., Edwards, R. L., Southon, J., Matsumoto, K., Feinberg, J. M., Sinha, A., et al. (2018). Atmospheric ¹⁴C/¹²C changes during the last glacial period from Hulu Cave. *Science*, 362(6420), 1293–1297. <https://doi.org/10.1126/science.aau0747>
- Chikamoto, M. O., Abe-Ouchi, A., Oka, A., Ohgaito, R., & Timmermann, A. (2012). Quantifying the ocean's role in glacial CO₂ reductions. *Climate of the Past*, 8(2), 545–563. <https://doi.org/10.5194/cp-8-545-2012>
- Chikamoto, M. O., Menviel, L., Abe-Ouchi, A., Ohgaito, R., Timmermann, A., Okazaki, Y., et al. (2012). Variability in North Pacific intermediate and deep water ventilation during Heinrich events in two coupled climate models. *Deep Sea Research Part II: Topical Studies in Oceanography*, 61–64, 114–126. <https://doi.org/10.1016/j.dsr2.2011.12.002>
- Ciais, P., Tagliabue, A., Cuntz, M., Bopp, L., Scholze, M., Hoffmann, G., et al. (2012). Large inert carbon pool in the terrestrial biosphere during the Last Glacial Maximum. *Nature Geoscience*, 5(1), 74–79. <https://doi.org/10.1038/ngeo1324>
- Cleroux, C., Demenocal, P., & Guilderson, T. (2011). Deglacial radiocarbon history of tropical Atlantic thermocline waters: Absence of CO₂ reservoir purging signal. *Quaternary Science Reviews*, 30(15–16), 1875–1882. <https://doi.org/10.1016/j.quascirev.2011.04.015>
- Cook, M., & Keigwin, L. D. (2015). Radiocarbon profiles of the NW Pacific from the LGM and deglaciation: Evaluating ventilation metrics and the effect of uncertain surface reservoir ages. *Paleoceanography*, 30(3), 174–195. <https://doi.org/10.1002/2014PA002649>
- Cornec, M., Claustre, H., Mignot, A., Guidi, L., Lacour, L., Poteau, A., et al. (2021). Deep chlorophyll maxima in the global ocean: Occurrences, drivers and characteristics. *Global Biogeochemical Cycles*, 35(4), e2020GB006759. <https://doi.org/10.1029/2020GB006759>
- Costa, K. M., McManus, J. F., & Anderson, R. F. (2017). Radiocarbon and stable isotope evidence for changes in sediment mixing in the North Pacific over the past 30 kyr. *Radiocarbon*, 60(1), 113–135. <https://doi.org/10.1017/RDC.2017.91>
- Craig, H. (1957). The natural distribution of radiocarbon and the exchange time of carbon dioxide between the atmosphere and the sea. *Tellus*, 9(1), 1–17. <https://doi.org/10.3402/tellusa.v9i1.9078>
- Curry, W. B., & Oppo, D. W. (2005). Glacial water mass geometry and the distribution of δ¹³C of ΣCO₂ in the western Atlantic Ocean. *Paleoceanography*, 20(1). <https://doi.org/10.1029/2004PA001021>
- Dai, Y., Yu, J., & Rafter, P. A. (2021). Deglacial ventilation changes in the deep Southwest Pacific. *Paleoceanography and Paleoclimatology*, 36(2), e2020PA004172. <https://doi.org/10.1029/2020PA004172>
- Damon, P. E., & Linick, T. W. (1986). Geomagnetic-heliomagnetic modulation of atmospheric radiocarbon production. *Radiocarbon*, 28(2A), 266–278. <https://doi.org/10.1017/s0033822200007360>
- Davies-Walczak, M., Mix, A. C., Stoner, J. S., Southon, J. R., Cheseby, M., & Xuan, C. (2014). Late glacial to Holocene radiocarbon constraints on North Pacific intermediate water ventilation and deglacial atmospheric CO₂ sources. *Earth and Planetary Science Letters*, 397, 57–66. <https://doi.org/10.1016/j.epsl.2014.04.004>
- de Boyer Montégut, C., Madec, G., Fischer, A. S., Lazar, A., & Iudicone, D. (2004). Mixed layer depth over the global ocean: An examination of profile data and a profile-based climatology. *Journal of Geophysical Research*, 109(C12). <https://doi.org/10.1029/2004JC002378>
- de la Fuente, M., Calvo, E., Skinner, L., Pelejero, C., Evans, D., Müller, W., et al. (2017). The evolution of deep ocean chemistry and respired carbon in the eastern equatorial Pacific over the last deglaciation. *Paleoceanography*, 32(12), 1371–1385. <https://doi.org/10.1002/2017PA003155>
- de la Fuente, M., Skinner, L., Calvo, E., Pelejero, C., & Cacho, I. (2015). Increased reservoir ages and poorly ventilated deep waters inferred in the glacial Eastern Equatorial Pacific. *Nature Communications*, 6(1), 7420. <https://doi.org/10.1038/ncomms8420>
- Delaygue, G., Bekki, S., & Bard, E. (2015). Modelling the stratospheric budget of beryllium isotopes. *Tellus B: Chemical and Physical Meteorology*, 67(1), 28582. <https://doi.org/10.3402/tellusb.v67.28582>

- De Pol-Holz, R., Keigwin, L. D., Southon, J., Hebbeln, D., & Mohtadi, M. (2010). No signature of abyssal carbon in intermediate waters off Chile during deglaciation. *Nature Geoscience*, 3, 192–195. <https://doi.org/10.1038/ngeo745>
- de Vries, H. (1958). Variation in concentration of radiocarbon with time and location on Earth. *Proceedings Koninklijke Nederlandse Akademie van Wetenschappen - Series B*, 61(2), 94–102.
- DeVries, T., & Primeau, F. (2010). An improved method for estimating water-mass ventilation age from radiocarbon data. *Earth and Planetary Science Letters*, 295(3), 367–378. <https://doi.org/10.1016/j.epsl.2010.04.011>
- DeVries, T., & Primeau, F. (2011). Dynamically and observationally constrained estimates of water-mass distributions and ages in the global ocean. *Journal of Physical Oceanography*, 41(12), 2381–2401. <https://doi.org/10.1175/jpo-d-10-05011.1>
- Dinauer, A., Adolphi, F., & Joos, F. (2020). Mysteriously high $\Delta^{14}\text{C}$ of the glacial atmosphere: Influence of ^{14}C production and carbon cycle changes. *Climate of the Past*, 16(4), 1159–1185. <https://doi.org/10.5194/cp-2019-159>
- Diz, P., & Barker, S. (2015). Linkages between rapid climate variability and deep-sea benthic foraminifera in the deep Subantarctic South Atlantic during the last 95kyr. *Paleoceanography*, 30(6), 601–611. <https://doi.org/10.1002/2015pa002784>
- Dolman, A. M., Groeneveld, J., Mollenhauer, G., Ho, S. L., & Laepple, T. (2021). Estimating bioturbation from replicated small-sample radiocarbon ages. *Paleoceanography and Paleoclimatology*, 36, e2020PA004142. <https://doi.org/10.1029/2020pa004142>
- Duplessy, J. C., Arnold, M., Bard, E., Juillet, L. A., Kallel, N., & Labeyrie, L. (1989). AMS (super 14) C study of transient events and of the ventilation rate of the Pacific intermediate water during the last deglaciation. *Radiocarbon*, 31(3), 10.
- Duplessy, J.-C., Shackleton, N. J., Fairbanks, R. G., Labeyrie, L., Oppo, D., & Kallel, N. (1988). Deep water source variations during the last climatic cycle and their impact on global deep water circulation. *Paleoceanography*, 3, 343–360. <https://doi.org/10.1029/pa003i003p00343>
- Eggelston, S., & Galbraith, E. D. (2018). The devil's in the disequilibrium: Multi-component analysis of dissolved carbon and oxygen changes under a broad range of forcings in a general circulation model. *Biogeosciences*, 15(12), 3761–3777. <https://doi.org/10.5194/bg-15-3761-2018>
- Elsasser, W., Ney, E. P., & Winckler, J. R. (1956). Cosmic-ray intensity and geomagnetism. *Nature*, 178, 1226–1227. <https://doi.org/10.1038/1781226a0>
- Eltgroth, S. F., Adkins, J. F., Robinson, L. F., Southon, J., & Kashgarian, M. (2006). A deep-sea coral record of North Atlantic radiocarbon through the Younger Dryas: Evidence for intermediate water/deepwater reorganization. *Paleoceanography*, 21(4). <https://doi.org/10.1029/2005PA001192>
- England, M. H. (1995). The age of water and ventilation timescales in a global ocean model. *Journal of Physical Oceanography*, 25(11), 2756–2777. [https://doi.org/10.1175/1520-0485\(1995\)025<2756:TAOWAV>2.0.CO;2](https://doi.org/10.1175/1520-0485(1995)025<2756:TAOWAV>2.0.CO;2)
- EPICA Community Members. (2006). One-to-one coupling of glacial variability in Greenland and Antarctica. *Nature*, 444, 195–198.
- Ezat, M. M., Rasmussen, T. L., Skinner, L. C., & Zamelczyk, K. (2019). Deep ocean ^{14}C ventilation age reconstructions from the Arctic Mediterranean reassessed. *Earth and Planetary Science Letters*, 518, 67–75. <https://doi.org/10.1016/j.epsl.2019.04.027>
- Ezat, M. M., Rasmussen, T. L., Thornalley, D. J. R., Olsen, J., Skinner, L. C., Hönisch, B., & Groeneveld, J. (2017). Ventilation history of Nordic Seas overflows during the last (de)glacial period revealed by species-specific benthic foraminiferal ^{14}C dates. *Paleoceanography*, 32(2), 172–181. <https://doi.org/10.1002/2016PA003053>
- Fagault, Y., Tuna, T., Rostek, F., & Bard, E. (2019). Radiocarbon dating small carbonate samples with the gas ion source of AixMICADAS. *Nuclear Instruments and Methods in Physics Research Section B: Beam Interactions with Materials and Atoms*, 455, 276–283. <https://doi.org/10.1016/j.nimb.2018.11.018>
- Fairbanks, R. G., Mortlock, R. A., Chiu, T.-C., Cao, L., Kaplan, A., Guilderson, T., et al. (2005). Radiocarbon calibration curve spanning 0–50,000 years BP based on paired $^{230}\text{Th}/^{234}\text{U}/^{238}\text{U}$ and ^{14}C dates on pristine corals. *Quaternary Science Reviews*, 24, 1781–1796. <https://doi.org/10.1016/j.quascirev.2005.04.007>
- Ferrari, R., Jansen, M. F., Adkins, J. F., Burke, A., Stewart, A. L., & Thompson, A. F. (2014). Antarctic sea ice control on ocean circulation in present and glacial climates. *Proceedings of the National Academy of Sciences of the United States of America*, 111(24), 8753–8758. <https://doi.org/10.1073/pnas.1323922111>
- Fiadiero, M. E. (1982). Three-dimensional modeling of tracers in the deep Pacific Ocean: Radiocarbon and the circulation. *Journal of Marine Research*, 40, 537–550.
- Fiedler, P. C., & Talley, L. D. (2006). Hydrography of the eastern tropical Pacific: A review. *Progress in Oceanography*, 69(2), 143–180. <https://doi.org/10.1016/j.pocean.2006.03.008>
- Francois, R., Altabet, M. A., Yu, E.-F., Sigman, D. M., Bacon, M. P., Frank, M., et al. (1997). Contribution of Southern Ocean surface-water stratification to low atmospheric CO_2 concentrations during the last glacial period. *Nature*, 389, 929–935. <https://doi.org/10.1038/40073>
- Frank, M., Schwarz, B., Baumann, S., Kubik, P. W., Suter, M., & Mangini, A. (1997). A 200 kyr record of cosmogenic radionuclide production rate and geomagnetic field intensity from ^{10}Be in globally stacked deep-sea sediments. *Earth and Planetary Science Letters*, 149(1), 121–129. [https://doi.org/10.1016/S0012-821X\(97\)00070-8](https://doi.org/10.1016/S0012-821X(97)00070-8)
- Freeman, E., Skinner, L. C., Tisserand, A., Dokken, T., Timmermann, A., Menviel, L., & Friedrich, T. (2015). An Atlantic-Pacific ventilation seesaw across the last deglaciation. *Earth and Planetary Science Letters*, 424, 237–244. <https://doi.org/10.1016/j.epsl.2015.05.032>
- Freeman, E., Skinner, L. C., Waelbroeck, C., & Hodell, D. (2016). Radiocarbon evidence for enhanced respired carbon storage in the deep Atlantic at the Last Glacial Maximum. *Nature Communications*, 7. <https://doi.org/10.1038/ncomms11998>
- Galbraith, E., & de Lavergne, C. (2019). Response of a comprehensive climate model to a broad range of external forcings: Relevance for deep ocean ventilation and the development of late Cenozoic ice ages. *Climate Dynamics*, 52(1), 653–679. <https://doi.org/10.1007/s00382-018-4157-8>
- Galbraith, E., Jaccard, S. L., Pedersen, T. F., Sigman, D. M., Haug, G. H., Cook, M., et al. (2007). Carbon dioxide release from the North Pacific abyss during the last deglaciation. *Nature*, 449, 890–893. <https://doi.org/10.1038/nature06227>
- Galbraith, E., Kwon, E. Y., Bianchi, D., Hain, M. P., & Sarmiento, J. L. (2015). The impact of atmospheric $p\text{CO}_2$ on carbon isotope ratios of the atmosphere and ocean. *Global Biogeochemical Cycles*, 29, 307–324. <https://doi.org/10.1002/2014GB004929>
- Galbraith, E., Kwon, E. Y., Gnanadesikan, A., Rodgers, K. B., Griffies, S. M., Bianchi, D., et al. (2011). Climate variability and radiocarbon in the CM2Mc Earth System Model. *Journal of Climate*, 24, 4230–4254. <https://doi.org/10.1175/2011jcli3919.1>
- Galbraith, E. D., & Skinner, L. C. (2020). The biological pump during the last glacial maximum. *Annual Review of Marine Science*, 12(1), 559–586. <https://doi.org/10.1146/annurev-marine-010419-010906>
- Ganopolski, A., & Brovkin, V. (2017). Simulation of climate, ice sheets and CO_2 evolution during the last four glacial cycles with an Earth system model of intermediate complexity. *Climate of the Past*, 13(12), 1695–1716. <https://doi.org/10.5194/cp-13-1695-2017>
- Gebbie, G., & Huybers, P. (2012). The mean age of ocean waters inferred from radiocarbon observations: Sensitivity to surface sources and accounting for mixing histories. *Journal of Physical Oceanography*, 42(2), 291–305. <https://doi.org/10.1175/jpo-d-11-043.1>
- Genty, D., & Massault, M. (1997). Bomb ^{14}C recorded in laminated speleothems: Calculation of dead carbon proportion. *Radiocarbon*, 33(1), 33–48. <https://doi.org/10.1017/s0033822200040881>

- Gersonde, R., Abelmann, A., Brathauer, U., Becquey, S., Bianchi, C., Cortese, G., et al. (2003). Last glacial sea surface temperatures and sea-ice extent in the Southern Ocean (Atlantic-Indian sector): A multiproxy approach. *Paleoceanography*, *18*(3). <https://doi.org/10.1029/2002PA000809>
- Gherardi, J.-M., Labeyrie, L., McManus, J. F., Francois, R., Skinner, L. C., & Cortijo, E. (2005). Evidence from the Northeastern Atlantic basin for variability of the meridional overturning circulation through the last deglaciation. *Earth and Planetary Science Letters*, *240*(3–4), 710–723. <https://doi.org/10.1016/j.epsl.2005.09.061>
- Godwin, H. (1962). Half-life of radiocarbon. *Nature*, *195*(4845), 984. <https://doi.org/10.1038/195984a0>
- Goldstein, S. J., Lea, D. W., Chakraborty, S., Kashgarian, M., & Murrell, M. T. (2001). Uranium-series and radiocarbon geochronology of deep-sea corals: Implications for Southern Ocean ventilation rates and the oceanic carbon cycle. *Earth and Planetary Science Letters*, *193*, 167–182. [https://doi.org/10.1016/s0012-821x\(01\)00494-0](https://doi.org/10.1016/s0012-821x(01)00494-0)
- Goodwin, P. (2012). An isopycnal box model with predictive deep-ocean structure for biogeochemical cycling applications. *Ocean Modelling*, *51*, 19–36. <https://doi.org/10.1016/j.ocemod.2012.04.005>
- Gorbarenko, S. A., Derkachev, A. N., Astakhov, A. S., Sauton, J. R., Nürnberg, D., & Shapovalov-Chuprynin, F. V. (2000). Data on mineral composition of volcanic glass and radiocarbon age of Upper Quaternary sediments from the Sea of Okhotsk. In Supplement to: Gorbarenko, S. A., Derkachev, A. N., Astakhov, A. S., Sauton, J. R., Nürnberg, D., & Shapovalov-Chuprynin, F. V. (2000). *Lithostratigraphy and tephrochronology of Upper Quaternary deposits from the Sea of Okhotsk. Tikhookeanskaya Geologiya (Pacific Geology)*, *19*(2), 58–72. PANGAEA.
- Goslar, T., Arnold, M., Bard, E., Kuc, T., Pazdur, M. F., Ralska-Jasiewiczowa, M., et al. (1995). High concentration of atmospheric ¹⁴C during the Younger Dryas cold episode. *Nature*, *377*(6548), 414–417. <https://doi.org/10.1038/377414a0>
- Gottschalk, J., Michel, E., Thöle, L. M., Studer, A. S., Hasenfratz, A. P., Schmid, N., et al. (2020). Glacial heterogeneity in Southern Ocean carbon storage abated by fast South Indian deglacial carbon release. *Nature Communications*, *11*(1), 6192. <https://doi.org/10.1038/s41467-020-20034-1>
- Gottschalk, J., Skinner, L. C., Jaccard, S. L., Menviel, L., Nehrbass-Ahles, C., & Waelbroeck, C. (2019). Southern Ocean link between changes in atmospheric CO₂ levels and northern-hemisphere climate anomalies during the last two glacial periods. *Quaternary Science Reviews*, *230*, 106067. <https://doi.org/10.1016/j.quascirev.2019.106067>
- Gottschalk, J., Skinner, L. C., Lippold, J., Vogel, H., Frank, N., Jaccard, S. L., & Waelbroeck, C. (2016). Biological and physical controls in the Southern Ocean on past millennial-scale atmospheric CO₂ changes. *Nature Communications*, *7*, 11539. <https://doi.org/10.1038/ncomms11539>
- Gottschalk, J., Skinner, L. C., Misra, S., Waelbroeck, C., Menviel, L., & Timmermann, A. (2015). Abrupt changes in the southern extent of North Atlantic deep water during Dansgaard-Oeschger events. *Nature Geoscience*, *8*(12), 950–954. <https://doi.org/10.1038/ngeo2558>
- Gottschalk, J., Szidat, S., Michel, E., Mazaud, A., Salazar, G., Battaglia, M., et al. (2018). Radiocarbon measurements of small-size foraminiferal samples with the Mini Carbon Dating System (MICADAS) at the University of Bern: Implications for paleoclimate reconstructions. *Radiocarbon*, *60*(2), 469–491. <https://doi.org/10.1017/RDC.2018.3>
- Grant, K. M., Rohling, E. J., Bar-Matthews, M., Ayalon, A., Medina-Elizalde, M., Ramsey, C. B., et al. (2012). Rapid coupling between ice volume and polar temperature over the past 150,000 years. *Nature*, *491*(7426), 744–747. <https://doi.org/10.1038/nature11593>
- Gray, W. R., Rae, J. W. B., Wills, R. C. J., Shevenell, A. E., Taylor, B., Burke, A., et al. (2018). Deglacial upwelling, productivity and CO₂ outgassing in the North Pacific Ocean. *Nature Geoscience*, *11*(5), 340–344. <https://doi.org/10.1038/s41561-018-0108-6>
- Guyodo, Y., & Valet, J.-P. (1999). Global changes in the Earth's magnetic field during the past 800 kyr. *Nature*, *399*, 249–252. <https://doi.org/10.1038/20420>
- Hain, M. P., Sigman, D. M., & Haug, G. H. (2011). Carbon dioxide effects of Antarctic stratification, North Atlantic Intermediate Water formation, and subantarctic nutrient drawdown during the last ice age: Diagnosis and synthesis in a geochemical box model. *Global Biogeochemical Cycles*, *24*(4). <https://doi.org/10.1029/2010GB003790>
- Hain, M. P., Sigman, D. M., & Haug, G. H. (2014). Distinct roles of the Southern Ocean and North Atlantic in the deglacial atmospheric radiocarbon decline. *Earth and Planetary Science Letters*, *394*, 198–208. <https://doi.org/10.1016/j.epsl.2014.03.020>
- Hall, T. M., & Haine, T. W. N. (2002). On ocean transport diagnostics: The idealized age tracer and the age spectrum. *Journal of Physical Oceanography*, *32*(6), 1987–1991. [https://doi.org/10.1175/1520-0485\(2002\)032<1987:ootdti>2.0.co;2](https://doi.org/10.1175/1520-0485(2002)032<1987:ootdti>2.0.co;2)
- Heaton, T. J., Köhler, P., Butzin, M., Bard, E., Reimer, R. W., Austin, W. E. N., et al. (2020). Marine20—The marine radiocarbon age calibration curve (0–55,000 cal BP). *Radiocarbon*, *62*(4), 779–820. <https://doi.org/10.1017/RDC.2020.68>
- Henry, L. G., McManus, J. F., Curry, W. B., Roberts, N. L., Piotrowski, A. M., & Keigwin, L. D. (2016). North Atlantic ocean circulation and abrupt climate change during the last glaciation. *Science*, *353*(6298), 470–474. <https://doi.org/10.1126/science.aaf5529>
- Hines, S. K. V., Southon, J. R., & Adkins, J. F. (2015). A high-resolution record of Southern Ocean intermediate water radiocarbon over the past 30,000 years. *Earth and Planetary Science Letters*, *432*, 46–58. <https://doi.org/10.1016/j.epsl.2015.09.038>
- Hines, S. K. V., Thompson, A. F., & Adkins, J. F. (2019). The role of the Southern Ocean in abrupt transitions and hysteresis in glacial ocean circulation. *Paleoceanography and Paleoclimatology*, *34*(4), 490–510. <https://doi.org/10.1029/2018pa003415>
- Hogg, A., Southon, J., Turney, C., Palmer, J., Bronk Ramsey, C., Fenwick, P., et al. (2016). Punctuated shutdown of Atlantic meridional overturning circulation during Greenland Stadial 1. *Scientific Reports*, *6*(1), 25902. <https://doi.org/10.1038/srep25902>
- Hogg, A. G., Heaton, T. J., Hua, Q., Palmer, J. G., Turney, C. S., Southon, J., et al. (2020). SHCal20 Southern Hemisphere Calibration, 0–55,000 years cal BP. *Radiocarbon*, *62*(4), 759–778. <https://doi.org/10.1017/RDC.2020.59>
- Hogg, A. G., Hua, Q., Blackwell, P. G., Niu, M., Buck, C. E., Guilderson, T. P., et al. (2013). SHCal13 Southern Hemisphere Calibration, 0–50,000 years cal BP. *Radiocarbon*, *55*(4), 1889–1903.
- Hönisch, B., Hemming, N. G., Archer, D., Siddall, M., & McManus, J. F. (2009). Atmospheric carbon dioxide concentration across the mid-Pleistocene transition. *Science*, *324*(5934), 1551–1554. <https://doi.org/10.1126/science.1171477>
- Hoogakker, B. A. A., Elderfield, H., Schmiedl, G., McCave, I. N., & Rickaby, R. E. M. (2015). Glacial-interglacial changes in bottom-water oxygen content on the Portuguese margin. *Nature Geoscience*, *8*(1), 40–43. <https://doi.org/10.1038/ngeo2317>
- Hoogakker, B. A. A., Lu, Z., Umling, N., Jones, L., Zhou, X., Rickaby, R. E. M., et al. (2018). Glacial expansion of oxygen-depleted seawater in the eastern tropical Pacific. *Nature*, *562*(7727), 410–413. <https://doi.org/10.1038/s41586-018-0589-x>
- Hughen, K., Eglinton, T., Xu, L., & Makou, M. (2004). Abrupt tropical vegetation response to rapid climate changes. *Science*, *304*, 1955–1959. <https://doi.org/10.1126/science.1092995>
- Hughen, K., Lehman, S., Southon, J., Overpeck, J., Marchal, O., Herring, C., & Turnbull, J. (2004). ¹⁴C activity and global carbon cycle changes over the past 50,000 years. *Science*, *303*, 202–207. <https://doi.org/10.1126/science.1090300>
- Hughen, K., Southon, J., Lehman, S., Bertrand, C., & Turnbull, J. (2006). Marine-derived ¹⁴C calibration and activity record over the past 50,000 years updated from the Cariaco Basin. *Quaternary Science Reviews*, *25*, 3216–3227. <https://doi.org/10.1016/j.quascirev.2006.03.014>
- Hughen, K. A., Overpeck, J. T., Lehmann, S. J., Kashgarian, M., Southon, J. R., & Peterson, L. C. (1998). A new ¹⁴C calibration data set for the last deglaciation based on marine varves. *Radiocarbon*, *40*(1), 483–494.
- Hughes, E. E., & Mann, W. B. (1964). The half-life of carbon-14: Comments on mass-spectrometric method. *International Journal of Applied Radiation and Isotopes*, *15*(3), 97–100. [https://doi.org/10.1016/0020-708x\(64\)90038-9](https://doi.org/10.1016/0020-708x(64)90038-9)

- Huybers, P., & Langmuir, C. (2009). Feedback between deglaciation, volcanism, and atmospheric CO₂. *Earth and Planetary Science Letters*, 286, 479–491. <https://doi.org/10.1016/j.epsl.2009.07.014>
- Huybers, P., & Langmuir, C. H. (2017). Delayed CO₂ emissions from mid-ocean ridge volcanism as a possible cause of late-Pleistocene glacial cycles. *Earth and Planetary Science Letters*, 457, 238–249. <https://doi.org/10.1016/j.epsl.2016.09.021>
- Ikehara, K., Danhara, T., Yamashita, T., Tanahashi, M., Morita, S., & Ohkushi, K. I. (2011). Paleoclimatographic control on a large marine reservoir effect offshore of Tokai, south of Japan, NW Pacific, during the last glacial maximum-deglaciation. *Quaternary International*, 246(1), 213–221. <https://doi.org/10.1016/j.quaint.2011.07.005>
- Ikehara, K., Ohkushi, K. I., Shibahara, A., & Hoshida, M. (2006). Change of bottom water conditions at intermediate depths of the Oyashio region, NW Pacific over the past 20,000 yrs. *Global and Planetary Change*, 53(1), 78–91. <https://doi.org/10.1016/j.gloplacha.2006.01.011>
- Ito, T., & Follows, M. J. (2005). Preformed phosphate, soft tissue pump and atmospheric CO₂. *Journal of Marine Research*, 63, 813–839. <https://doi.org/10.1357/0022240054663231>
- Ito, T., & Follows, M. J. (2013). Air-sea disequilibrium of carbon dioxide enhances the biological carbon sequestration in the Southern Ocean. *Global Biogeochemical Cycles*, 27, 1129–1138. <https://doi.org/10.1002/2013GB004682>
- Jaccard, S. L., & Galbraith, E. (2012). Large climate-driven changes of oceanic oxygen concentrations during the last deglaciation. *Nature Geoscience*, 5, 151–156. <https://doi.org/10.1038/ngeo1352>
- Jaccard, S. L., Galbraith, E. D., Martínez-García, A., & Anderson, R. F. (2016). Covariation of deep Southern Ocean oxygenation and atmospheric CO₂ through the last ice age. *Nature*, 530(7589), 207–210. <https://doi.org/10.1038/nature16514>
- Jahn, A., Lindsay, K., Giraud, X., Gruber, N., Otto-Bliesner, B. L., Liu, Z., & Brady, E. C. (2015). Carbon isotopes in the ocean model of the Community Earth System Model (CESM1). *Geoscientific Model Development*, 8(8), 2419–2434. <https://doi.org/10.5194/gmd-8-2419-2015>
- Jeltsch-Thömmes, A., & Joos, F. (2020). Modeling the evolution of pulse-like perturbations in atmospheric carbon and carbon isotopes: The role of weathering–sedimentation imbalances. *Climate of the Past*, 16(2), 423–451. <https://doi.org/10.5194/cp-16-423-2020>
- Jenkins, W. J., Lott, D. E., German, C. R., Cahill, K. L., Goudreau, J., & Longworth, B. (2018). The deep distributions of helium isotopes, radiocarbon, and noble gases along the U.S. GEOTRACES East Pacific Zonal Transect (GP16). *Marine Chemistry*, 201, 167–182. <https://doi.org/10.1016/j.marchem.2017.03.009>
- Johnson, G. C. (2008). Quantifying Antarctic bottom water and North Atlantic deep water volumes. *Journal of Geophysical Research*, 113. <https://doi.org/10.1029/2007JC004477>
- Jones, C. D., Arora, V., Friedlingstein, P., Bopp, L., Brovkin, V., Dunne, J., et al. (2016). C4MIP – The coupled climate–carbon cycle model intercomparison project: Experimental protocol for CMIP6. *Geoscientific Model Development*, 9(8), 2853–2880. <https://doi.org/10.5194/gmd-9-2853-2016>
- Jones, D. C., Ito, T., Takano, Y., & Hsu, W.-C. (2014). Spatial and seasonal variability of the air-sea equilibration timescale of carbon dioxide. *Global Biogeochemical Cycles*, 28(11), 1163–1178. <https://doi.org/10.1002/2014GB004813>
- Keigwin, L. D. (2004). Radiocarbon and stable isotope constraints on Last Glacial Maximum and Younger Dryas ventilation in the western North Atlantic. *Paleoceanography*, 19(4), 1–15. <https://doi.org/10.1029/2004pa001029>
- Keigwin, L. D., & Lehman, S. J. (2015). Radiocarbon evidence for a possible abyssal front near 3.1 km in the glacial equatorial Pacific Ocean. *Earth and Planetary Science Letters*, 425, 93–104. <https://doi.org/10.1016/j.epsl.2015.05.025>
- Keigwin, L. D., Sachs, J. P., Rosenthal, Y., & Boyle, E. (2005). The 8200 year B.P. event in the slope water system, western subpolar North Atlantic. *Paleoceanography*, 20. <https://doi.org/10.1029/2004pa001074>
- Keigwin, L. D., & Schlegel, M. A. (2002). Ocean ventilation and sedimentation since the glacial maximum at 3 km in the western North Atlantic. *Geochemistry, Geophysics, Geosystems*, 3, <https://doi.org/10.1029/2001gc000283>
- Keigwin, L. D., & Swift, S. A. (2017). Carbon isotope evidence for a northern source of deep water in the glacial western North Atlantic. *Proceedings of the National Academy of Sciences*, 114, 2831–2835. <https://doi.org/10.1073/pnas.1614693114>
- Kennett, J. P., & Ingram, B. L. (1995). A 20,000-year record of ocean circulation and climate change from the Santa Barbara basin. *Nature*, 377(6549), 510–514. <https://doi.org/10.1038/377510a0>
- Key, R. M., Kozyr, A., Sabine, C., Lee, K., Wanninkhof, R., Bullister, J. L., et al. (2004). A global ocean carbon climatology: Results from the Global Data Analysis Project (GLODAP). *Global Biogeochemical Cycles*, 18(4), 1–23. <https://doi.org/10.1029/2004gb002247>
- Khatiwal, S., Muglia, J., & Schmittner, A. (2019). Air-sea disequilibrium enhances ocean carbon storage during glacial periods. *Science Advances*, 5, 1–10. <https://doi.org/10.1126/sciadv.aaw4981>
- Khatiwal, S., Visbeck, M., & Cane, M. A. (2005). Accelerated simulation of passive tracers in ocean circulation models. *Ocean Modelling*, 9, 51–69. <https://doi.org/10.1016/j.ocemod.2004.04.002>
- Kitagawa, H., & van der Plicht, J. (2000). Atmospheric radiocarbon calibration beyond 11,900 cal BP from Lake Suigetsu laminated sediments. *Radiocarbon*, 42(3), 369–380. <https://doi.org/10.1017/s0033822200030319>
- Kobayashi, H., & Oka, A. (2018). Response of atmospheric pCO₂ to glacial changes in the Southern Ocean amplified by carbonate compensation. *Paleoceanography and Paleoclimatology*, 33(11), 1206–1229. <https://doi.org/10.1029/2018pa003360>
- Koeve, W., Wagner, H., Kähler, P., & Oschlies, A. (2015). ¹⁴C-age tracers in global ocean circulation models. *Geoscientific Model Development*, 8(7), 2079–2094. <https://doi.org/10.5194/gmd-8-2079-2015>
- Köhler, P., Fischer, H., Munhoven, G., & Zeebe, R. E. (2005). Quantitative interpretation of atmospheric carbon records over the last glacial termination. *Global Biogeochemical Cycles*, 19, 1–24.
- Köhler, P., Knorr, G., & Bard, E. (2014). Permafrost thawing as a possible source of abrupt carbon release at the onset of the Bølling/Allerød. *Nature Communications*, 5, 5520. <https://doi.org/10.1038/ncomms6520>
- Köhler, P., Muscheler, R., & Fischer, H. (2006). A model-based interpretation of low-frequency changes in the carbon cycle during the last 120,000 years and its implications for the reconstruction of atmospheric Δ¹⁴C. *Geochemistry, Geophysics, Geosystems*, 7(11), 1–22.
- Korff, S. A., & Mendell, R. B. (1980). Variations in radiocarbon production in the Earth's atmosphere. *Radiocarbon*, 22(2), 159–165. <https://doi.org/10.1017/s0033822200009425>
- Kovaltsov, G. A., Mishev, A., & Usoskin, I. G. (2012). A new model of cosmogenic production of radiocarbon ¹⁴C in the atmosphere. *Earth and Planetary Science Letters*, 337, 114–120. <https://doi.org/10.1016/j.epsl.2012.05.036>
- Kromer, B. (2009). Radiocarbon and dendrochronology. *Dendrochronologia*, 27(1), 15–19. <https://doi.org/10.1016/j.dendro.2009.03.001>
- Kurie, F. N. D. (1934). A new mode of disintegration induced by neutrons. *Physical Review*, 45(12), 904. <https://doi.org/10.1103/PhysRev.45.904>
- Kwon, E. Y., & Primeau, F. (2006). Optimization and sensitivity study of a biogeochemistry ocean model using an implicit solver and in situ phosphate data. *Global Biogeochemical Cycles*, 20(4). <https://doi.org/10.1029/2005GB002631>
- Kwon, E. Y., Sarmiento, J. L., Toggweiler, J. R., & DeVries, T. (2011). The control of atmospheric pCO₂ by ocean ventilation change: The effect of the oceanic storage of biogenic carbon. *Global Biogeochemical Cycles*, 25(3), GB3026. <https://doi.org/10.1029/2011GB004059>

- Laj, C., Kissel, C., & Beer, J. (2004). High resolution global paleointensity stack since 75 kyr (GLOPIS-75) calibrated to absolute values. In *Timescales of the paleomagnetic field* (pp. 255–265). American Geophysical Union.
- Laj, C., Kissel, C., Mazaud, A., Michel, E., Muscheler, R., & Beer, J. (2002). Geomagnetic field intensity, North Atlantic Deep Water circulation and atmospheric $\Delta^{14}\text{C}$ during the last 50 kyr. *Earth and Planetary Science Letters*, 200, 177–190. [https://doi.org/10.1016/s0012-821x\(02\)00618-0](https://doi.org/10.1016/s0012-821x(02)00618-0)
- Lal, D., & Peters, B. (1967). Cosmic ray produced radioactivity on the Earth. In K. Sitte (Ed.), *Kosmische Strahlung II/Cosmic Rays II. Handbuch der Physik/Encyclopedia of Physics*. Springer. https://doi.org/10.1007/978-3-642-46079-1_7
- Lambeck, K., & Chappell, J. (2001). Sea level change through the last glacial cycle. *Science*, 292, 679–686. <https://doi.org/10.1126/science.1059549>
- Lande, R., & Wood, A. M. (1987). Suspension times of particles in the upper ocean. *Deep Sea Research Part A. Oceanographic Research Papers*, 34(1), 61–72. [https://doi.org/10.1016/0198-0149\(87\)90122-1](https://doi.org/10.1016/0198-0149(87)90122-1)
- Landschützer, P., Laruelle, G. G., Roobaert, A., & Regnier, P. (2020). A uniform $p\text{CO}_2$ climatology combining open and coastal oceans. *Earth System Science Data*, 12(4), 2537–2553. <https://doi.org/10.5194/essd-12-2537-2020>
- Leduc, G., Vidal, L., Tachikawa, K., Rostek, F., Sonzogni, C., Beaufort, L., & Bard, E. (2007). Moisture transport across Central America as a positive feedback on abrupt climatic changes. *Nature*, 445, 908–911. <https://doi.org/10.1038/nature05578>
- LeGrand, P., & Wunsch, C. (1995). Constraints from paleotracer data on the North Atlantic circulation during the last glacial maximum. *Paleoceanography*, 10(6), 1011–1045. <https://doi.org/10.1029/95pa01455>
- Levin, I., Kromer, B., Wagenbach, D., & Münich, K. O. (1987). Carbon isotope measurements of atmospheric CO_2 at a coastal station in Antarctica. *Tellus B*, 39(1–2), 89–95. <https://doi.org/10.1111/j.1600-0889.1987.tb00273.x>
- Li, T., Robinson, L. F., Chen, T., Wang, X. T., Burke, A., Rae, J. W. B., et al. (2020). Rapid shifts in circulation and biogeochemistry of the Southern Ocean during deglacial carbon cycle events. *Science Advances*, 6(42), eabb3807. <https://doi.org/10.1126/sciadv.abb3807>
- Libby, W. F. (1946). Atmospheric helium three and radiocarbon from cosmic radiation. *Physical Review*, 69(11–12), 671–672. <https://doi.org/10.1103/PhysRev.69.671.2>
- Libby, W. F. (1955). *Radioactive dating*. University of Chicago Press.
- Libby, W. F., Anderson, E. C., & Arnold, J. R. (1949). Age determination by radiocarbon content: World-wide assay of natural radiocarbon. *Science*, 109(2827), 227–228. <https://doi.org/10.1126/science.109.2827.227>
- Lindsay, C. M., Lehman, S. J., Marchitto, T. M., Carriquiry, J. D., & Ortiz, J. D. (2016). New constraints on deglacial marine radiocarbon anomalies from a depth transect near Baja California. *Paleoceanography*, 31(8), 1103–1116. <https://doi.org/10.1002/2015pa002878>
- Lindsay, C. M., Lehman, S. J., Marchitto, T. M., & Ortiz, J. D. (2015). The surface expression of radiocarbon anomalies near Baja California during deglaciation. *Earth and Planetary Science Letters*, 422, 67–74. <https://doi.org/10.1016/j.epsl.2015.04.012>
- Lippold, J., Luo, Y., Francois, R., Allen, S. E., Gherardi, J., Pichat, S., et al. (2012). Strength and geometry of the glacial Atlantic Meridional Overturning Circulation. *Nature Geoscience*, 5(11), 813–816. <https://doi.org/10.1038/ngeo1608>
- Lougheed, B. C., Metcalfe, B., Ninnemann, U. S., & Wacker, L. (2018). Moving beyond the age–depth model paradigm in deep-sea palaeoclimate archives: Dual radiocarbon and stable isotope analysis on single foraminifera. *Climate of the Past*, 14(4), 515–526. <https://doi.org/10.5194/cp-14-515-2018>
- Lund, D. C., Adkins, J. F., & Ferrari, R. (2011). Abyssal Atlantic circulation during the Last Glacial Maximum: Constraining the ratio between transport and vertical mixing. *Paleoceanography*, 26. <https://doi.org/10.1029/2010pa001938>
- Lund, D. C., Mix, A. C., & Southon, J. (2011). Increased ventilation age of the deep northeast Pacific Ocean during the last deglaciation. *Nature Geoscience*, 4(11), 771–774. <https://doi.org/10.1038/ngeo1272>
- Lund, D. C., Tassin, A. C., Hoffman, J. L., & Schmittner, A. (2015). Southwest Atlantic water mass evolution during the last deglaciation. *Paleoceanography*, 30(5), 477–494. <https://doi.org/10.1002/2014pa002657>
- Magana, A. L., Southon, J. R., Kennett, J. P., Roark, E. B., Sarnthein, M., & Stott, L. D. (2010). Resolving the cause of large differences between deglacial benthic foraminifera radiocarbon measurements in Santa Barbara Basin. *Paleoceanography*, 25(4). <https://doi.org/10.1029/2010pa002011>
- Mangini, A., Lomitschka, M., Eichstadter, R., Frank, N., Vogler, S., Bonani, G., et al. (1998). Coral provides way to age deep water. *Nature*, 392, 347–348. <https://doi.org/10.1038/32804>
- Mann, W. B., Marlow, W. F., & Hughes, E. E. (1961). The half-life of carbon-14. *International Journal of Applied Radiation and Isotopes*, 11(1), 57–67. [https://doi.org/10.1016/0020-708x\(61\)90132-6](https://doi.org/10.1016/0020-708x(61)90132-6)
- Marchal, O. (2005). Optimal estimation of atmospheric ^{14}C production over the Holocene: Paleoclimate implications. *Climate Dynamics*, 24(1), 71–88. <https://doi.org/10.1007/s00382-004-0476-z>
- Marchal, O., & Curry, W. B. (2008). On the abyssal circulation in the glacial Atlantic. *Journal of Physical Oceanography*, 38, 2014–2037. <https://doi.org/10.1175/2008jpo3895.1>
- Marchal, O., & Zhao, N. (2021). On the estimation of deep Atlantic ventilation from fossil radiocarbon records. Part I: Modern reference estimates. *Journal of Physical Oceanography*, 51(6), 1843–1873. <https://doi.org/10.1175/jpo-d-20-0153.1>
- Marchitto, T. M., & Broecker, W. (2006). Deep water mass geometry in the glacial Atlantic Ocean: A review of constraints from the paleonutrient proxy Cd/Ca. *Geochemistry, Geophysics, Geosystems*, 7(12), 1–16. <https://doi.org/10.1029/2006gc001323>
- Marchitto, T. M., Lehman, S. J., Otiz, J. D., Flückiger, J., & van Geen, A. (2007). Marine radiocarbon evidence for the mechanism of deglacial atmospheric CO_2 rise. *Science*, 316, 1456–1459. <https://doi.org/10.1126/science.1138679>
- Marchitto, T. M., Lynch-Stieglitz, J., & Hemming, S. R. (2005). Deep Pacific CaCO_3 compensation and glacial-interglacial atmospheric CO_2 . *Earth and Planetary Science Letters*, 231, 317–336. <https://doi.org/10.1016/j.epsl.2004.12.024>
- Marcott, S. A., Bauska, T. K., Buizert, C., Steig, E. J., Rosen, J. L., Cuffey, K. M., et al. (2014). Centennial-scale changes in the global carbon cycle during the last deglaciation. *Nature*, 514(7524), 616–619. <https://doi.org/10.1038/nature13799>
- Martin, W. R., McNichol, A. P., & McCorkle, D. C. (2000). The radiocarbon age of calcite dissolving at the sea floor: Estimates from pore water data. *Geochimica et Cosmochimica Acta*, 64(8), 1391–1404. [https://doi.org/10.1016/S0016-7037\(99\)00424-X](https://doi.org/10.1016/S0016-7037(99)00424-X)
- Martinez-Boti, M. A., Marino, G., Foster, G. L., Ziveri, P., Henehan, M. J., Rae, J. W. B., et al. (2015). Boron isotope evidence for oceanic carbon dioxide leakage during the last deglaciation. *Nature*, 518(7538), 219–222. <https://doi.org/10.1038/nature14155>
- Masarik, J., & Beer, J. (1999). Simulation of particle fluxes and cosmogenic nuclide production in the Earth's atmosphere. *Journal of Geophysical Research*, 104(D10), 12099–12111. <https://doi.org/10.1029/1998jd200091>
- Matsumoto, K. (2007). Radiocarbon-based circulation age of the world oceans. *Journal of Geophysical Research*, 112(C9), 1–7. <https://doi.org/10.1029/2007jc004095>
- Max, L., Lembke-Jene, L., Riethdorf, J. R., Tiedemann, R., Nürnberg, D., Kühn, H., & Mackensen, A. (2014). Pulses of enhanced North Pacific Intermediate Water ventilation from the Okhotsk Sea and Bering Sea during the last deglaciation. *Climate of the Past*, 10(2), 591–605. <https://doi.org/10.5194/cp-10-591-2014>

- Mazaud, A., Laj, C., Bard, E., Arnold, M., & Tric, E. (1991). Geomagnetic-field control of ^{14}C production over the last 80 Ky: Implications for the radiocarbon time-scale. *Geophysical Research Letters*, *18*(10), 1885–1888. <https://doi.org/10.1029/91gl02285>
- McCulloch, M., Taviani, M., Montagna, P., López Correa, M., Remia, A., & Mortimer, G. (2010). Proliferation and demise of deep-sea corals in the Mediterranean during the Younger Dryas. *Earth and Planetary Science Letters*, *298*(1), 143–152. <https://doi.org/10.1016/j.epsl.2010.07.036>
- McElhinny, M. W., & Senanayake, W. E. (1982). Variations in the geomagnetic dipole 1: The past 50,000 years. *Journal of Geomagnetism and Geoelectricity*, *34*(1), 39–51. <https://doi.org/10.5636/jgg.34.39>
- McManus, J. F., Francois, R., Gherardi, J.-M., Keigwin, L. D., & Brown-Leger, S. (2004). Collapse and rapid resumption of the Atlantic meridional circulation linked to deglacial climate changes. *Nature*, *428*, 834–837. <https://doi.org/10.1038/nature02494>
- Meissner, K. J., Schmittner, A., Weaver, A. J., & Adkins, J. F. (2003). Ventilation of the North Atlantic Ocean during the Last Glacial Maximum: A comparison between simulated and observed radiocarbon ages. *Paleoceanography*, *18*(2), 1–13. <https://doi.org/10.1029/2002pa000762>
- Mekik, F. (2014). Radiocarbon dating of planktonic foraminifer shells: A cautionary tale. *Paleoceanography*, *29*(1), 13–29. <https://doi.org/10.1002/2013pa002532>
- Ménabréaz, L., Thouveny, N., Bourlès, D. L., & Vidal, L. (2014). The geomagnetic dipole moment variation between 250 and 800 ka BP reconstructed from the authigenic $^{10}\text{Be}/^9\text{Be}$ signature in West Equatorial Pacific sediments. *Earth and Planetary Science Letters*, *385*, 190–205. <https://doi.org/10.1016/j.epsl.2013.10.037>
- Menviel, L., England, M. H., Meissner, K. J., Mouchet, A., & Yu, J. (2014). Atlantic-Pacific seesaw and its role in outgassing CO_2 during Heinrich events. *Paleoceanography*, *29*(1), 58–70. <https://doi.org/10.1002/2013pa002542>
- Menviel, L., Spence, P., & England, M. H. (2015). Contribution of enhanced Antarctic Bottom Water formation to Antarctic warm events and millennial-scale atmospheric CO_2 increase. *Earth and Planetary Science Letters*, *413*, 37–50. <https://doi.org/10.1016/j.epsl.2014.12.050>
- Menviel, L., Spence, P., Yu, J., Chamberlain, M. A., Matear, R. J., Meissner, K. J., & England, M. H. (2018). Southern Hemisphere westerlies as a driver of the early deglacial atmospheric CO_2 rise. *Nature Communications*, *9*(1), 2503. <https://doi.org/10.1038/s41467-018-04876-4>
- Menviel, L., Yu, J., Joos, F., Mouchet, A., Meissner, K. J., & England, M. H. (2017). Poorly ventilated deep ocean at the Last Glacial Maximum inferred from carbon isotopes: A data-model comparison study. *Paleoceanography*, *32*(1), 2–17. <https://doi.org/10.1002/2016pa003024>
- Menviel, L. C., Spence, P., Skinner, L. C., Tachikawa, K., Friedrich, T., Missiaen, L., & Yu, J. (2020). Enhanced mid-depth southward transport in the Northeast Atlantic at the last glacial maximum despite a weaker AMOC. *Paleoceanography and Paleoclimatology*, *35*(2), e2019PA003793. <https://doi.org/10.1029/2019pa003793>
- Missiaen, L., Wacker, L., Lougheed, B. C., Skinner, L., Hajdas, I., Nouet, J., et al. (2020). Radiocarbon dating of small-sized foraminifer samples: Insights into marine sediment mixing. *Radiocarbon*, *62*(2), 313–333. <https://doi.org/10.1017/RDC.2020.13>
- Mix, A. C., Lund, D. C., Pisias, N. G., Boden, P., Bornmalm, L., Lyle, M., & Pyke, J. (1999). Rapid climate oscillations in the Northeast Pacific during the last deglaciation reflect Northern and Southern Hemisphere sources. In P. U. Clark, R. S. Webb, & L. D. Keigwin (Eds.), *Mechanisms of global climate change at millennial time scales* (pp. 127–148). American Geophysical Union. <https://doi.org/10.1029/gm112p0127>
- Miyake, F., Masuda, K., & Nakamura, T. (2013). Another rapid event in the carbon-14 content of tree rings. *Nature Communications*, *4*(1), 1748. <https://doi.org/10.1038/ncomms2783>
- Mollenhauer, G., Kienast, M., Lamy, F., Meggers, H., Schneider, R. R., Hayes, J. M., & Eglinton, T. I. (2005). An evaluation of ^{14}C age relationships between co-occurring foraminifera, alkenones, and total organic carbon in continental margin sediments. *Paleoceanography*, *20*. <https://doi.org/10.1029/2004PA001103>
- Mollenhauer, G., Kusch, S., Eglinton, T. I., & Pearson, A. (2019). Compound-specific radiocarbon measurements. In J. K. Cochran, H. J. Bokuniewicz, & P. L. Yager (Eds.), *Encyclopedia of ocean sciences* (3rd ed., pp. 235–244). Academic Press. <https://doi.org/10.1016/b978-0-12-409548-9.11432-0>
- Monnin, E., Indermuhle, A., Dallenbach, A., Fluckiger, J., Stauffer, B., Stocker, T. F., et al. (2001). Atmospheric CO_2 concentrations over the last glacial termination. *Science*, *291*, 112–114. <https://doi.org/10.1126/science.291.5501.112>
- Mook, W. G., & van der Plicht, J. (1999). Reporting ^{14}C activities and concentrations. *Radiocarbon*, *41*(3), 227–239. <https://doi.org/10.1017/s0033822200057106>
- Mouchet, A. (2013). The ocean bomb radiocarbon inventory revisited. *Radiocarbon*, *55*(3), 1580–1594.
- Muglia, J., Skinner, L. C., & Schmittner, A. (2018). Weak overturning circulation and high Southern Ocean nutrient utilization maximized glacial ocean carbon. *Earth and Planetary Science Letters*, *496*, 47–56. <https://doi.org/10.1016/j.epsl.2018.05.038>
- Müller, S. A., Joos, F., Edwards, N. R., & Stocker, T. F. (2006). Water mass distribution and ventilation time scales in a cost-efficient, three-dimensional ocean model. *Journal of Climate*, *19*, 5479–5499. <https://doi.org/10.1175/JCLI3911.1>
- Murayama, M., Taira, A., Iwakura, H., Matsumoto, E., & Nakamura, T. (1992). Northwest Pacific deep water ventilation rate during the past 35,000 years with the AMS ^{14}C foraminifera ages. *Summaries of Researches Using AMS at Nagoya University* (Vol. 3, pp. 114–121). Nagoya University Center for Chronological Research.
- Muscheler, R., Beer, J., Kubik, P. W., & Synal, H.-A. (2005). Geomagnetic field intensity during the last 60,000 years based on ^{10}Be and ^{36}Cl from the Summit ice cores and ^{14}C . *Quaternary Science Reviews*, *24*, 1846–1860. <https://doi.org/10.1016/j.quascirev.2005.01.012>
- Muscheler, R., Beer, J., Wagner, G., & Finkel, R. C. (2000). Changes in deep-water formation during the Younger Dryas event inferred from ^{10}Be and ^{14}C records. *Nature*, *408*, 567–570. <https://doi.org/10.1038/35046041>
- Muscheler, R., Beer, J., Wagner, G., Laj, C., Kissel, C., Raisbeck, G. M., et al. (2004). Changes in the carbon cycle during the last deglaciation as indicated by the comparison of ^{10}Be and ^{14}C records. *Earth and Planetary Science Letters*, *219*, 325–340. [https://doi.org/10.1016/s0012-821x\(03\)00722-2](https://doi.org/10.1016/s0012-821x(03)00722-2)
- Muschitiello, F., D'Andrea, W. J., Schmittner, A., Heaton, T. J., Balascio, N. L., deRoberts, N., et al. (2019). Deep-water circulation changes lead North Atlantic climate during deglaciation. *Nature Communications*, *10*(1). <https://doi.org/10.1038/s41467-019-09237-3>
- Nehrbass-Ahles, C., Shin, J., Schmitt, J., Bereiter, B., Joos, F., Schilt, A., et al. (2020). Abrupt CO_2 release to the atmosphere under glacial and early interglacial climate conditions. *Science*, *369*(6506), 1000–1005. <https://doi.org/10.1126/science.aay8178>
- Ng, H. C., Robinson, L. F., McManus, J. F., Mohamed, K. J., Jacobel, A. W., Ivanovic, R. F., et al. (2018). Coherent deglacial changes in western Atlantic Ocean circulation. *Nature Communications*, *9*(1), 2947. <https://doi.org/10.1038/s41467-018-05312-3>
- Niu, M., Heaton, T. J., Blackwell, P. G., & Buck, C. E. (2013). The Bayesian approach to radiocarbon calibration curve estimation: The Intcal13, Marine13, and SHcal13 methodologies. *Radiocarbon*, *55*(4), 1905–1922. https://doi.org/10.2458/azu_js_rc.55.17222
- Oeschger, H., Siegenthaler, U., Schotterer, U., & Gugelmann, A. (1975). A box diffusion model to study the carbon dioxide exchange in nature. *Tellus*, *27*(2), 168–192. <https://doi.org/10.1111/j.2153-3490.1975.tb01671.x>
- Ohkouchi, N., Eglinton, T. I., Keigwin, L. D., & Hayes, J. M. (2002). Spatial and temporal offsets between proxy records in a sediment drift. *Science*, *298*, 1224–1227. <https://doi.org/10.1126/science.1075287>
- Okazaki, Y., Kimoto, K., Asahi, H., Sato, M., Nakamura, Y., & Harada, N. (2014). Glacial to deglacial ventilation and productivity changes in the southern Okhotsk Sea. *Palaeogeography, Palaeoclimatology, Palaeoecology*, *395*, 53–66. <https://doi.org/10.1016/j.palaeo.2013.12.013>

- Okazaki, Y., Sagawa, T., Asahi, H., Horikawa, K., & Onodera, J. (2012). Ventilation changes in the western North Pacific since the last glacial period. *Climate of the Past*, 8(1), 17–24. <https://doi.org/10.5194/cp-8-17-2012>
- Okazaki, Y., Timmermann, A., Menviel, L., Harada, N., Abe-Ouchi, A., Chikamoto, M. O., et al. (2010). Deepwater formation in the North Pacific during the last glacial termination. *Science*, 329(5988), 200–204. <https://doi.org/10.1126/science.1190612>
- Olsson, I. U., Karlen, I., Turnbull, A. H., & Prosser, N. J. D. (1962). A determination of the half-life of C-14 with a proportional counter. *Arkiv för Fysik*, 22(3), 237–255.
- Orr, J. C., Najjar, R. G., Sabine, C., & Joos, F. (2000). *Abiotic-HOWTO. Technical report, revision: 1.16*. Retrieved from <http://ocmip5.ipsl.jussieu.fr/OCMIP/phase2/simulations/Abiotic/HOWTO-Abiotic.html>
- Ortiz, J. D., O'Connell, S. B., DelViscio, J., Dean, W., Carriquiry, J. D., Marchitto, T., et al. (2004). Enhanced marine productivity off western North America during warm climate intervals of the past 52 k.y. *Geology*, 32(6), 521–524. <https://doi.org/10.1130/g20234.1>
- Pailler, D., & Bard, E. (2002). High frequency palaeoceanographic changes during the past 140,000 yr recorded by the organic matter in sediments of the Iberian Margin. *Palaeogeography, Palaeoclimatology, Palaeoecology*, 181, 431–452. [https://doi.org/10.1016/s0031-0182\(01\)00444-8](https://doi.org/10.1016/s0031-0182(01)00444-8)
- Peck, V. L., Hall, I. R., Zahn, R., Elderfield, H., Grousset, F., Hemming, S. R., & Scourse, J. D. (2006). High resolution evidence for linkages between NW European ice sheet instability and Atlantic Meridional Overturning Circulation. *Earth and Planetary Science Letters*, 243(3), 476–488. <https://doi.org/10.1016/j.epsl.2005.12.023>
- Pedro, J. B., Jochum, M., Buizert, C., He, F., Barker, S., & Rasmussen, S. O. (2018). Beyond the bipolar seesaw: Toward a process understanding of interhemispheric coupling. *Quaternary Science Reviews*, 192, 27–46. <https://doi.org/10.1016/j.quascirev.2018.05.005>
- Peterson, C. D., Lisiecki, L., & Stern, J. V. (2014). Deglacial whole-ocean $\delta^{13}\text{C}$ change estimated from 480 benthic foraminiferal records. *Paleoceanography*, 29, 549–563. <https://doi.org/10.1002/2013pa002552>
- Povinec, P. P., Litherland, A. E., & von Reden, K. F. (2009). Development in radiocarbon technologies: From the Libby counter to compound-specific AMS analyses. *Radiocarbon*, 51(1), 45–78. <https://doi.org/10.1017/s0033822200033701>
- Primeau, F. (2005). Characterizing transport between the surface mixed layer and the ocean interior with a forward adjoint global ocean transport model. *Journal of Physical Oceanography*, 35, 545–564. <https://doi.org/10.1175/jpo2699.1>
- Primeau, F., & Deleersnijder, E. (2009). On the time to tracer equilibrium in the global ocean. *Ocean Science*, 5(1), 13–28. <https://doi.org/10.5194/os-5-13-2009>
- Rae, J. W. B., Burke, A., Robinson, L. F., Adkins, J. F., Chen, T., Cole, C., et al. (2018). CO_2 storage and release in the deep Southern Ocean on millennial to centennial timescales. *Nature*, 562(7728), 569–573. <https://doi.org/10.1038/s41586-018-0614-0>
- Rae, J. W. B., Sarnthein, M., Foster, G. L., Ridgwell, A., Grootes, P. M., & Elliott, T. (2014). Deep water formation in the North Pacific and deglacial CO_2 rise. *Paleoceanography*, 29(6), 645–667. <https://doi.org/10.1002/2013PA002570>
- Rafter, P. A., Carriquiry, J. D., Herguera, J.-C., Hain, M. P., Solomon, E. A., & Southon, J. R. (2019). Anomalous >2000-year-old surface ocean radiocarbon age as evidence for deglacial geologic carbon release. *Geophysical Research Letters*, 46(23), 13950–13960. <https://doi.org/10.1029/2019gl085102>
- Rafter, P. A., Herguera, J. C., & Southon, J. R. (2018). Extreme lowering of deglacial seawater radiocarbon recorded by both epifaunal and infaunal benthic foraminifera in a wood-dated sediment core. *Climate of the Past*, 14(12), 1977–1989. <https://doi.org/10.5194/cp-14-1977-2018>
- Raisbeck, G. M., Yiou, F., Jouzel, J., Petit, J. R., Barkov, N. I., & Bard, E. (1992). ^{10}Be deposition at Vostok, Antarctica, during the last 50,000 years and its relationship to possible cosmogenic production variations during this period. In E. Bard & W. S. Broecker (Eds.), *The last deglaciation: Absolute and radiocarbon chronologies* (pp. 127–139). Springer Verlag. https://doi.org/10.1007/978-3-642-76059-4_9
- Reimer, P. J., Austin, W. E. N., Bard, E., Bayliss, A., Blackwell, P. G., Bronk Ramsey, C., et al. (2020). The Intcal20 Northern Hemisphere radiocarbon age calibration curve (0–55 cal kBP). *Radiocarbon*, 62, 1–757. <https://doi.org/10.1017/RDC.2020.41>
- Reimer, P. J., Baillie, M. G. L., Bard, E., Bayliss, A., Beck, J. W., Blackwell, P. G., et al. (2009). Intcal09 and Marine09 radiocarbon age calibration curves, 0–50,000 years cal BP. *Radiocarbon*, 51(4), 1111–1150. <https://doi.org/10.1017/s0033822200034202>
- Reimer, P. J., Baillie, M. G. L., Bard, E., Bayliss, A., Warren Beck, J., Bertrand, C. J. H., et al. (2004). INTCAL04 Terrestrial radiocarbon age calibration, 0–26 cal kyr BP. *Radiocarbon*, 46(3), 1029–1058.
- Reimer, P. J., Bard, E., Bayliss, A., Beck, J. W., Blackwell, P. G., Ramsey, C. B., et al. (2013). Intcal13 and Marine13 radiocarbon age calibration curves, 0–50,000 years cal BP. *Radiocarbon*, 55(4), 1869–1887. https://doi.org/10.2458/azu_js_rc.55.16947
- Reimer, P. J., & Reimer, R. W. (2001). A marine reservoir correction database and on-line interface. *Radiocarbon*, 43(2A), 461–463.
- Revelle, R., & Suess, H. E. (1957). Carbon dioxide exchange between atmosphere and ocean and the question of an increase of atmospheric CO_2 during the past decades. *Tellus*, 9(1), 18–27. <https://doi.org/10.3402/tellusa.v9i1.9075>
- Rhodes, R. H., Brook, E. J., Chiang, J. C. H., Blunier, T., Maselli, O. J., McConnell, J. R., et al. (2015). Enhanced tropical methane production in response to iceberg discharge in the North Atlantic. *Science*, 348(6238), 1016–1019. <https://doi.org/10.1126/science.1262005>
- Ridgwell, A., Hargreaves, J. C., Edwards, N. R., Annan, J. D., Lenton, T. M., Marsh, R., et al. (2007). Marine geochemical data assimilation in an efficient Earth System Model of global biogeochemical cycling. *Biogeosciences*, 4(1), 87–104. <https://doi.org/10.5194/bg-4-87-2007>
- Roberts, M. L., & Southon, J. R. (2007). A preliminary determination of the absolute $^{14}\text{C}/^{12}\text{C}$ ratio of OX-I. *Radiocarbon*, 49(2), 441–445.
- Robinson, L. F., Adkins, J. F., Keigwin, L. D., Southon, J., Fernandez, D. P., Wang, S.-L., & Scheirer, D. S. (2005). Radiocarbon variability in the western North Atlantic during the last deglaciation. *Science*, 310, 1469–1473. <https://doi.org/10.1126/science.1114832>
- Rodgers, K. B., Mikaloff-Fletcher, S. E., Bianchi, D., Beaulieu, C., Galbraith, E. D., Gnanadesikan, A., et al. (2011). Interhemispheric gradient of atmospheric radiocarbon reveals natural variability of Southern Ocean winds. *Climate of the Past*, 7(4), 1123–1138. <https://doi.org/10.5194/cp-7-1123-2011>
- Ronge, T. A., Prange, M., Mollenhauer, G., Ellinghausen, M., Kuhn, G., & Tiedemann, R. (2020). Radiocarbon evidence for the contribution of the southern Indian Ocean to the evolution of atmospheric CO_2 over the last 32,000 years. *Paleoceanography and Paleoclimatology*, 35(3), e2019PA003733. <https://doi.org/10.1029/2019PA003733>
- Ronge, T. A., Sarnthein, M., Roberts, J., Lamy, F., & Tiedemann, R. (2019). East Pacific Rise core PS75/059-2: Glacial-to-deglacial stratigraphy revisited. *Paleoceanography and Paleoclimatology*, 34(4), 432–435. <https://doi.org/10.1029/2019PA003569>
- Ronge, T. A., Tiedemann, R., Lamy, F., Köhler, P., Alloway, B. V., De Pol-Holz, R., et al. (2016). Radiocarbon constraints on the extent and evolution of the South Pacific glacial carbon pool. *Nature Communications*, 7. <https://doi.org/10.1038/ncomms11487>
- Roth, R., & Joos, F. (2013). A reconstruction of radiocarbon production and total solar irradiance from the Holocene ^{14}C and CO_2 records: Implications of data and model uncertainties. *Climate of the Past*, 9(4), 1879–1909. <https://doi.org/10.5194/cp-9-1879-2013>
- Sadatzi, H., Maffezzoli, N., Dokken, T. M., Simon, M. H., Berben, S. M. P., Fahl, K., et al. (2020). Rapid reductions and millennial-scale variability in Nordic Seas sea ice cover during abrupt glacial climate changes. *Proceedings of the National Academy of Sciences*, 117(47), 29478–29486. <https://doi.org/10.1073/pnas.2005849117>
- Sarmiento, J. L., & Gruber, N. (2006). *Ocean biogeochemical dynamics* (p. 503). Princeton University Press.

- Sarmiento, J. L., & Toggweiler, R. (1984). A new model for the role of the oceans in determining atmospheric $p\text{CO}_2$. *Nature*, *308*, 621–624. <https://doi.org/10.1038/308621a0>
- Sarnthein, M., Balmer, S., Grootes, P., & Mudelsee, M. (2015). Planktic and benthic ^{14}C reservoir ages for three ocean basins, calibrated by a suite of ^{14}C plateaus in the glacial-to-deglacial Suigetsu atmospheric ^{14}C record. *Radiocarbon*, *57*(1), 129–151. https://doi.org/10.2458/azu_rc.57.17916
- Sarnthein, M., Grootes, P. M., Kennett, J. P., & Nadeau, M.-J. (2007). ^{14}C reservoir ages show deglacial changes in ocean currents and carbon cycle. In A. Schmittner, C. H. Chiang, & S. R. Hemming (Eds.), *Ocean circulation: Mechanisms and impacts* (pp. 175–196). AGU. <https://doi.org/10.1029/173gm13>
- Sarnthein, M., Küssner, K., Grootes, P. M., Ausin, B., Eglinton, T., Muglia, J., et al. (2020). Plateaus and jumps in the atmospheric radiocarbon record – Potential origin and value as global age markers for glacial-to-deglacial paleoceanography, a synthesis. *Climate of the Past*, *16*(6), 2547–2571. <https://doi.org/10.5194/cp-16-2547-2020>
- Sarnthein, M., Schneider, B., & Grootes, P. M. (2013). Peak glacial ^{14}C ventilation ages suggest major draw-down of carbon into the abyssal ocean. *Climate of the Past Discussions*, *9*, 925–965. <https://doi.org/10.5194/cp-9-2595-2013>
- Sauzède, R., Claustre, H., Jamet, C., Uitz, J., Ras, J., Mignot, A., & D'Ortenzio, F. (2015). Retrieving the vertical distribution of chlorophyll a concentration and phytoplankton community composition from in situ fluorescence profiles: A method based on a neural network with potential for global-scale applications. *Journal of Geophysical Research: Oceans*, *120*(1), 451–470. <https://doi.org/10.1002/2014JC010355>
- Schmitt, J., Schneider, R., Elsig, J., Leuenberger, D., Lourantou, A., Chappellaz, J., et al. (2012). Carbon isotope constraints on the deglacial CO_2 rise from ice cores. *Science*, *336*(6082), 711–714. <https://doi.org/10.1126/science.1217161>
- Schroder-Ritzrau, A., Mangini, A., & Lomitschka, M. (2003). Deep-sea corals evidence periodic reduced ventilation in the North Atlantic during the LGM/Holocene transition. *Earth and Planetary Science Letters*, *216*, 399–410. [https://doi.org/10.1016/s0012-821x\(03\)00511-9](https://doi.org/10.1016/s0012-821x(03)00511-9)
- Schüpbach, S., Fischer, H., Bigler, M., Erhardt, T., Gfeller, G., Leuenberger, D., et al. (2018). Greenland records of aerosol source and atmospheric lifetime changes from the Eemian to the Holocene. *Nature Communications*, *9*(1), 1476. <https://doi.org/10.1038/s41467-018-03924-3>
- Shackleton, N. J., Duplessy, J.-C., Arnold, M., Maurice, P., Hall, M. A., & Cartlidge, J. (1988). Radiocarbon age of last glacial Pacific deep water. *Nature*, *335*(6192), 708–711. <https://doi.org/10.1038/335708a0>
- Shao, J., Stott, L. D., Gray, W. R., Greenop, R., Pecher, I., Neil, H. L., et al. (2019). Atmosphere-ocean CO_2 exchange across the last deglaciation from the boron isotope proxy. *Paleoceanography and Paleoclimatology*, *34*(10), 1650–1670. <https://doi.org/10.1029/2018PA003498>
- Siani, G., Michel, E., De Pol-Holz, R., DeVries, T., Lamy, F., Carel, M., et al. (2013). Carbon isotope records reveal precise timing of enhanced Southern Ocean upwelling during the last deglaciation. *Nature Communications*, *4*. <https://doi.org/10.1038/ncomms3758>
- Siani, G., Paterne, M., Michel, E., Sulpizio, R., Sbrana, A., Arnold, M., & Haddad, G. (2001). Mediterranean Sea surface radiocarbon reservoir age changes since the last glacial maximum. *Science*, *294*, 1917–1920. <https://doi.org/10.1126/science.1063649>
- Siegenthaler, U. (1983). Uptake of excess CO_2 by an outcrop-diffusion model ocean. *Journal of Geophysical Research*, *88*, 3599–3608. <https://doi.org/10.1029/jc088ic06p03599>
- Siegenthaler, U., Heimann, M., & Oeschger, H. (1980). ^{14}C variations caused by changes in the global carbon cycle. *Radiocarbon*, *22*(2), 177–191. <https://doi.org/10.1017/s0033822200009449>
- Siegenthaler, U., & Wenk, T. (1984). Rapid atmospheric CO_2 variations and ocean circulation. *Nature*, *308*(5960), 624–626. <https://doi.org/10.1038/308624a0>
- Sigman, D. M., Hain, M. P., & Haug, G. H. (2010). The polar ocean and glacial cycles in atmospheric CO_2 . *Nature*, *466*, 47–55. <https://doi.org/10.1038/nature09149>
- Sikes, E. L., Allen, K. A., & Lund, D. C. (2017). Enhanced $\delta^{13}\text{C}$ and $\delta^{18}\text{O}$ differences between the South Atlantic and South Pacific during the last glaciation: The deep gateway hypothesis. *Paleoceanography*, *32*(10), 1000–1017. <https://doi.org/10.1002/2017PA003118>
- Sikes, E. L., Cook, M. S., & Guilderson, T. P. (2016). Reduced deep ocean ventilation in the Southern Pacific Ocean during the last glaciation persisted into the deglaciation. *Earth and Planetary Science Letters*, *438*, 130–138. <https://doi.org/10.1016/j.epsl.2015.12.039>
- Sikes, E. L., Elmore, A. C., Allen, K. A., Cook, M. S., & Guilderson, T. P. (2016). Glacial water mass structure and rapid $\delta^{18}\text{O}$ and $\delta^{13}\text{C}$ changes during the last glacial termination in the Southwest Pacific. *Earth and Planetary Science Letters*, *456*, 87–97. <https://doi.org/10.1016/j.epsl.2016.09.043>
- Sikes, E. L., & Guilderson, T. P. (2016). Southwest Pacific Ocean surface reservoir ages since the last glaciation: Circulation insights from multiple-core studies. *Paleoceanography*, *31*(2), 298–310. <https://doi.org/10.1002/2015PA002855>
- Sikes, E. L., Samson, C. R., Guilderson, T. P., & Howard, W. R. (2000). Old radiocarbon ages in the southwest Pacific Ocean during the last glacial period and deglaciation. *Nature*, *405*, 555–559. <https://doi.org/10.1038/35014581>
- Simon, Q., Thouveny, N., Bourlès, D. L., Valet, J.-P., & Bassinot, F. (2020). Cosmogenic ^{10}Be production records reveal dynamics of geomagnetic dipole moment (GDM) over the Laschamp excursion (20–60 ka). *Earth and Planetary Science Letters*, *550*, 116547. <https://doi.org/10.1016/j.epsl.2020.116547>
- Singarayer, J. S., Richards, D. A., Ridgwell, A., Valdes, P. J., Austin, W. E. N., & Beck, J. W. (2008). An oceanic origin for the increase of atmospheric radiocarbon during the Younger Dryas. *Geophysical Research Letters*, *35*(14). <https://doi.org/10.1029/2008gl034074>
- Skinner, L., Freeman, E., Hodell, D., Waelbroeck, C., Vasquez Riveiros, N., & Scrivner, A. (2021). Atlantic Ocean ventilation changes across the last deglaciation and their carbon cycle implications. *Paleoceanography and Paleoclimatology*, *36*(2), e2020PA004074. <https://doi.org/10.1029/2020pa004074>
- Skinner, L., McCave, I. N., Carter, L., Fallon, S., Scrivner, A., & Primeau, F. (2015). Reduced ventilation and enhanced magnitude of the deep Pacific carbon pool during the last glacial period. *Earth and Planetary Science Letters*, *411*, 45–52. <https://doi.org/10.1016/j.epsl.2014.11.024>
- Skinner, L., Menviel, L., Broadfield, L., Gottschalk, J., & Greaves, M. (2020). Southern Ocean convection amplified past Antarctic warming and atmospheric CO_2 rise during Heinrich Stadial 4. *Communications Earth & Environment*, *1*(1), 23. <https://doi.org/10.1038/s43247-020-00024-3>
- Skinner, L., Muschitiello, F., & Scrivner, A. E. (2019). Marine reservoir age variability over the last deglaciation: Implications for marine carbon cycling and prospects for regional radiocarbon calibrations. *Paleoceanography and Paleoclimatology*, *34*(11), 1807–1815. <https://doi.org/10.1029/2019pa003667>
- Skinner, L., Sadekov, A., Brandon, M., Greaves, M., Plancherel, Y., de la Fuente, M., et al. (2019). Rare Earth Elements in the service of paleoceanography: A novel microanalysis approach. *Geochimica et Cosmochimica Acta*, *245*, 118–132. <https://doi.org/10.1016/j.gca.2018.10.027>
- Skinner, L. C., & Elderfield, H. (2005). Constraining ecological and biological bias in planktonic foraminiferal Mg/Ca and $\delta^{18}\text{O}_{\text{cc}}$: A multi-species approach to proxy calibration testing. *Paleoceanography*, *20*, 1–15. <https://doi.org/10.1029/2004pa001058>
- Skinner, L. C., Fallon, S., Waelbroeck, C., Michel, E., & Barker, S. (2010). Ventilation of the deep Southern Ocean and deglacial CO_2 rise. *Science*, *328*, 1147–1151. <https://doi.org/10.1126/science.1183627>
- Skinner, L. C., Primeau, F., Freeman, E., de la Fuente, M., Goodwin, P., Gottschalk, J., et al. (2017). Radiocarbon constraints on the glacial ocean circulation and its impact on atmospheric CO_2 . *Nature Communications*, *8*, 16010. <https://doi.org/10.1038/ncomms16010>

- Skinner, L. C., Scrivner, A., Vance, D., Barker, S., Fallon, S., & Waelbroeck, C. (2013). North Atlantic versus Southern Ocean contributions to a deglacial surge in deep ocean ventilation. *Geology*, *41*, 667–670. <https://doi.org/10.1130/G34133.1>
- Skinner, L. C., & Shackleton, N. J. (2004). Rapid transient changes in northeast Atlantic deep-water ventilation-age across Termination I. *Paleoceanography*, *19*, 1–11. <https://doi.org/10.1029/2003pa000983>
- Skinner, L. C., & Shackleton, N. J. (2006). Deconstructing Terminations I and II: Revisiting the glacioeustatic paradigm based on deep-water temperature estimates. *Quaternary Science Reviews*, *25*, 3312–3321. <https://doi.org/10.1016/j.quascirev.2006.07.005>
- Skinner, L. C., Waelbroeck, C., Scrivner, A., & Fallon, S. (2014). Radiocarbon evidence for alternating northern and southern sources of ventilation of the deep Atlantic carbon pool during the last deglaciation. *Proceedings of the National Academy of Sciences*, *111*(15), 5480–5484. <https://doi.org/10.1073/pnas.1400668111>
- Sortor, R. N., & Lund, D. C. (2011). No evidence for a deglacial intermediate water $\Delta^{14}\text{C}$ anomaly in the SW Atlantic. *Earth and Planetary Science Letters*, *310*(1–2), 65–72. <https://doi.org/10.1016/j.epsl.2011.07.017>
- Soulet, G. (2015). Methods and codes for reservoir-atmosphere ^{14}C age offset calculations. *Quaternary Geochronology*, *29*, 97–103. <https://doi.org/10.1016/j.quageo.2015.05.023>
- Soulet, G., Skinner, L., Beaupre, S. R., & Galy, V. (2016). A note on reporting of reservoir ^{14}C disequilibria and age offsets. *Radiocarbon*, *57*(6), 205–211. <https://doi.org/10.1017/RDC.2015.22>
- Southon, J., Noronha, A. L., Cheng, H., Edwards, R. L., & Wang, Y. (2012). A high-resolution record of atmospheric ^{14}C based on Hulu Cave speleothem H82. *Quaternary Science Reviews*, *33*, 32–41. <https://doi.org/10.1016/j.quascirev.2011.11.022>
- Spolaor, A., Vallelonga, P., Turetta, C., Maffezzoli, N., Cozzi, G., Gabrieli, J., et al. (2016). Canadian Arctic sea ice reconstructed from bromine in the Greenland NEEM ice core. *Scientific Reports*, *6*(1), 33925. <https://doi.org/10.1038/srep33925>
- Stern, J. V., & Lisiecki, L. E. (2013). North Atlantic circulation and reservoir age changes over the past 41,000 years. *Geophysical Research Letters*, *40*(14), 3693–3697. <https://doi.org/10.1002/grl.50679>
- Stocker, T. F., & Johnsen, S. J. (2003). A minimum thermodynamic model for the bipolar seesaw. *Paleoceanography*, *18*(4). <https://doi.org/10.1029/2003pa000920>
- Stocker, T. F., & Wright, D. G. (1996). Rapid changes in ocean circulation and atmospheric radiocarbon. *Paleoceanography*, *11*(6), 773–795. <https://doi.org/10.1029/96pa02640>
- Stoner, J. S., Laj, C., Channell, J. E. T., & Kissel, C. (2002). South Atlantic and North Atlantic geomagnetic paleointensity stacks (0–80 ka): Implications for inter-hemispheric correlation. *Quaternary Science Reviews*, *21*, 1141–1151. [https://doi.org/10.1016/s0277-3791\(01\)00136-6](https://doi.org/10.1016/s0277-3791(01)00136-6)
- Stott, L., Davy, B., Shao, J., Coffin, R., Pecher, I., Neil, H., et al. (2019). CO_2 release from Pockmarks on the Chatham Rise-Bounty Trough at the glacial termination. *Paleoceanography and Paleooclimatology*, *34*(11), 1726–1743. <https://doi.org/10.1029/2019pa003674>
- Stott, L., Southon, J., Timmermann, A., & Koutavas, A. (2009). Radiocarbon age anomaly at intermediate water depth in the Pacific Ocean during the last deglaciation. *Paleoceanography*, *24*(2). <https://doi.org/10.1029/2008PA001690>
- Stott, L. D. (2020). Assessing the stratigraphic integrity of planktic and benthic ^{14}C records in the western Pacific for $\Delta^{14}\text{C}$ reconstructions at the last glacial termination. *Radiocarbon*, *62*(5), 1389–1402. <https://doi.org/10.1017/RDC.2020.82>
- Stuiver, M. (1961). Variations in radiocarbon concentration and sunspot activity. *Journal of Geophysical Research*, *66*(1), 273–276. <https://doi.org/10.1029/JZ066i001p00273>
- Stuiver, M., Pearson, G. W., & Braziunas, T. (1986). Radiocarbon calibration of marine samples back to 9000 cal yr BP. *Radiocarbon*, *28*(2B), 980–1021. <https://doi.org/10.1017/s0033822200060264>
- Stuiver, M., & Polach, H. A. (1977). Reporting of ^{14}C data. *Radiocarbon*, *19*(3), 355–363. <https://doi.org/10.1017/s0033822200003672>
- Stuiver, M., Reimer, P. J., Bard, E., Beck, J. W., Burr, G. S., Hughen, K. A., et al. (1998). INTCAL98 radiocarbon age calibration, 24,000–0 cal BP. *Radiocarbon*, *40*(3), 1041–1083. <https://doi.org/10.1017/s0033822200019123>
- Takahashi, T., Sutherland, S. C., Wanninkhof, R., Sweeney, C., Feely, R. A., Chipman, D. W., et al. (2009). Climatological mean and decadal change in surface ocean $p\text{CO}_2$, and net sea-air CO_2 flux over the global oceans. *Deep Sea Research Part II: Topical Studies in Oceanography*, *56*(8), 554–577. <https://doi.org/10.1016/j.dsr2.2008.12.009>
- Telesniński, M. M., Ezat, M. M., Muschitiello, F., Bauch, H. A., & Spielhagen, R. F. (2021). Ventilation history of the Nordic Seas deduced from pelagic-benthic radiocarbon age offsets. *Geochemistry, Geophysics, Geosystems*, *22*(4), e2020GC009132. <https://doi.org/10.1029/2020GC009132>
- Thiagarajan, N., Subhas, A. V., Southon, J. R., Eiler, J. M., & Adkins, J. F. (2014). Abrupt pre-Bölling-Allerød warming and circulation changes in the deep ocean. *Nature*, *511*(7507), 75–78. <https://doi.org/10.1038/nature13472>
- Thornalley, D. J. R., Barker, S., Broecker, W., Elderfield, H., & McCave, I. N. (2011). The deglacial evolution of North Atlantic deep convection. *Science*, *331*, 202–205. <https://doi.org/10.1126/science.1196812>
- Thornalley, D. J. R., Bauch, H. A., Gebbie, G., Guo, W., Ziegler, M., Bernasconi, S. M., et al. (2015). A warm and poorly ventilated deep Arctic Mediterranean during the last glacial period. *Science*, *349*(6249), 706–710. <https://doi.org/10.1126/science.aaa9554>
- Toggweiler, J. R. (1999). Variation of atmospheric CO_2 by ventilation of the ocean's deepest water. *Paleoceanography*, *14*(5), 571–588. <https://doi.org/10.1029/1999pa900033>
- Toggweiler, J. R., Dixon, K., & Bryan, K. (1989). Simulations of radiocarbon in a coarse-resolution world ocean model: 1. Steady state prebomb distributions. *Journal of Geophysical Research*, *94*(C6), 8217–8241. <https://doi.org/10.1029/jc094ic06p08217>
- Toggweiler, J. R., & Sarmiento, J. L. (1985). Glacial to interglacial changes in atmospheric carbon dioxide: The critical role of ocean surface water in high latitudes. In *The carbon cycle and atmospheric CO_2 : Natural variations Archean to present* (pp. 163–184). American Geophysical Union.
- Tschumi, T., Joos, F., Gehlen, M., & Heinze, C. (2011). Deep ocean ventilation, carbon isotopes, marine sedimentation and the deglacial CO_2 rise. *Climate of the Past*, *7*, 771–800. <https://doi.org/10.5194/cp-7-771-2011>
- Umling, N. E., & Thunell, R. C. (2017). Synchronous deglacial thermocline and deep-water ventilation in the eastern equatorial Pacific. *Nature Communications*, *8*, 14203. <https://doi.org/10.1038/ncomms14203>
- Umling, N. E., & Thunell, R. C. (2018). Mid-depth respired carbon storage and oxygenation of the eastern equatorial Pacific over the last 25,000 years. *Quaternary Science Reviews*, *189*, 43–56. <https://doi.org/10.1016/j.quascirev.2018.04.002>
- Volk, T., & Hoffert, M. I. (1985). Ocean carbon pumps: Analysis of relative strengths and efficiencies in ocean-driven atmospheric CO_2 changes. In *The carbon cycle and atmospheric CO_2 : Natural variations Archean to present*. American Geophysical Union.
- Wacker, L., Lippold, J., Molnár, M., & Schulz, H. (2013). Towards radiocarbon dating of single foraminifera with a gas ion source. *Nuclear Instruments and Methods in Physics Research Section B: Beam Interactions with Materials and Atoms*, *294*, 307–310. <https://doi.org/10.1016/j.nimb.2012.08.038>
- Waelbroeck, C., Duplessy, J.-C., Michel, E., Labeyrie, L., Paillard, D., & Duprat, J. (2001). The timing of the last deglaciation in North Atlantic climate records. *Nature*, *412*, 724–727. <https://doi.org/10.1038/35089060>

- Walker, B. D., Beaupré, S. R., Guilderson, T. P., McCarthy, M. D., & Druffel, E. R. M. (2016). Pacific carbon cycling constrained by organic matter size, age and composition relationships. *Nature Geoscience*, 9(12), 888–891. <https://doi.org/10.1038/ngeo2830>
- Wan, S., & Jian, Z. (2014). Deep water exchanges between the South China Sea and the Pacific since the last glacial period. *Paleoceanography*, 29(12), 1162–1178. <https://doi.org/10.1002/2013PA002578>
- Wang, Y. J., Cheng, H., Edwards, R. L., An, Z. S., Wu, J. Y., Shen, C.-C., & Dorale, J. A. (2001). A high-resolution absolute-dated late Pleistocene monsoon record from Hulu Cave, China. *Science*, 294, 2345–2348. <https://doi.org/10.1126/science.1064618>
- Wanninkhof, R., Park, G.-H., Takahashi, T., Sweeney, C., Feely, R., Nojiri, Y., et al. (2013). Global ocean carbon uptake: Magnitude, variability and trends. *Biogeosciences*, 10(3), 1983–2000. <https://doi.org/10.5194/bg-10-1983-2013>
- Watson, A. J., Vallis, G. K., & Nikurashin, M. (2015). Southern Ocean buoyancy forcing of ocean ventilation and glacial atmospheric CO₂. *Nature Geoscience*, 8(11), 861–864. <https://doi.org/10.1038/ngeo2538>
- Watt, D. E., Ramsden, D., & Wilson, H. W. (1961). The half-life of carbon-14. *International Journal of Applied Radiation and Isotopes*, 11(1), 68–74. [https://doi.org/10.1016/0020-708x\(61\)90133-8](https://doi.org/10.1016/0020-708x(61)90133-8)
- Waugh, D., & Hall, T. (2002). Age of stratospheric air: Theory observations, and models. *Review of Geophysics*, 40(4), 1–1–1–26. <https://doi.org/10.1029/2000RG000101>
- Welte, C., Wacker, L., Hattendorf, B., Christl, M., Fohlmeister, J., Breitenbach, S. F. M., et al. (2016). Laser ablation – Accelerator mass spectrometry: An approach for rapid radiocarbon analyses of carbonate archives at high spatial resolution. *Analytical Chemistry*, 88(17), 8570–8576. <https://doi.org/10.1021/acs.analchem.6b01659>
- Williams, P. M., & Druffel, E. R. M. (1987). Radiocarbon in dissolved organic-matter in the central North Pacific Ocean. *Nature*, 330, 246–248. <https://doi.org/10.1038/330246a0>
- Williams, R. G., & Follows, M. (2011). *Ocean dynamics and the carbon cycle: Principals and mechanisms*. Cambridge University Press.
- Willis, E. H., Tauber, H., & Münnich, K. O. (1960). Variations in the atmospheric radiocarbon concentration over the past 1300 years. *Radiocarbon*, 3, 1–4. <https://doi.org/10.1017/s1061592x00020548>
- Wilson, D. J., Crocket, K. C., van de Fliedert, T., Robinson, L. F., & Adkins, J. F. (2014). Dynamic intermediate ocean circulation in the North Atlantic during Heinrich Stadial 1: A radiocarbon and neodymium isotope perspective. *Paleoceanography*, 29(11), 1072–1093. <https://doi.org/10.1002/2014PA002674>
- Winterfeld, M., Mollenhauer, G., Dumann, W., Köhler, P., Lembke-Jene, L., Meyer, V. D., et al. (2018). Deglacial mobilization of pre-aged terrestrial carbon from degrading permafrost. *Nature Communications*, 9(1), 3666. <https://doi.org/10.1038/s41467-018-06080-w>
- Wolff, E., Fischer, H., & Rothlisberger, R. (2009). Glacial terminations as southern warmings without northern control. *Nature Geoscience*, 2, 206–209. <https://doi.org/10.1038/ngeo442>
- Wycech, J., Kelly, D. C., & Marcott, S. (2016). Effects of seafloor diagenesis on planktic foraminiferal radiocarbon ages. *Geology*, 44(7), 551–554. <https://doi.org/10.1130/g37864.1>
- Yokoyama, Y., Esat, T. M., Thompson, W. G., Thomas, A. L., Webster, J. M., Miyairi, Y., et al. (2018). Rapid glaciation and a two-step sea level plunge into the Last Glacial Maximum. *Nature*, 559(7715), 603–607. <https://doi.org/10.1038/s41586-018-0335-4>
- Yu, J., Anderson, R. F., Jin, Z., Rae, J. W. B., Opdyke, B. N., & Eggins, S. M. (2013). Responses of the deep ocean carbonate system to carbon reorganization during the Last Glacial–interglacial cycle. *Quaternary Science Reviews*, 76, 39–52. <https://doi.org/10.1016/j.quascirev.2013.06.020>
- Yu, J., Anderson, R. F., & Rohling, E. J. (2014). Deep ocean carbonate chemistry and glacial–interglacial atmospheric CO₂ changes. *Oceanography*, 27(1), 16–25. <https://doi.org/10.5670/oceanog.2014.04>
- Zeebe, R. E., & Wolf-Gladrow, D. (2001). *CO₂ in seawater: Equilibrium, kinetics, isotopes*. Elsevier.
- Zhao, N., & Keigwin, L. D. (2018). An atmospheric chronology for the glacial–deglacial Eastern Equatorial Pacific. *Nature Communications*, 9(1), 3077. <https://doi.org/10.1038/s41467-018-05574-x>
- Zhao, N., Marchal, O., Keigwin, L., Amrhein, D., & Gebbie, G. (2018). A synthesis of deglacial deep-sea radiocarbon records and their (in) consistency with modern ocean ventilation. *Paleoceanography and Paleoclimatology*, 33(2), 128–151. <https://doi.org/10.1002/2017pa003174>